# Iron-Oxide-Supported Nanocarbon in Lithium-Ion Batteries, Medical, Catalytic, and Environmental Applications

**Jiří Tuček,[†] Kingsley Christian Kemp,[‡] Kwang Soo Kim,[‡,*] and Radek Zbořil[†,*]**

[†]Regional Centre of Advanced Technologies and Materials, Departments of Physical Chemistry and Experimental Physics, Faculty of Science, Palacky University, 17. listopadu 1192/12, 771 46 Olomouc, Czech Republic, and [‡]Center for Superfunctional Materials, Department of Chemistry, School of Natural Science, Ulsan National Institute of Science and Technology (UNIST), UNIST-gil 50, Ulsan 689-798, Korea

**ABSTRACT** Owing to the three different orbital hybridizations carbon can adopt, the existence of various carbon nanoallotropes differing also in dimensionality has been already affirmed with other structures predicted and expected to emerge in the future. Despite numerous unique features and applications of 2D graphene, 1D carbon nanotubes, or 0D fullerenes, nanodiamonds, and carbon quantum dots, which have been already heavily explored, any of the existing carbon allotropes do not offer competitive magnetic properties. For challenging applications, carbon nanoallotropes are functionalized with magnetic species, especially of iron oxide nature, due to their interesting magnetic properties (superparamagnetism and strong magnetic response under external magnetic fields), easy availability, biocompatibility, and low cost. In addition, combination of iron oxides (magnetite, maghemite, hematite) and carbon nanostructures brings enhanced electrochemical performance and (photo)catalytic capability due to synergetic and cooperative effects. This work aims at reviewing these advanced applications of iron-oxide-supported nanocarbon composites where iron oxides play a diverse role. Various architectures of carbon/iron oxide nanocomposites, their synthetic procedures, physicochemical properties, and applications are discussed in details. A special attention is devoted to hybrids of carbon nanotubes and rare forms (mesoporous carbon, nanofoam) with magnetic iron oxide carriers for advanced environmental technologies. The review also covers the huge application potential of graphene/iron oxide nanocomposites in the field of energy storage, biomedicine, and remediation of environment. Among various discussed medical applications, magnetic composites of zero-dimensional fullerenes and carbon dots are emphasized as promising candidates for complex theranostics and dual magneto-fluorescence imaging.

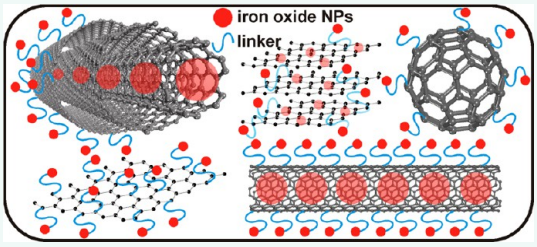


**KEYWORDS:** carbon allotropes · carbon nanotube · fullerene · graphene · graphene oxide · carbon quantum dot · mesoporous carbon · carbon foam · core–shell nanoparticles · functionalization · $\gamma$-$Fe_2O_3$ · $\alpha$-$Fe_2O_3$ · $Fe_3O_4$

Carbon is an essential element of all organic compounds and is regarded as a building stone of all living organisms. In nature, elemental carbon exists in two well-known forms, that is, soft graphite and hard diamond. Thus, carbon is said to display allotropy, a feature of a chemical element to occur in several different stable structural forms with significantly different physical properties. Nanotechnology approaches, which underwent a dramatic boom in the late 20th century, have given rise to other structurally distinct forms of carbon, often referred to as carbon nanomaterials. They include fullerene,[1] nanodiamond,[2] carbon quantum dots,[3,4] carbon nanotubes[5] and nanofibers,[6] carbon nanobuds,[7] graphene,[8−10] carbon nanohorns,[11] and carbon (graphene) nanoribbons.[12−14] With respect to their dimensionalities, carbon nanomaterials can be divided into three groups: (i) zero-dimensional (0D) structures such as fullerene, carbon quantum dots, and nanodiamonds, (ii) one-dimensional (1D) structures such as carbon nanotubes and carbon nanohorns, and (iii) two-dimensional (2D) structures such as graphene, carbon (graphene) nanoribbons, and few-layered graphenes. (Graphite and diamond are classified as 3D carbon allotropes.) Other classification criteria involve types of

* Address correspondence to radek.zboril@upol.cz, kimks@unist.ac.kr.

Received for review April 3, 2014 and accepted July 7, 2014.

**Published online July 07, 2014**
10.1021/nn501836x

**VOCABULARY:** **Allotropy** - a property of a chemical element showing potentiality to exist in two or more distinct forms differing in the crystal structure and having thus significantly distinct physical properties; **Nanocomposite** - a system composed of two or more phases, where at least one of the components has one, two, or three dimensions of less than 100 nm; **Functionalization** - a process of modification of (nano)material contact surface with substances of diverse chemical nature enriching the combined architecture with physical, chemical, or biological features that are different from those exhibited by the (nano)material alone; **Covalent functionalization** - a type of functionalization when the two or more chemically or physically distinct species in a nanocomposite are combined together *via* functional groups (*e.g.*, $-OH$, $-COOH$, $-OOH$, $-F$, $-NH_2$, $-SH$, $-OP(=O)(OH)_2$), establishing covalent bonds among the components involved in the nanocomposite. This, among others, enables to alter the properties of individual nanocomposite components *via* cooperation and synergetic effects, bringing new functions, features, and capabilities of the nanocomposite, enhancing its application potential; **Physical adsorption** - a process of nanocomposite formation when various structures, substances, and/or compounds are adsorbed on a surface of a given nanomaterial, exploiting its large surface area. The physical adsorption is mediated by forces of physical nature acting between nanocomposite components including electrostatic Coulomb forces, unbalanced valence forces of atoms at the surface, van der Waals forces, *etc.*; **Superparamagnetism** - a magnetic phenomenon when a nanoparticle's magnetic moment (*i.e.*, a superspin—a vector sum of all atomic (ion) magnetic moments inside the nanoparticle) spontaneously fluctuates between directions along easy axes of magnetization established by the nanoparticle magnetic anisotropy; in each direction, the superspin stays for a certain time before flipping known as the relaxation time. The nanoparticle's superspin oscillations are triggered by a temperature when a thermal energy exceeds energy of anisotropy barrier(s) separating energetically favorable superspin directions. The temperature at which superparamagnetic fluctuations occur (the so-called blocking temperature) depends, among other factors, on the particle size, material's magnetic anisotropy energy constant, strength of external magnetic field, and characteristic time of the measuring technique. In other words, at a certain temperature, nanoparticles become superparamagnetic once their size falls down below a threshold limit particular for any material showing long-range magnetic ordering in the bulk form; **Bioimaging** - imaging of tissues and organs in the living organisms employing (nano)materials as contrast or photoluminescence-active agents. Nanoparticles showing a superparamagnetic property (*e.g.*, iron oxide nanoparticles) are often used in magnetic resonance imaging (MRI) and magnetic particle imaging (MPI) diagnostic approaches, whereas quantum dots (of carbon nature) play a significant role in diagnostics exploiting their fluorescent properties; **Magnetic delivery** - a way to deliver a biologically active compound (*e.g.*, a drug) to a target place in a living organism employing a magnetic nanoparticle as its carrier; the complex can be easily magnetized by a homogeneous external magnetic field and controllably driven to a particular site by magnetic forces generated by a magnetic field gradient; **Lithium-ion battery** - a member of a class of rechargeable battery types based on passage of lithium ions from the negative electrode to the positive electrode during discharge and back when charging undergoing intercalation and deintercalation processes, respectively.

covalent bonds ($sp^2$ and $sp^3$) between carbon atoms in a respective carbon nanoallotrope or morphological features of carbon nanoallotropes (*e.g.*, empty internal space *vs* "flat" or curved structures). Besides these carbon nanomaterials, which have been extensively covered in the literature, other nanosized members of the carbon family have been reported, such as carbon nanofoam[15] and aggregated diamond nanorods.[16,17] In terms of orbital hybridization, carbon is found to display $sp^3$, $sp^2$, and $sp^1$ configurations, allowing existence a great variety of crystalline and disordered structures. According to the recent theoretical studies, other possible forms of carbon have been predicted, including body-centered tetragonal carbon (bct carbon),[18] T-carbon,[19] M-carbon,[20] nanorope,[21] and prismane $C_8$.[22] Thus, in the near future, new carbon nanoallotropes are expected to emerge, enriching significantly the carbon family. The structures of the most frequently studied carbon (nano)allotropes are depicted in Figure 1.

Despite many unique material features, carbon (nano)allotropes show they miss some properties, which restricts their application portfolio and makes them unfit for some practical fields. Thus, carbon nanomaterials are frequently surface-modified by suitable functional groups to enable attachment of various organic and inorganic substances in order to enrich the properties and, hence, the application potential of the resulting hybrid system.[23−28] The covalent or noncovalent attachment of various compounds may tune the physicochemical features of the carbon nanomaterials due to synergetic effects and bring new characteristics that are not shown by the carbon nanostructures alone. These nanocomposite systems then become competitive materials in various fields where carbon nanomaterials themselves are not so attractive or they offer a good substitute for other (nano)materials with worse efficiency in a given application. One of the properties that carbon nanomaterials do not possess is a magnetic response if placed under external magnetic fields (or the response is very small as, for example, in graphene[29] or fullerene[30]). Thus, there have been a series of successful attempts reported to endow carbon-based nanocomposites with magnetic properties. Out of all

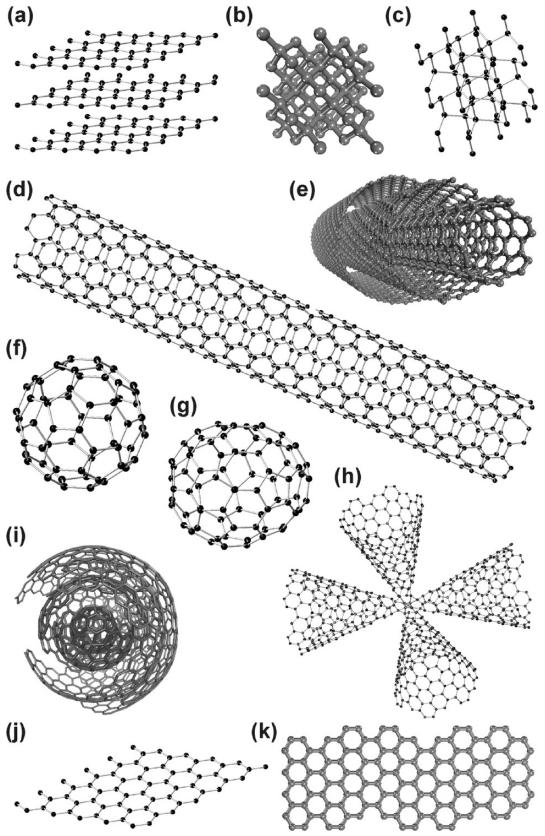


**Figure 1. Allotropes of carbon: (a) graphite; (b) diamond; (c) lonsdaleite; (d) single-walled carbon nanotube; (e) multi-walled carbon nanotube; (f) fullerene $C_{60}$; (g) fullerene $C_{76}$; (h) carbon nanohorns; (i) onion-like carbon; (j) graphene; (k) carbon nanoribbons.**

the possible magnetic substances that carbon nanomaterials can be decorated with, nanosized iron oxides [especially, $\gamma$-$Fe_2O_3$ (maghemite) and $Fe_3O_4$ (magnetite)] hold a paramount position.[31] They show not only interesting magnetic properties (*e.g.*, a strong magnetic response under small applied magnetic fields, superparamagnetism, tunable heating performance in alternating magnetic fields) but also favorable biochemical characteristics (*e.g.*, biocompatibility, biodegradability, nontoxicity).[32,33] In addition, combination of iron oxides and carbon nanostructures brings enhanced electrochemical performance and (photo)catalytic capability of the hybrids due to cooperative effects, thus making them very promising, for example, in the field of chemical degradation of various organic and/or inorganic compounds and in energy storage. Besides this, iron oxide/carbon nanoallotrope composites show improved sensing properties, providing feasible detection of various organic compounds and biomolecules.

In these nanocomposites, iron oxides play two roles. They are considered to behave passively when they act as an agent providing the hybrid with the capability to be targeted or separated by applying a magnetic field gradient (*e.g.*, removal of the pollutants adsorbed on the surface of a magnetic nanocomposite, carriers of compounds to be delivered to a target site). On the other hand, they perform an active function if the hybrid is designed for diagnostic (MRI imaging) and/or theranostic (biological imaging and therapy) purposes or photocatalytic applications. In addition, iron oxides are found to be extremely valuable in nanocomposites explored for anode materials for lithium-ion batteries as they readily undergo conversion- or displacement-type reactions (*i.e.*, $MO_x + xLi^+ + xe^- \leftrightarrow M + LiO_2$, where M is the metal) to store energy. Similarly, different carbon allotropes show different applicability as their physicochemical properties are governed by their structure and dimensionality. For example, to form a more conductive material, it is beneficial to introduce highly conductive graphene. However, for some photocatalytic applications, it may be more effective to exploit the photoactive carbon quantum dots.

In this review, in order to highlight the extraordinary position of carbon nanomaterials in the current materials science, we first provide an overview of the basic carbon (nano)allotropes, their physicochemical properties, preparation routes, and applicability in various practical fields. Afterward, we review the syntheses, properties, and current or proposed applications of carbon nanostructures functionalized with nanosized iron oxides. Specific attention is devoted to nanocomposites containing iron oxides with carbon nanotubes, graphene and graphene oxide, fullerenes, carbon quantum dots, mesoporous carbon, and carbon foam. Future perspectives and directions in the field of magnetic carbon nanocomposites are also discussed with regard to their application potential.

**Overview of Basic Carbon Allotropes, Their Physicochemical Properties, Syntheses, and Applications.** *Diamond and Graphite.* Diamond, the hardest known natural mineral, has tetrahedrally coordinated $sp^3$ carbon atoms that form an extended three-dimensional network adopting features of the face-centered cubic Bravais lattice. In contrast, graphite has three-coordinated $sp^2$ carbon atoms arranged in a honeycomb lattice with layered planar structure, where the sheets of the carbon atoms are held together by weak van der Waals forces. The different layout of carbon atoms in the lattice of diamond and graphite endows them with completely different physical properties (*e.g.*, graphite is opaque and metallic to earthy-looking, whereas diamond is transparent and brilliant).

*Fullerenes.* In 1985, a new carbon allotrope, known as fullerene, was discovered by Kroto *et al.*[1] while studying the nature of carbon in interstellar space. It was named after Richard Buckminster Fuller, a visionary architect famous for the design of geodesic domes which have structural characteristics resembling those of spherical fullerenes. In fullerenes, the closed-cage structure is established by the presence of five-membered rings; the arrangement of carbon atoms is

not planar but rather slightly pyramidalized as a result of a "pseudo" $sp^3$ bonding component present in the essentially $sp^2$ carbons.[34] Among the known forms of fullerenes, $C_{60}$ is regarded as the most symmetrical and stable fullerene molecule.[34] It consists of 20 hexagonal and 12 disjoint pentagonal faces where a carbon atom is located at each corner of the individual polygons; the polygons are arranged into highly symmetric truncated icosahedrons. The van der Waals diameter of $C_{60}$ is ~1.1 nm, and its nucleus-to-nucleus diameter is ~0.71 nm.[35] The $C_{60}$ molecule is often said to be not "superaromatic" because of its tendency to avoid formation of double bonds in the pentagonal rings.[25] As a result, poor electron delocalization is observed, and thus the $C_{60}$ molecule, behaving like an electrophile with a large electron-acceptor capability (*i.e.*, able to reversibly accept up to six electrons), reacts readily with electron-rich species.[34] Besides $C_{60}$, other fullerenes have been reported, such as $C_{70}$, $C_{76}$, $C_{82}$, and $C_{84}$.[36] $C_{60}$ and other larger fullerenes are routinely produced by a low-pressure method in which an electric discharge is passed across a gap between two carbon electrodes in a helium atmosphere.[34] Alternatively, they can be formed using laser vaporization of carbon or arc vaporization of graphite in an inert atmosphere.[37] From the viewpoint of physical properties, fullerenes and their derivatives have generated significant interest due to their remarkable optical characteristics,[38] heat resistance,[39] superconductivity,[40] and ferromagnetic behavior with Curie temperatures (up to ~33 K) much higher than those reported for any organic magnets.[41,42] Most of the fullerene derivatives are described as soft organic ferromagnets when the low-temperature long-range magnetic ordering is, among other factors, governed mainly by orientational ordering of $C_{60}^-$ ions, short $C_{60}$–$C_{60}$ distances along the fullerene *c* structural axis, and presence of ions of a charge transfer compound.[41,42] Fullerenes are frequently functionalized (see Figure 2) with a variety of organic and inorganic compounds to extend their range of potential applications. Functionalized

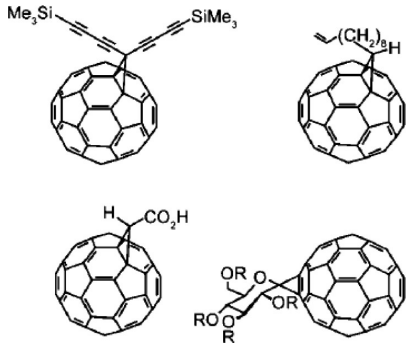


**Figure 2. Covalent chemical functionalization of fullerene surface (silane, alkene, carboxylate, and carbohydrate modifications). Reprinted with permission from ref 24. Copyright 1996 American Association for the Advancement of Science.**

fullerenes have found promising applications in the field of medicine (antioxidants and neuroprotective agents,[43] enzyme inhibition,[44] antimicrobial activity[45]), electronics (organic solar cells,[46–49] liquid crystals,[50] photocurrent generation devices,[51] *etc.*), and catalysis (sensors).[52] The discovery of fullerenes stimulated an eminent interest in carbon chemistry, which in turn intensified attempts to produce new carbon-based nanostructures.

*Carbon Nanotubes.* In 1991, Iijima discovered a new structural form of carbon, known as multiwalled carbon nanotubes, in a carbon soot prepared by an arc-discharge method;[5] 2 years later, he observed single-walled carbon nanotubes.[53] A single-walled carbon nanotube is a graphene sheet that is rolled to form a cylinder with a typical diameter from ~0.4 to ~2 nm.[54,55] In contrast, a multiwalled carbon nanotube comprises concentric cylinders with an interlayer spacing of 0.34 nm and a typical diameter ranging from ~2 to ~25 nm; the rolled graphene sheets are held together by van der Waals interactions.[54,55] The length of single-walled and multiwalled carbon nanotubes can reach hundreds of micrometers or even centimeters.[56] The aspect ratio (*i.e.*, length-to-diameter ratio) frequently exceeds 10 000, and thus, carbon nanotubes have been suggested to be the most anisotropic materials ever produced. Besides the diameter and length, chirality (the angle between the hexagons and the nanotube axis) is another key parameter of the carbon nanotube.[54,55,57–60] Depending on the chirality, the carbon atoms around the nanotube circumference can be arranged in several ways of which arm chair, zigzag, and chiral patterns (see Figure 3) are the most common examples.[54,55,57–60] In carbon nanotubes, the carbon atoms are held together by $sp^2$ bonds, endowing them with a unique strength. It turns out that the properties of carbon nanotubes significantly depend on the way the graphene sheets are rolled, their diameter and length, their morphology, and defects. Carbon nanotubes are found to be among the strongest and stiffest materials yet discovered and existing in nature (Young's modulus of ~1.2 TPa and tensile strength of ~100 GPa, about 100 times higher than steel).[54,55,57–60] The electrical properties of carbon nanotubes are markedly

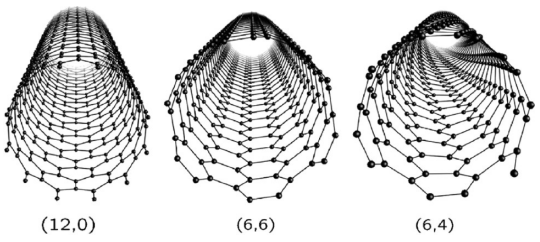


**Figure 3. Structure of (12,0) zigzag, (6,6) armchair, and (6,4) chiral single-walled carbon nanotube. Reprinted with permission from ref 59. Copyright 2007 American Physical Society.**

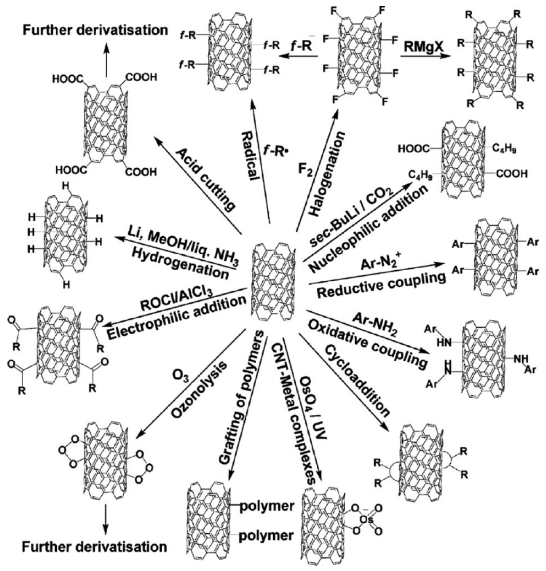


**Figure 4. Surface functionalization of the carbon nanotubes with various functional groups. Reprinted with permission from ref 61. Copyright 2010 Royal Society of Chemistry.**

governed by their chirality and diameter; single-walled carbon nanotubes can be either a metal, semiconductor, or small-gap semiconductor. Because the nanotube diameter lies in the nanometer range, electrons propagate only along the axis of the nanotube and their transport involves quantum effects. Thus, carbon nanotubes are sometimes referred to as one-dimensional conductors. The remarkable optical properties of carbon nanotubes include absorption, photoluminescence, and Raman scattering.[54,55,57−60] Moreover, carbon nanotubes possess excellent thermal and chemical stability. Owing to their large surface area, they can be readily functionalized; three different approaches are possible (see examples in Figure 4):[23,61] (i) covalent attachment of chemical groups through reactions on the $\pi$-conjugated skeleton of carbon nanotubes, (ii) noncovalent adsorption of various functional molecules, and (iii) endohedral filling of their inner empty cavity. Three main methods are used to produce carbon nanotubes,[57,60] such as electric arc-discharge (EAD), laser ablation (LAB), and chemical vapor deposition (CVD). EAD- and LAB-based synthetic procedures involve vaporization of graphite samples, whereas in the CVD-based method (exploited for commercial production of high-purity carbon nanotubes), carbon-containing vapor is passed over supported metal catalyst nanoparticles (nickel, cobalt, iron) in a furnace. Up to now, carbon nanotubes have been applied or proposed as attractive candidates in many fields of human activity including strength reinforcement elements in composites, components in energy and gas storage devices, building blocks in nanoelectronics (*e.g.*, transistors and logic, memory, and sensory devices), fillers in polymer matrixes, molecular tanks, and tools in medicine (*e.g.*, drug delivery

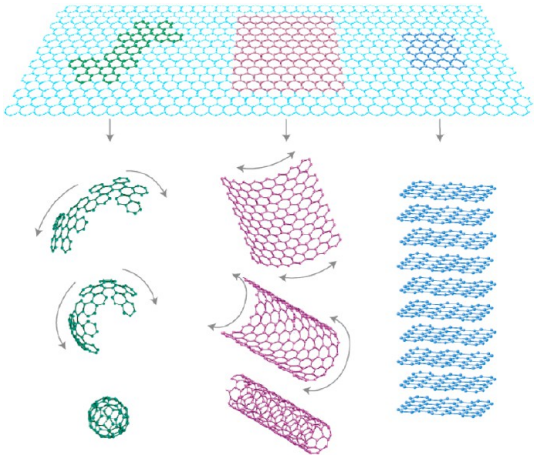

**Figure 5. Graphene as a building block of a fullerene, carbon nanotube, and graphite. Reprinted with permission from ref 66. Copyright 2007 Nature Publishing Group.**

carriers, components in gene delivery systems, and photothermal therapy).[57,60] Besides application-related areas, carbon nanotubes are widely considered a suitable model system for studying various quantum phenomena occurring in quasi-1D solids, such as single-electron charging,[62] ballistic transport,[63] weak localization,[64] and quantum interference.[65]

*Graphene.* Graphene (sometimes referred to as "the thinnest material in our universe"), a flat 2D planar monolayer of $sp^2$-bonded carbon atoms arranged in a two-dimensional hexagonal honeycomb lattice and first isolated in 2004,[8] constitutes another carbon allotrope that can be viewed as the building unit of 3D graphite (stacking of graphene sheets), 1D carbon nanotubes (rolling of a graphene sheet), or 0D fullerenes (wrapping of a graphene sheet) (see Figure 5).[66] In graphene, two equivalent carbon sublattices can be identified. There are three extremely strong $\sigma$ bonds connecting each carbon to its three nearest neighbors, giving rise to the mechanical stability of the sheet; each carbon atom has a $\pi$ orbital contributing to a delocalized network of electrons, which is responsible for its electron conductivity.[67−71] In order to maintain stability, the graphene layer contains "intrinsic" ripples with an amplitude of ~1 nm. The ripples can be induced externally to tune the local electrical and optical features of graphene to meet the requirements of a given application. Proper graphene behaves as a semimetal or zero-gap semiconductor. Besides this, graphene shows unique physical properties, including large values of intrinsic mobility (~200 000 $cm^2\ V^{-1}\ s^{-1}$), Young's modulus (~1 TPa), theoretical surface area (~2630 $m^2\ g^{-1}$), thermal conductivity (~5000 $Wm^{-1}\ K^{-1}$), and optical transmittance (~97.7%).[26,67−69] Moreover, in the field of physics, graphene has been used to study interesting physical phenomena, such as ambipolar field effects,[70,71] the quantum Hall effect at room temperature,[72] single-molecule adsorption events,[73] giant magnetoresistance,[74] DNA sequencing,[75,76] *etc.*

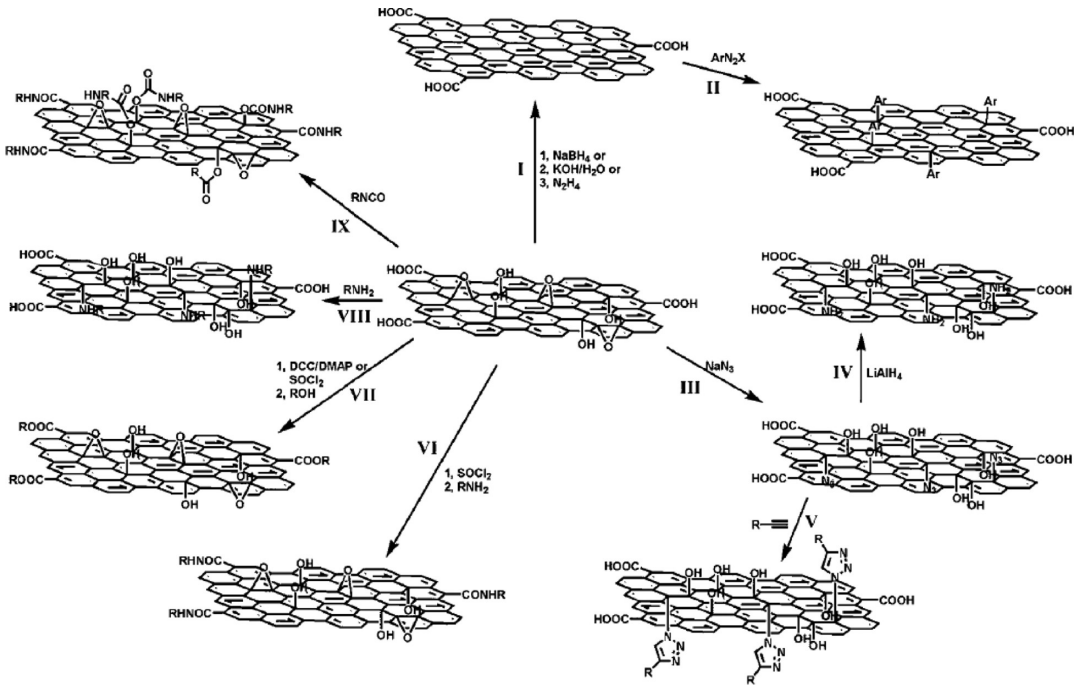


**Figure 6. Covalent functionalization of graphene or graphene oxide: I, reduction of graphene oxide into graphene employing various approaches; II, covalent functionalization of reduced graphene through diazonium reaction; III, functionalization of graphene oxide upon reaction of graphene oxide and sodium azide; IV, reduction of azide-functionalized graphene oxide toward amino-functionalized graphene oxide; V, functionalization of azide-functionalized graphene oxide; VI, functionalization of graphene oxide with alkyl chains; VII, esterification of graphene oxide; VIII, nucleophilic ring-opening reaction; IX, modification of graphene oxide with organic isocyanates. Reprinted with permission from ref 77. Copyright 2010 Royal Society of Chemistry.**

If the size of the graphene sheet is reduced below 100 nm in all dimensions, graphene quantum dots are formed that show physical phenomena governed by size and edge crystallography. Graphene can be prepared by mechanical exfoliation, epitaxial growth, chemical vapor deposition, and chemical exfoliation;[8−10,26,67−69] currently, mechanical exfoliation is considered the most convenient method for providing high-quality graphene samples. As in the case of carbon nanotubes, graphene (and graphene oxide) can be functionalized covalently (see examples in Figure 6) and/or noncovalently with various functional groups for secondary attachment of organic or inorganic compounds.[27,28,77] The covalent modification of graphene sheet involves formation of oxygenated species such as carboxyl, epoxy, and hydroxyl on the graphene surface generating graphene oxide; these oxygenated functional groups are then exploited for covalent attachment of other compounds.[77] On the other hand, noncovalent functionalization is based on van der Waals forces and/or $\pi-\pi$ stacking of aromatic molecules on the graphene sheet.[77] Owing to the superior properties of graphene and its derivatives,[27,78] a wide spectrum of applications has been proposed, including lightweight, thin, and flexible yet durable display screens,[79] field-effect ballistic transistors,[80−83] as an active component in electrochromic devices (in the form of graphene oxide),[84] transparent conducting electrodes in liquid-crystal displays,[85] organic photovoltaic cells,[86] organic light-emitting diodes,[87] components in optical modulators,[88] and conductive plates in ultracapacitors.[89] Besides exploitations in technical branches, graphene, graphene oxide, and graphene quantum dots have been shown to be promising candidates in various fields of medicine, including drug/gene delivery[90] and cancer therapy,[91] biosensing,[92−94] and bioimaging.[95] However, the practical introduction of graphene into composite materials is hampered by low production yields and product purity.

*Carbon Quantum Dots.* Recently, carbon quantum dots (or carbon nanoparticles) have attracted significant interest owing to their unique quantum size effects and strongly size-dependent electronic, optical, and electrochemical properties.[96] Carbon quantum dots are carbon nanocrystals with a size in all dimensions less than 10 nm and are composed of graphitic ($sp^2$) carbon. Besides many fascinating optical features such as photoluminescence tuned by dot size and surface functional groups (see Figure 7),[97−102] nonlinear optical response,[103] photoinduced electron transfer,[104] and electrochemiluminescence,[105] carbon quantum dots offer several advantages over heavy-metal-containing semiconductor-based quantum dots, including chemical inertness, biocompatibility, and low toxicity.[96] They can be prepared using both bottom-up and top-down approaches. The bottom-up preparation methods are based on using molecular precursors (*e.g.*, citric acid, glucose, resin), whereas the top-down synthesis

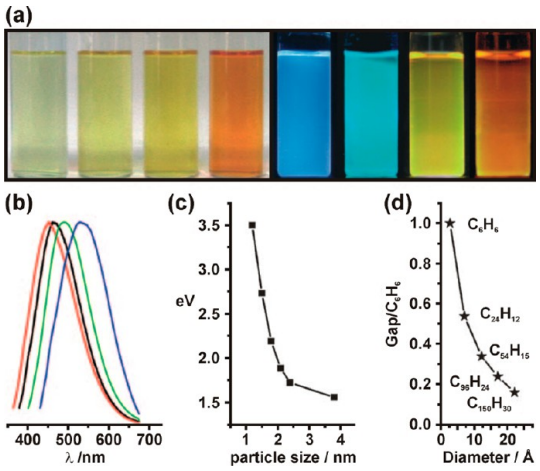


**Figure 7. Photoluminescence properties of carbon quantum dots: (a) differently sized carbon quantum dots illuminated under white (left) and UV light (right; 365 nm); (b) photoluminescence spectra of differently sized carbon quantum dots (red, black, green, and blue lines represent photoluminescence spectra of blue, green, yellow, and red emission carbon quantum dots, respectively); (c) dependence of photoluminescence properties of carbon quantum dots on their size; (d) relationship between HOMO−LUMO gap and the size of graphene fragments. Reprinted with permission from ref 97. Copyright 2010 Wiley-VCH.**

procedures start with larger carbon (nano)materials (*e.g.*, nanodiamonds, graphite, carbon nanotubes, carbon soots, activated carbon, graphene oxide). Carbon quantum dots and their functionalized analogues have been utilized mainly in medicine for diagnostic purposes (bioimaging and biosensing).[106,107]

**Iron-Oxide-Functionalized Carbon Nanotubes for Medical Applications and Water Treatment.** In general, a nanocomposite is a system composed of two or more phases, where at least one of the components has one, two, or three dimensions of less than 100 nm. Nanocomposite systems can be found in nature, or they can be prepared by a variety of synthetic procedures. The reason for combining two or more phases together is that a nanomaterial can be produced with interesting properties stemming from the components involved. In other words, due to synergy, nanocomposite materials show desirable combinations of physicochemical properties that are not found in the individual components. The resulting nanocomposite may then exhibit a multifunctional character with several modes of action simultaneously.

It is known that the properties of carbon nanotubes can be improved or tuned by chemical modification to meet the requirements of a given application.[23,108,109] Hence, to increase the application potential of carbon nanotubes, it is necessary to modify them with relevant functional groups and/or nanoparticles in order to integrate them into desired structures or attach suitable nano-objects. It has been shown that decoration of carbon nanotubes with compounds of different chemical nature can improve their dispersity in solvents[110] and/or provide them with new optical, electrical, and magnetic properties.[111−114] As they have small size, large surface-area-to-volume ratio, a layered structure, and high chemical stability, carbon nanotubes are frequently used as a supporting material for transition metal nanoparticles acting as catalysts, increasing their distribution and thus catalytic efficiency of the carbon nanotube−metal nanoparticle nanocomposite.[115] In addition, because of their well-defined tubular morphology (hollow cavities) and high aspect ratio, carbon nanotubes can be used as templates for the preparation of other nano-objects or as nanosized reaction vessels.[116−118] Recently, it has been shown that chemical reactions, especially their course and final phase composition of products, can proceed in a confined space (*i.e.*, within the nanochannels of carbon nanotubes) in a manner significantly different than that observed in a size-unrestricted environment.[119−122] In addition, the confinement can modify the structure and physicochemical properties of the nanomaterials grown inside the channels of carbon nanotubes. In particular, the redox properties of substances confined inside the carbon nanotubes can easily be modified, yielding hybrids appealing for many catalytic reactions that highly depend on the redox state of the active components.[121,122] Moreover, theoretical studies have predicted that deviation of the graphene layers from planarity induces the $\pi$-electron density to shift from the concave inner surface to the convex outer surface, resulting in an electron-deficient interior surface and an electron-enriched exterior surface of the carbon nanotubes.[123,124] Hence, a substance in contact with either surface may show altered structural and electronic properties depending on the type and degree of its attachment.

Carbon nanotubes, no matter whether single-walled or multiwalled of nature, are diamagnetic[125] (with a very weak field-induced magnetization having an opposite orientation with respect to the direction of the applied magnetic field), which precludes their use in any magnetism-based applications. However, once functionalized with magnetic nanoparticles, they can be used in various applications, such as for components in magnetic data storage devices,[126] toners and inks for xerography,[127] contrast agents in magnetic resonance imaging,[128] magnetic composites for drug delivery,[129] ferrofluids,[130] materials absorbing in the microwave domain of the electromagnetic spectrum,[131] optical transducers designed for wearable electronics,[132,133] advanced catalysts and sensors controllable and separable by external magnetic fields,[134] magnetically separable adsorbents for removing various inorganic and organic pollutants from aqueous solutions, *etc.* (see below for detailed discussion of applications of carbon nanotube/iron oxide-based hybrids).[135−144]

There are two possible approaches for decorating carbon nanotubes with magnetic nanoparticles: (i)

attaching them to the exterior surface of carbon nanotubes or (ii) placing them inside the channels of carbon nanotubes. Modification of the exterior surface of carbon nanotubes can be achieved in two ways, that is, by covalent attachment of chemical groups stemming from a suitable compound covering the nanoparticle surface through reactions onto a $\pi$-conjugated skeleton of carbon nanotubes and/or by noncovalent adsorption or polymer-mediated wrapping of various functional groups from the substance covalently or noncovalently bound to the surface of a nanoparticle.[23] To place nanoparticles inside carbon nanotubes, two strategies are often used which differ in the number of preparation steps:[145−149] (i) to cut the end of carbon nanotubes and fill them with liquid-containing precursors for formation of metal and/or metal oxide nanoparticles (a two-step process) or (ii) to grow metal and/or metal oxide nanoparticles simultaneously with evolution of the carbon nanotube skeleton (a one-step process).

*Filling the Carbon Nanotubes with Magnetic Nanoparticles.* In order to prepare nanoparticle-filled carbon nanotubes, the phenomenon of spontaneous penetration of fluids (*i.e.*, molten substances containing precursors for formation of metal and/or metal oxide nanoparticles) into wettable capillaries is frequently employed.[123,150] There are two factors determining the degree of nanotube filling, that is, the surface tension of the fluid[151] and the contact angle between the pore walls and the fluid.[122] It is known that carbon nanotubes are wettable for liquids if their surface tension is below 100−200 mN/m.[152] However, in the early stage of this method, a few drawbacks have been reported including hardly controllable opening of the nanotube ends, low filling efficiency (low level of filling), presence of knars inside the carbon nanotubes, reactions with carbon due to high melting points of metal sources, formation of admixtures of iron and carbon (*e.g.*, $Fe_3C$), *etc.*[153] Improvements of the filling method have been suggested, such as the use of template to aid growth of the carbon nanotubes. It has been shown that if carbon nanotubes are synthesized within the pores of an alumina (aluminum oxide) template (by a method of noncatalytic chemical vapor deposition), we get nanotubes with open ends and free of catalyst particles (see Figure 8).[117,133] Such prepared nanotubes can be easily filled with suspensions of functional nanoparticles and then separated from the alumina membrane (see Figure 9).[133] This strategy provides, among others, to load carbon nanotubes with nanoparticles in large amounts. The magnetic properties of carbon nanotubes filled with magnetic nanoparticles depend on the amount and the way they are organized inside the nanotubes. However, it is generally difficult to control the distribution of magnetic nanoparticles inside the channels of carbon nanotubes, resulting in undesired agglomeration driven by strong interparticle

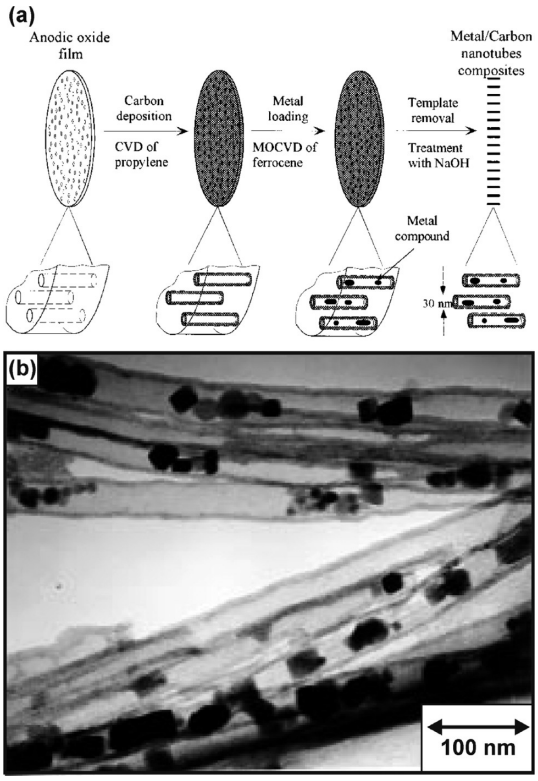


**Figure 8. (a) Scheme of the preparation of carbon nanotubes with open ends. (b) Transmission electron microscopy (TEM) image demonstrating inclusion of iron oxide nanoparticles inside carbon nanotubes. Reprinted from ref 117. Copyright 1998 American Chemical Society.**

magnetic interactions. Sometimes, to improve the magnetic properties of the magnetic nanoparticle-filled carbon nanotubes, an external magnetic field is applied during the synthesis as it affects the magnetic anisotropy of the formed hybrid.[133] In addition, an external magnetic field may assist the penetration of magnetic nanoparticles into the nanotube channels by overcoming possible opposing forces (*e.g.*, friction with the nanotube walls). For nanotubes with very small diameter, it is believed that the filling process is predominantly driven by capillary forces with almost negligible effect of the external magnetic field.

The methods used to prepare carbon nanotubes filled with magnetic nanoparticles include the arc-discharge evaporation technique,[154] capillary action-based technique,[150] wet chemical method,[155] template carbonization method,[117] spray pyrolysis,[145] catalyzed hydrocarbon pyrolysis,[156] condensed phase electrolysis,[157] *etc.* In principle, wet chemical approaches are considered the most simple and versatile methods for catalysis in terms of applicability to most metals. It has been shown that shortening the carbon nanotubes reduces the transport resistance associated with filling the nanotube channels with solutions of precursors for formation of iron oxide nanoparticles.[122] Nanotube shortening can be achieved by, for example, a controlled oxidation process catalyzed by

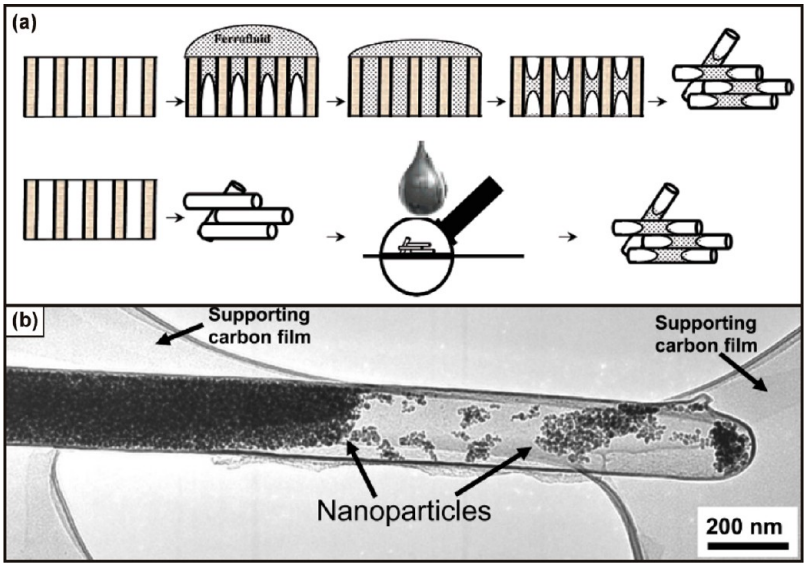


**Figure 9. (a) Strategy for filling carbon nanotubes with magnetic nanoparticles. (b) TEM image showing iron oxide nanoparticles inside carbon nanotubes. Reprinted from ref 133. Copyright 2005 American Chemical Society.**

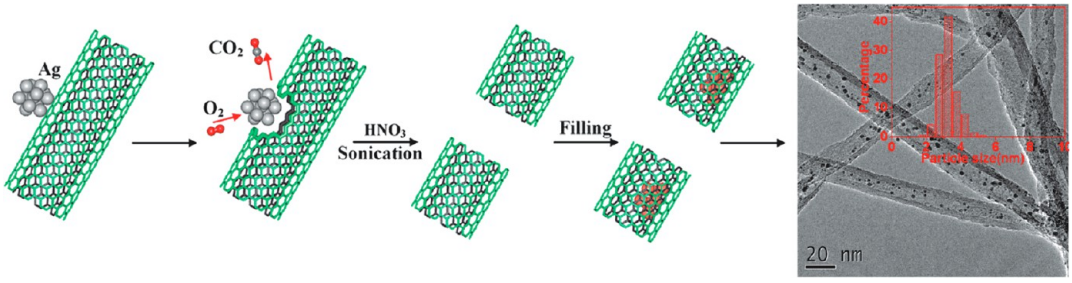


**Figure 10. Procedure for cutting carbon nanotubes and filling them with magnetic nanoparticles. The inset shows their particle size distribution inside the carbon nanotubes. Reprinted from ref 122. Copyright 2011 American Chemical Society.**

Ag nanoparticles (see Figure 10).[122] In addition, it has been suggested that ultrasonic treatment and stirring may expel air from the nanotube cavity, making it easier for the precursor-containing fluid to enter the nanotube channels.[122] Alternatively, the nanotube channels can be filled with iron oxide precursors in a vapor state. This is usually achieved by employing the metal−organic chemical vapor deposition (MOCVD) technique.[117] It has been identified that the pressure of the vapor and MOCVD temperature and time period greatly influence the size and number of iron oxide nanoparticles formed inside the carbon nanotube.

The most frequently used precursors for iron oxide nanoparticle synthesis include iron(III) nitrate ($Fe(NO_3)_3$),[121,158,159] iron pentacarbonyl ($Fe(CO)_5$),[160] ferrocene ($Fe(C_5H_5)_2$),[117,145,146,161−163] ferrocene−$Fe_3(CO)_{12}$ mixture,[145] and the Fe−urea coordination complex ($Fe[(NH_2)_2CO]_6(NO_3)_3$).[145] In most cases, iron nanoparticles are formed in the first step; these iron nanoparticles are then subjected to oxidation to obtain iron oxide phases ($Fe_3O_4$ or $\gamma$-$Fe_2O_3$). Before filling the nanotubes with iron precursors, it is advisible to wash them to remove any catalyst that could give rise to formation of unwanted phases, degrading the properties of the hybrid.

Besides the strategy to fill nanotubes with a ferrofluid or iron oxide precursor in solution, prepared in a separate step, magnetic nanoparticle-loaded nanotubes can be synthesized in a single step when the nanotube skeleton and magnetic nanoparticles are formed simultaneously (*i.e.*, *in situ* synthesis). In such cases, the suitably chosen precursor (*e.g.*, ferrocene) acts as a source for both the carbon nanotubes and iron and/or iron oxide nanoparticles.[145]

*Decorating the Exterior Surface of Carbon Nanotubes with Magnetic Nanoparticles.* As it turns out, filling carbon nanotubes with nano-objects is not such a trivial process as a series of problems must be overcome to obtain a hybrid with the required chemical composition and properties. Thus, another approach to functionalize carbon nanotubes has been suggested based on modification of their outer surfaces.[23,108,109] It is well-known that the convex surface of carbon nanotubes can be used to transfer mass or ions, support host compounds (*e.g.*, organic small molecules, complexes, surfactants, macromolecules, metals,

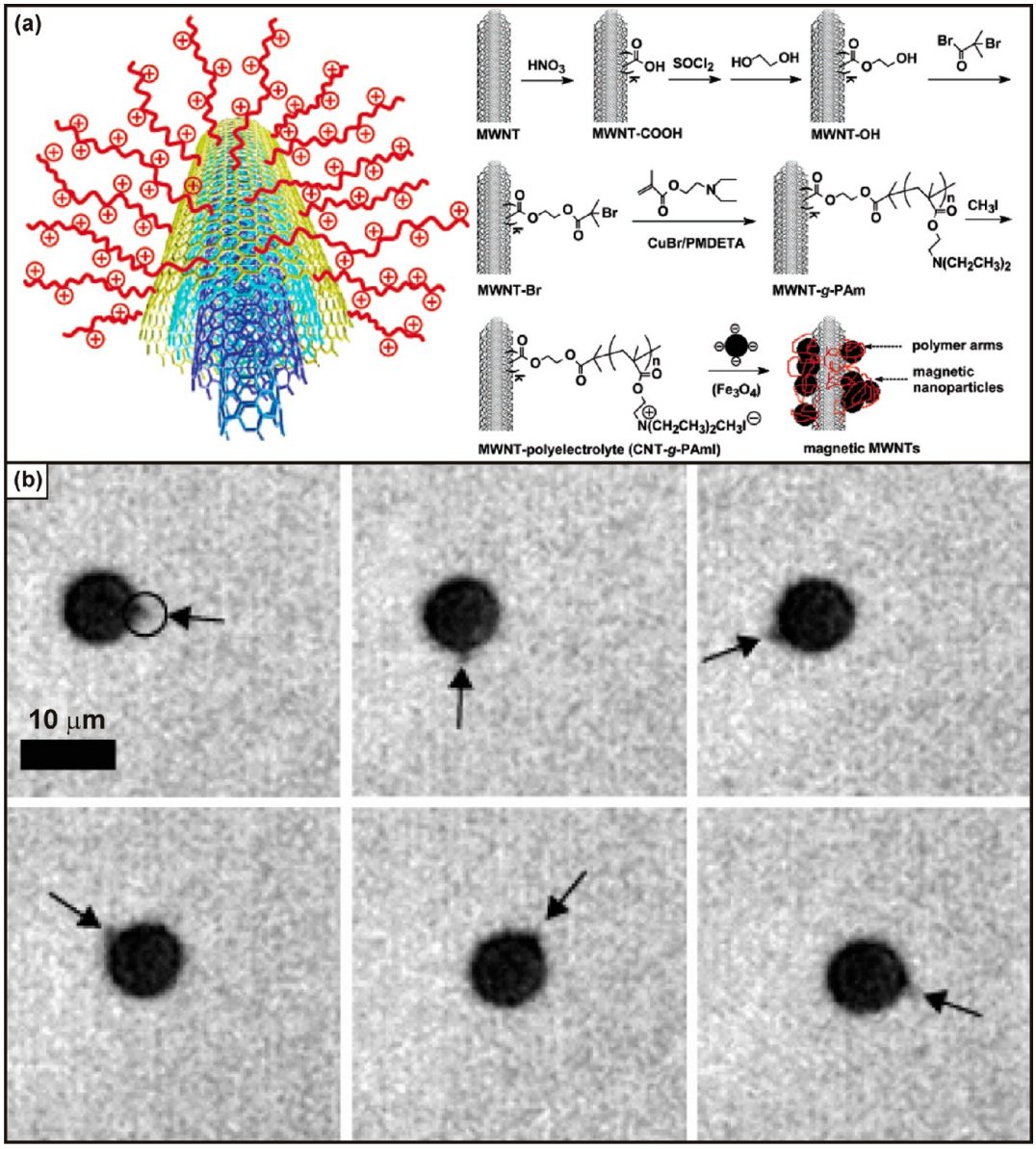


**Figure 11. (a) Cartoon of cationic multiarm multiwalled carbon-nanotube-based "nanocatcher" and scheme of synthetic steps towards polyelectrolyte-grafted multiwalled carbon nanotubes functionalized with anionic $Fe_3O_4$ nanoparticles (MWNT = multiwalled carbon nanotube, MWNT-*g*-PAm = polyamine-grafted multiwalled carbon nanotube, MWNT-*g*-PAmI = polyelectrolyte-grafted multiwalled carbon nanotube). (b) TEM images showing manipulation of sheep red blood cells with magnetic hybrids attached to the cell (magnetic nanotubes are indicated by black arrow; the frequency and intensity of the magnetic field used were 0.5 Hz and 12.7 A/m, respectively). Reprinted from ref 153. Copyright 2006 American Chemical Society.**

oxides, and quantum dots), and act as a substrate. In general, the attachment of nanoparticles on the exterior surface of carbon nanotubes can be realized in two ways:[164−172] by direct or indirect connection. In the case of direct linkage, the large surface area of both carbon nanotubes and nanoparticles promotes physical adsorption, establishing noncovalent interaction between the two counterparts holding them together. Another possibility involves charging the surface of a nanoparticle and carbon nanotube with an opposite charge; the binding then occurs by evolution of electrostatic interactions between the nanocomposite components.[134,153] For an indirect connection, a compound and/or functional group (*e.g.*, −OH, −COOH) mediating a bond between the nanoparticle and carbon nanotube is required. In such a strategy, the surfaces of either nanoparticles or carbon nanotubes or both of them are functionalized with suitable substances favoring the formation of a link, particularly of covalent nature. It has been reported that if the connection between the carbon nanotube and the surface-modifying substance (*e.g.*, pyrene) exploits the $\pi-\pi$ stacking interactions[173] the attachment is weak and may get weaker due to the weight of nanoparticles. Regardless of the strategy, the loading capability mainly depends on the available surface

which is generally much larger for single-walled carbon nanotubes than for multiwalled counterparts. Alternatively, the guest compounds can be attached to the nanotube outer surface by chemical vapor deposition.[174]

The examples of loading of iron oxide nanoparticles on the exterior surface of nanotubes are shown in Figures 11−15. The synthetic procedure toward magnetic multiwalled carbon nanotubes, depicted in Figure 11a, involves two stages:[153] (i) covalent grafting of cationic polymeric chains onto the surface of the multiwalled carbon nanotubes forming nanocatchers (see Figure 11a), and (ii) attachment of iron oxide nanoparticles to the polyelectrolyte-coated multiwalled carbon nanotubes. First step involves oxidation of multiwalled carbon nanotubes using fuming $HNO_3$ followed by reaction with thionyl chloride and glycol to produce the ester. Transformation of this group into 2-bromodimethylpropionyl residue constitutes the key step for further polymerization with diethylaminoethyl methacrylate. Reaction with methyl iodine provides the positively charged dimethylamino groups which can then electrostatically react with anionic $Fe_3O_4$ nanoparticles. The prepared nanocomposite was successfully tested for biomanipulation purposes as shown in Figure 11b.

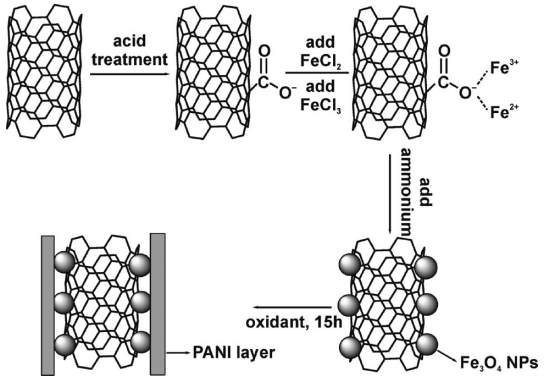


**Figure 12. Schematic representation of the preparation steps toward the carbon nanotube/$Fe_3O_4$/PANI hybrid (NPs = nanoparticles). Reprinted with permission from ref 175. Copyright 2008 Elsevier B. V.**

Figure 12 shows an alternative synthetic process toward assembly of functionalized carbon nanotubes decorated with both $Fe_3O_4$ nanoparticles and polyaniline molecules.[175] The first step involves oxidation of carbon nanotubes in strong acid followed by *in situ* synthesis of $Fe_3O_4$ under basic conditions ($NH_3$) and in nitrogen atmosphere. Further functionalization was obtained by adding aniline under mild oxidative condition ($FeCl_3$) after 15 h at low temperature (0−5 °C).

The synthetic steps needed for the preparation of PEG-grafted carbon nanotubes functionalized further with magnetic iron oxide/silica nanoparticles are presented in Figure 13.[171] First step uses a mixture of nitric and sulfuric acid followed by silanization using $SiCl_4$ in basic conditions. This precursor can be used to produce PEG-functionalized carbon nanotubes by reaction with the silane moieties that can be used to assemble magnetic heterosystems by interaction with the preformed core−shell $Fe_3O_4/SiO_2$ nanoparticles.

A sophisticated way to covalently attach iron oxide nanoparticles on the exterior surface of carbon nanotubes is shown in Figure 14.[168] The synthesis of the carbon nanotube/iron oxide hybrid involves oxidation of the carbon nanotube surface under strong acid conditions followed by some dehydration to afford alcoholic residues (−OH) due to high-temperature heating (1 h, 120 °C) within the reaction. Activation of the acid group of the poly(acrylic acid) (PAA) with *N*,*N*′-dicyclohexylcarbodiimide (DCC) and 4-dimethylaminopyridine (DMAP) allows formation of an ester group in which PAA becomes directly attached to the surface of the carbon nanotubes. The free carboxylate residues of PAA were then reacted with amino-functionalized $Fe_3O_4$ nanoparticles, and amide bonds were formed, affording carbon nanotube/$Fe_3O_4$ nanocomposites.

A simple procedure toward carbon nanotube/iron oxide hybrids is depicted in Figure 15.[172] First, carbon nanotubes were reacted under mild conditions (60 °C)

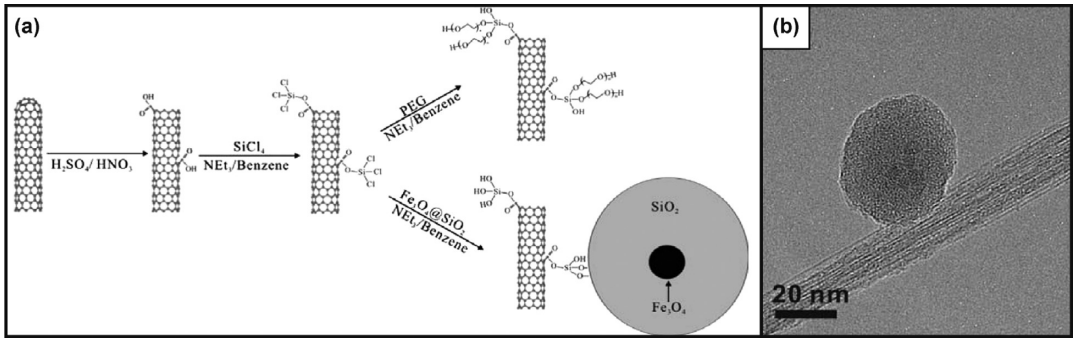


**Figure 13. (a) Scheme of reaction pathway toward PEG-grafted carbon nanotubes with possible further functionalization by magnetic iron oxide silica nanoparticles. (b) Representative TEM image of the carbon nanotube/$Fe_3O_4/SiO_2$ nanoparticle hybrid ($Fe_3O_4$ nanoparticles encapsulated within silica sphere with a diameter of ~35 nm). Reprinted with permission from ref 171. Copyright 2009 Elsevier B. V.**

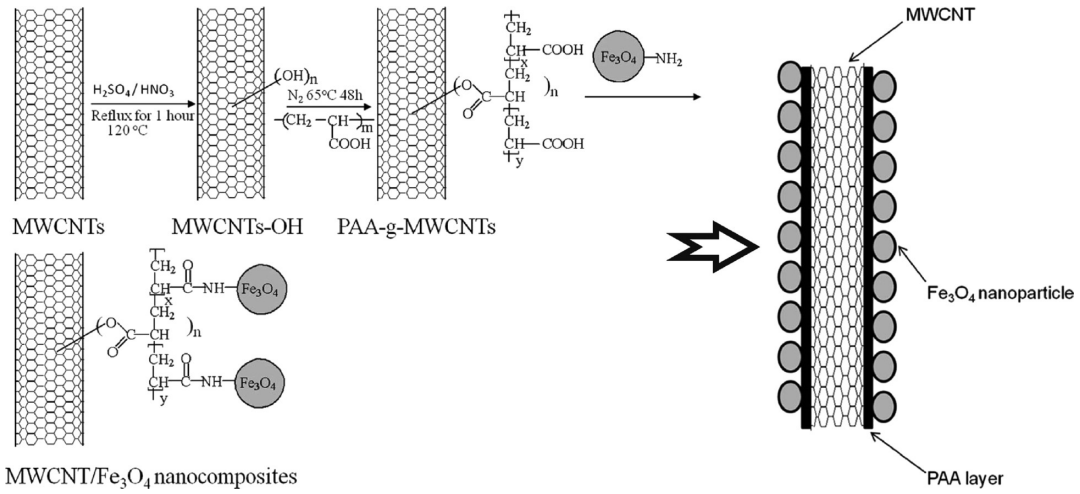


**Figure 14. Scheme describing the synthetic protocol toward magnetic carbon nanotube/$Fe_3O_4$ nanocomposites (MWCNT = multiwalled carbon nanotube, PAA-*g*-MWCNT = poly(acrylic acid) (PAA)-grafted multiwalled carbon nanotube). Reprinted with permission from ref 168. Copyright 2010 Wiley Periodicals, Inc.**

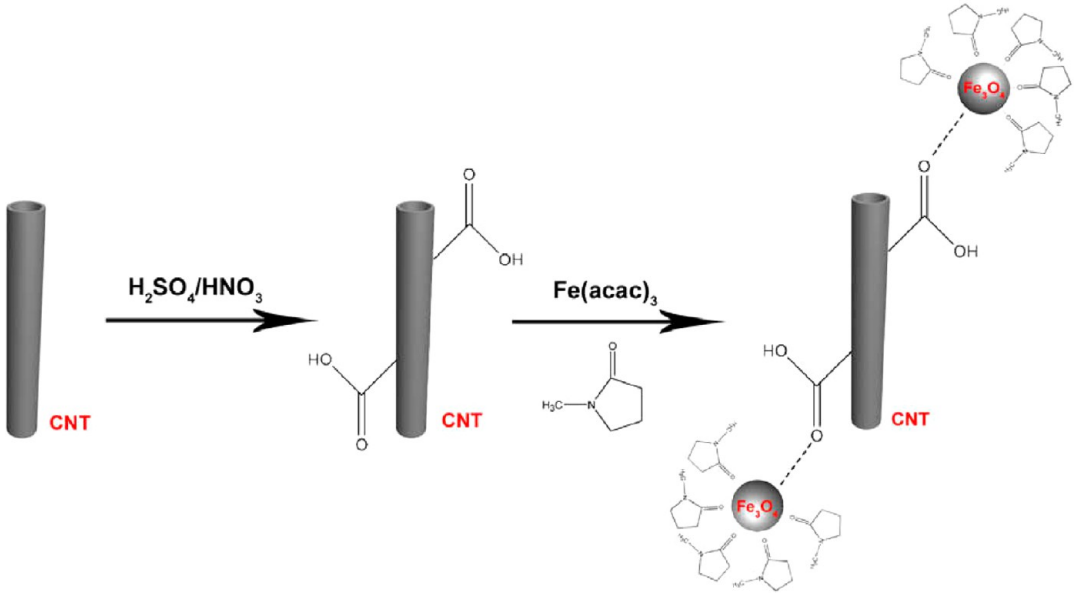


**Figure 15. Scheme of preparation steps toward carbon nanotube/iron oxide hybrids employing *N*-methylpyrrolidone as a capping agent (CNT = carbon nanotube). Reprinted with permission from ref 172. Copyright 2009 Elsevier B. V.**

with strong acid mixture ($H_2SO_4$/$HNO_3$) to promote formation of acid groups on the exterior wall of carbon nanotubes. Then, the oxidized intermediate was reacted *in situ* with ferric acetylacetonate (Fe(acac)$_3$) using *N*-methylpyrrolidone as the nanoparticle's capping agent to give the carbon nanotube/iron oxide assembly.

*Overview of Applications of Carbon Nanotube/Iron Oxide Hybrids.* As already briefly outlined above, carbon nanotubes functionalized with magnetic iron oxide nanoparticles have been used in various applications in the biomedical, environmental, electronics, and other fields. The utilization of the inherent physical properties of the carbon nanotubes can be tuned when using magnetic carbon nanotube composite materials as the carbon nanotubes can be aligned by application of an external magnetic field.[126,133,176] It is believed that owing to the magnetic alignment in these composite materials they can then be applied in filters, wearable electronics, changeable diffraction gratings, data storage, memory devices, polarizers, *etc*. Additionally, the alignment of magnetic carbon nanotube additives in the matrix of other materials can enhance the properties of these materials. This has been shown for polymers, where an increase in the mechanical strength and conductivity has been demonstrated by adding magnetic carbon nanotubes.[177,178] Kim and colleagues[177] showed that the orientation of the carbon nanotubes in the polymer matrix can affect the conductivity of the polymer in

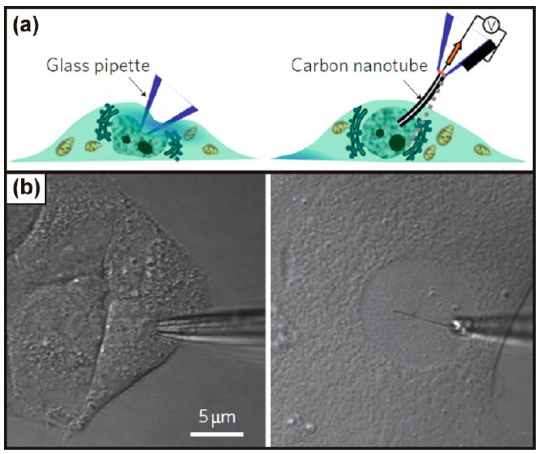


Figure 16. Comparison between cellular endoscopes and glass pipettes. (a) Scheme showing a conventional glass pipet (left) and a nanotube endoscope (right). (b) HeLa cell (left) being injected by a 1 mm commercial glass pipet, and a primary rat hepatocyte nucleus (right) being interrogated by a 100 nm nanotube endoscope. Reprinted with permission from ref 181. Copyright 2011 Macmillan Publishers Limited.

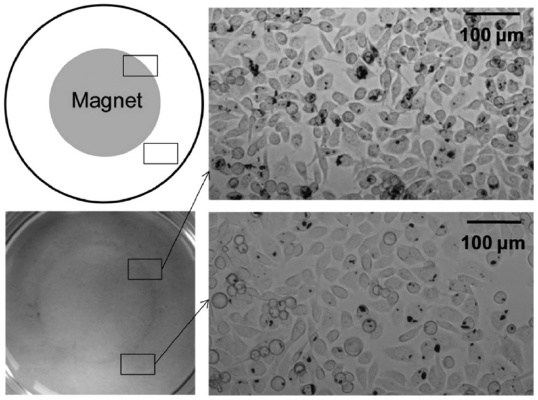


Figure 17. Magnetically based modulation of the uptake of carbon nanotube/iron oxide hybrids by the PC3 tumor cells (the cells incubated with 10 mg $mL^{-1}$ of magnetic carbon nanotubes for 20 h in the presence of a magnet placed underneath the culture dish). The magnetic hybrids were attracted to the area with the highest magnetic gradient at the periphery of the magnet, resulting in a higher cellular uptake (top) compared to the regions outside the magnet (bottom). Reprinted with permission from ref 186. Copyright 2013 Royal Society of Chemistry.

different directions, with a higher conductivity in directions parallel to the external magnetic field. Recently, Cava *et al.*[179] prepared iron-oxide-filled carbon nanotubes and tested them successfully as functional components in resistive memory devices. It was demonstrated that the electronic properties of these hybrids are governed by hopping charge transfer phenomena that occur both between the nanotube shells and between the iron oxide filling and the nanotube. Along with iron oxide oxygen migration, these processes promote bipolar resistive switching between the two different electronic states. Thus, if an external electric field is applied in different directions, the hybrid is still found in the same electronic conditions unless the space charge at the filling changes its polarization.

Some of the most interesting applications of carbon nanotube/iron oxide composite materials come from the biomedical field. Works by Freedman *et al.*[180] and Singhal *et al.*[181] have shown that a magnetic carbon-nanotube-tipped pipet can be used to transfer liquid into and within a single cell, as well as for fluorescence and electrochemical probing of the cell (see Figure 16). Interestingly, the use of this carbon-nanotube-based cellular endoscope allows for the magnetic relocation of the tip in the cell by application of a magnetic field. This provides far more precise probing of the cell than can be achieved when using normal techniques.

Since the report by Syljukić and colleagues[182] showed that the assumed hydrogen peroxide detection ability of carbon nanotubes is actually due to iron oxide nanoparticles, there has been an increase in the use of the carbon nanotube/iron oxide composites as sensors. These magnetic carbon-nanotube-based materials have now been applied as electrochemical biosensors (paracetemol,[183] glucose,[184] and dopamine[134]) and gas sensors[162] by taking advantage of the inherent conductivity of carbon nanotubes.

The magnetic properties of these composites have allowed them to be applied as contrast agents in MRI diagnostic techniques[185,186] (see Figure 17) as well as in magnetic field directed fluorescence and surface-enhanced Raman spectroscopy cell imaging.[187,188] Interestingly, Lu and co-workers[189] have shown that by directing the magnetic carbon nanotube/doxorubicin composite with an external magnetic field, chemotherapeutic drugs can be delivered directly to cancer cells. Additionally, the magnetic carbon nanotube/doxorubicin composite displayed an enhanced cytoxicity toward cancer cells, indicating the unique application of these types of drugs.

Carbon nanotube/iron-oxide-based nanocomposites have also been used in water purification as adsorbents. The benefit of these types of adsorbents is that they are easily influenced by external magnetic forces. As such, separation of the adsorbents with adsorbed pollutants from the clean water is easier than in other purification methods. It has been shown that these materials can successfully remove inorganic [Ni(II),[190] Sr(II),[190] Cr(III) (see Figure 18),[191] Eu(III),[142] As(III),[192] As(IV),[192] Pb(II),[193] *etc.*] as well as organic pollutants (methylene blue,[194] neutral red,[194] 1-napthol,[193] brilliant cresyl blue,[143] *etc.*) from contaminated water. Normally, the adsorption capacity of the nanocomposite is larger than that of the unmodified carbon nanotubes due to additional surface area brought by iron oxide nanoparticles. Remarkably, in some circumstances (pH, ionic strength), the adsorption capacity of the nanocomposite material is larger than the sum of the separate components.[190] Other novel and

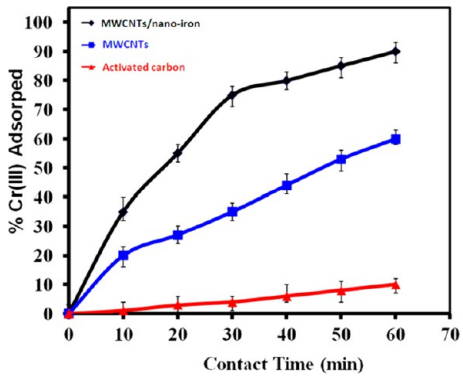


**Figure 18. Dependence of the contact time on the amount of Cr(III) adsorbed on different adsorbents (conditions: initial chromium concentration = 20 ppm; dosage of adsorbent = 50 mg; pH = 6; agitation speed = 150 rpm). The carbon nanotube/iron oxide nanocomposite shows a higher adsorption capability due additional adsorbing sites provided by the oxygen atoms of iron oxide nanoparticles. Reprinted with permission from ref 191. Copyright 2011 Elsevier Ltd.**

appealing applications of magnetic carbon nanotubes include catalysis,[195,196] magnetorheological fluids,[197] and chromatography in a single carbon nanotube.[198]

**Composites of Graphene and Graphene Oxide with Iron Oxides in Energy Storage, Medical, Sensing, Catalytic, and Environmental Applications.** Currently, graphene is one of the most studied nanomaterials because of its remarkable and application-appealing physicochemical properties. However, pristine graphene is nonmagnetic unless other nonmagnetic atoms (*e.g.*, fluorine) are added or some carbon atoms are removed, forming vacancies.[29] In order to create magnetic graphene, defects (*e.g.*, defects at the edges, introduction of foreign nonmagnetic atoms or vacancies) must be located far away from each other and their concentration should be relatively low to avoid cancelation of their magnetic behavior and/or graphene disintegration.[29] It has been reported that inhomogeneity of the graphene surface hinders the establishment of long-range ferromagnetic ordering between unpaired spins. Thus, only small regions in graphene show a magnetic response, often of superparamagnetic nature, making it impossible to identify the type of magnetic order (*i.e.*, ferromagnetic, antiferromagnetic, or ferrimagnetic alignment).[199] Moreover, the magnetic signal of these localized domains is often very small and hardly detectable. If graphene could be made magnetic in a controllable manner, it would open doorways for its use in various spintronic applications based on magnetic semiconductors.

To endow graphene with magnetic properties (*e.g.*, superparamagnetism, strong magnetic response under small applied magnetic fields[200]), the graphene surface can be decorated with magnetic nanoparticles of transition metal oxides, most frequently, iron oxides.[27] Both theoretical and experimental studies have demonstrated that incorporation of magnetic nanoparticles on graphene not only introduces interesting magnetic properties but can also be used to tune the surface morphology, electronic structure, and other intrinsic characteristics of graphene.[201−204] More specifically, the intrinsic properties of graphene can be altered by fine control of the surface coverage and distribution of the nanoparticles over the graphene surface. In addition, nanoparticles, both magnetic and nonmagnetic, are believed to act as stabilizers, preventing the aggregation of individual graphene sheets due to the strong van der Waals interactions between the graphene layers.[205] In this way, the unique properties of graphene sheets can be maintained even in a dry state.[206] On the other hand, the graphene structure, acting as a substrate, may have a positive impact on the growth mechanism of magnetic hybrid components, yielding nano-objects with well-defined size, particle size distribution, shape, and form (*e.g.*, iron oxide nanosheets).[207] As such, the nanocomposite's magnetic properties are significantly distinct from those exhibited by nanoparticle assemblies prepared without a graphene template.

In particular, graphene/iron oxide nanocomposites have been proposed to be promising candidates in a variety of fields, including biomedicine (especially in biodiagnostics),[208−210] catalysis,[211,212] magnetic and electric energy storage (*e.g.*, electrode materials in supercapacitors),[89,213−215] and water treatment and soil remediation.[216,217] In biomedical fields concerned with the transport of drugs to desired sites in living organisms, these hybrids have been suggested to work very effectively as drug carriers due to their large surface areas, stability for the adsorption of biomolecules, and capability to control their motion inside the bloodstream by applying an external magnetic field.[218] Recently, iron oxide nanoparticles as anode materials for lithium-ion batteries were found to show improved performance once incorporated on the surface of graphene sheets (see below for detailed discussion of applications of graphene/iron oxide-based hybrids).[219−222]

In general, nanoparticles can be attached to the surface of graphene in two ways:[27,223−227] covalent linkage and physical adsorption. Physical adsorption is driven, in most cases, by van der Waals forces, resulting in weak interactions between the nanoparticles and graphene which can be destroyed if the nanocomposite is exposed to an unfavorable environment. In addition, the physical adsorption process is difficult to control and can lead to aggregation of nanoparticles on the surface of graphene, significantly decreasing the surface area of the nanocomposite and, in the case of magnetic nanoparticles, negatively affecting the magnetic properties of the hybrid due to evolution of magnetic interparticle interactions of both dipole−dipole and exchange type. On the other hand, the establishment of covalent bonds between

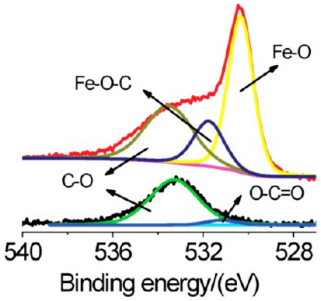


**Figure 19. Representative O 1s X-ray photoelectron spectra of the pure graphene nanosheets and graphene/iron oxide nanocomposite showing positioning of Fe−O−C (∼532 eV) bonds. The presence of Fe−C bonds is signaled by a peak at ∼707.5 eV in the Fe 2p X-ray photoelectron spectrum. Reprinted with permission from ref 232. Copyright 2011 Royal Society of Chemistry.**

nanoparticles and a graphene sheet promotes a much stronger interaction accompanied by significant modification of the geometric and electronic structure of graphene due to $sp^2$-to-$sp^3$ hybridization change. The covalent linkage can be either direct or indirect in nature. To establish a covalent link indirectly, a surfactant, such as an organic compound or a polymer-containing functional group (*i.e.*, organic molecular chains in most cases), is used as a mediator of the bond between the magnetic nanoparticles and the graphene surface. In this approach, the surface of either the magnetic nanoparticles or graphene is functionalized with a suitable organic compound, resulting in a hybrid assembly where both components may affect each other *via* the organic linker. In order to achieve strong covalent coupling, magnetic nanoparticles must be attached directly to the graphene surface. It is assumed that two types of bonds can develop between the two components: (i) Fe−O−C bonds[228,229] (see Figure 19) and (ii) a direct Fe−C bond.[230−232] If a covalent strategy is adopted, magnetic nanoparticles are homogeneously distributed over the graphene surface, avoiding thus formation of nanoparticle aggregates.

In the case of physical adsorption,[227] the synthetic protocol involves simple mixing of graphene and iron oxide nanoparticles prepared separately. However, several other methods to prepare graphene/iron oxide nanocomposites have been reported in the literature. Generally, they are divided according to the complexity of the synthesis and number of reaction steps. Most of the early preparation routes toward graphene/iron oxide covalently linked hybrids generally require three steps:[203,204,232,233] (i) synthesis of graphene by reduction of graphite oxide and/or graphene oxide, (ii) surface modification of graphene by a suitable organic compound or polymer (*e.g.*, poly(sodium 4-styrenesulfonate), 4-aminophenoxyphthalonitrile) to provide chemical groups for attaching iron oxide nanoparticles, and (iii) preparation of iron oxide nanoparticles, either surface chemically modified or not, and then mixing them with surface-functionalized graphene. However, multistep synthetic procedures are often time-consuming and difficult to control, resulting in hybrids with random and inhomogeneous coverage of the graphene surface by iron oxide nanoparticles. Additionally, in these reactions, a significant fraction of graphene sheets are not coated with iron oxide nanoparticles as they are stacked together due to van der Waals interactions. Thus, one-step syntheses are favored as both nanocomposite components are formed *in situ*; the reaction can more easily be optimized (*e.g.*, the size of nanoparticles, the degree and uniformity of nanoparticle distribution over the graphene surface), and the physicochemical properties of the hybrids can be readily tuned with regard to the specific application requirements.[221,234,235] The techniques employed to prepare graphene/iron oxide hybrids often involve either solvothermal or hydrothermal methods or traditional chemical vapor deposition technique.[208,221,236]

The synthesis of maghemite/graphene composites has been shown to proceed through solution deposition of an Fe(III) salt[237] or Fe(II) complexes[238] onto graphene oxide. This deposited material is then calcined or dried under an open atmosphere to promote the formation of maghemite ($\gamma$-$Fe_2O_3$). An alternative method to decorate graphene sheets using maghemite is to deposit preformed nanoparticles on exfoliated graphene oxide and followed by subsequent reduction of the graphene oxide.[239]

The most common synthetic routes for the formation of magnetite/graphene involve the simple chemical reduction of $Fe^{3+}$/$Fe^{2+}$ ions in the presence of graphene oxide in solution as has been shown by Chandra *et al.*[240] The other method involves the reduction of Fe(III) ions in the presence of graphene oxide.[207,241] Alternatively, Li *et al.*[242] showed that a magnetite/graphene oxide composite can be synthesized by the simple solution phase mixing of graphene oxide in the presence of preformed magnetite nanoparticles. In a report by Guo *et al.*,[243] it was suggested that both magnetic iron oxides form when an $Fe^{3+}$ salt is reduced in the presence of graphene oxide. In this study, the authors showed that lepidocrocite ($\gamma$-FeOOH) is formed during the reduction process. As it is known that lepidocrocite can be transformed to either maghemite and/or magnetite, this assumption is not unreasonable.[244]

As it turns out, graphene oxide, produced by oxidative exfoliation of graphite, is most frequently used as a graphene precursor because of its low cost and massive scalability.[245] More importantly, graphene oxide has a variety of oxygen-containing functional groups on its surface, including epoxy (C−O−C), hydroxyl (−OH), and carboxyl (−COOH) groups.[246] The presence of these groups provides opportunities for the immobilization of a diverse spectrum of

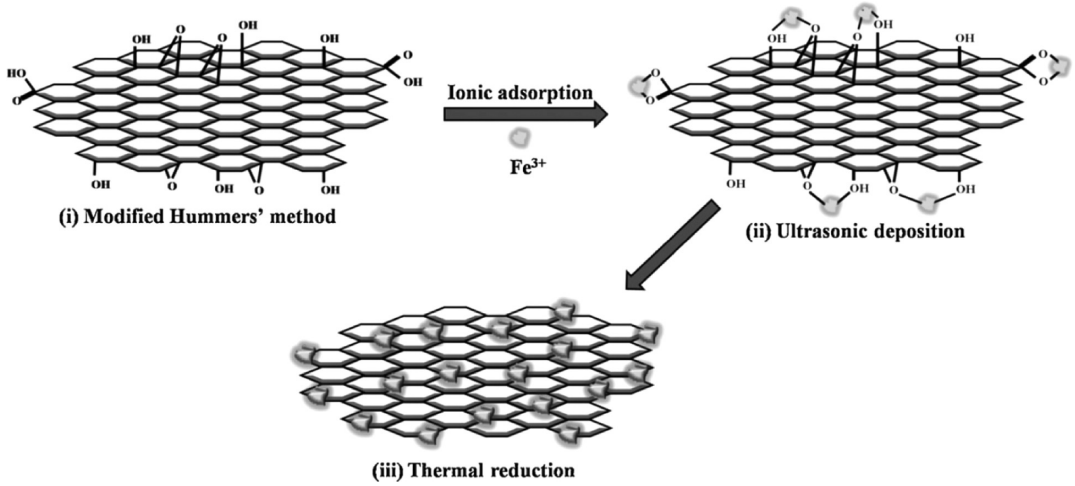


**Figure 20. Scheme showing the reaction steps for preparation of a graphene/iron oxide hybrid where the two components are linked via hydroxyl groups. Reprinted with permission from ref 222. Copyright 2011 Elsevier Ltd.**

substances, such as fluorescent molecules, drugs, inorganic nanoparticles, biomolecules, metals, *etc*. Owing to these functional groups, graphene oxide sheets are hydrophilic and readily dispersible in water. As a precursor for iron oxide nanoparticles, mixed aqueous solutions of $Fe^{2+}$ and $Fe^{3+}$ compounds (*e.g.*, $FeSO_4$ and $Fe_2(SO_4)_3$),[203] FeOOH,[233] ferric triacetylacetonate,[221] $FeCl_3$,[204] $Fe(NO_3)_3$,[222,232,246] and $Fe(CO)_5$ (ref 234) have already been used.

*Exemplary Preparation Routes toward Graphene/Iron Oxide Hybrids*. Typically, graphene/iron oxide nanocomposites are synthesized adopting the protocol shown in Figure 20.[222] First, as mentioned above, graphene oxide is prepared by the modified Hummers' method (*i.e.*, exfoliation of natural graphite powders). The advantage of working with graphene oxide springs from a large amount of oxide functional groups available which strongly react with $Fe^{3+}$ ions. In this way, $Fe^{3+}$ ions are firmly attached to the surface oxides. The dried graphene sheets obtained are then thermally treated under a $H_2$ atmosphere which promotes reduction of graphene oxide sheets as well as adhesion between reduced graphene oxide sheets and the formed $Fe_3O_4$ nanoparticles.[222]

Another synthetic protocol, as mentioned above, consists of the direct growth of FeOOH nanorods on the surface of graphene sheets followed by electrochemical transformation of FeOOH to $Fe_3O_4$ nanoparticles (see Figure 21).[233] The formation of the graphene/iron oxide hybrids occurs in three steps: (i) preparation of partially reduced graphene oxide or graphene oxide sheets, (ii) mixing of partially reduced graphene oxide or graphene oxide sheets with an $FeCl_3$ aqueous solution, and (iii) hydrolysis of the attached $Fe^{3+}$ ions. Iron oxide nanoparticles grow directly on the graphene surface, ensuring that the resulting hybrid has excellent capacitive properties.

Alternatively, graphene/iron oxide hybrids can be prepared following the reaction scheme shown in Figure 22.[247] In this synthesis, graphene oxide sheets are dispersed into 1-methyl-2-pyrrolidone solution using sonication. This dispersion is then heated, and a ferric triacetylacetonate solution is added dropwise. This addition induces formation of iron oxide nanoparticles which are attached to the surface of graphene oxide *via* metal−carboxyl bonds (confirmed by appearance of a peak at 1680 $cm^{-1}$ in the Fourier transform infrared spectrum of the hybrid; see Figure 22).[247]

To control the nucleation and growth of iron oxide nano-objects on the surface of graphene, the procedure shown schematically in Figure 23 has been proposed.[248] Reduced graphene oxide and iron(II) acetylacetonate are used as a substrate and iron oxide precursor, respectively. Chemically reduced graphene oxide is dispersed in a solution of ethylene glycol using polyvinylpyrrolidone as a dispersing agent. Subsequently, the suspension is mixed with iron(II) acetylacetonate employing an ultrasonication process, and the solution is heated to 170 °C for 30 min, which promotes nucleation of iron glycolate on the graphene oxide surface. The prolonged reaction time induces formation of iron glycolate nanoribbons; the hybrid is then thermally annealed at different temperatures (250−400 °C) to yield iron oxide nanoribbons. More importantly, the as-prepared iron oxide nanoribbons show a large aspect ratio and porous structure favoring, for example, the rapid diffusion of lithium ions from the electrolyte to electrode, and flexible graphene matrix provides a space for volume changes of iron oxide during the cycling processes. Thus, the large specific capacity and stable cyclability (see Figure 23) of iron oxide nanoribbons make the graphene/$Fe_3O_4$ hybrids promising candidates as anode materials in lithium-ion batteries (see Figure 24).[222]

To increase the cycling performance of graphene/iron oxide anodes in lithium-ion batteries, an architecture comprising graphene nanosheets with continuous iron oxide nanofilms directly anchored on their

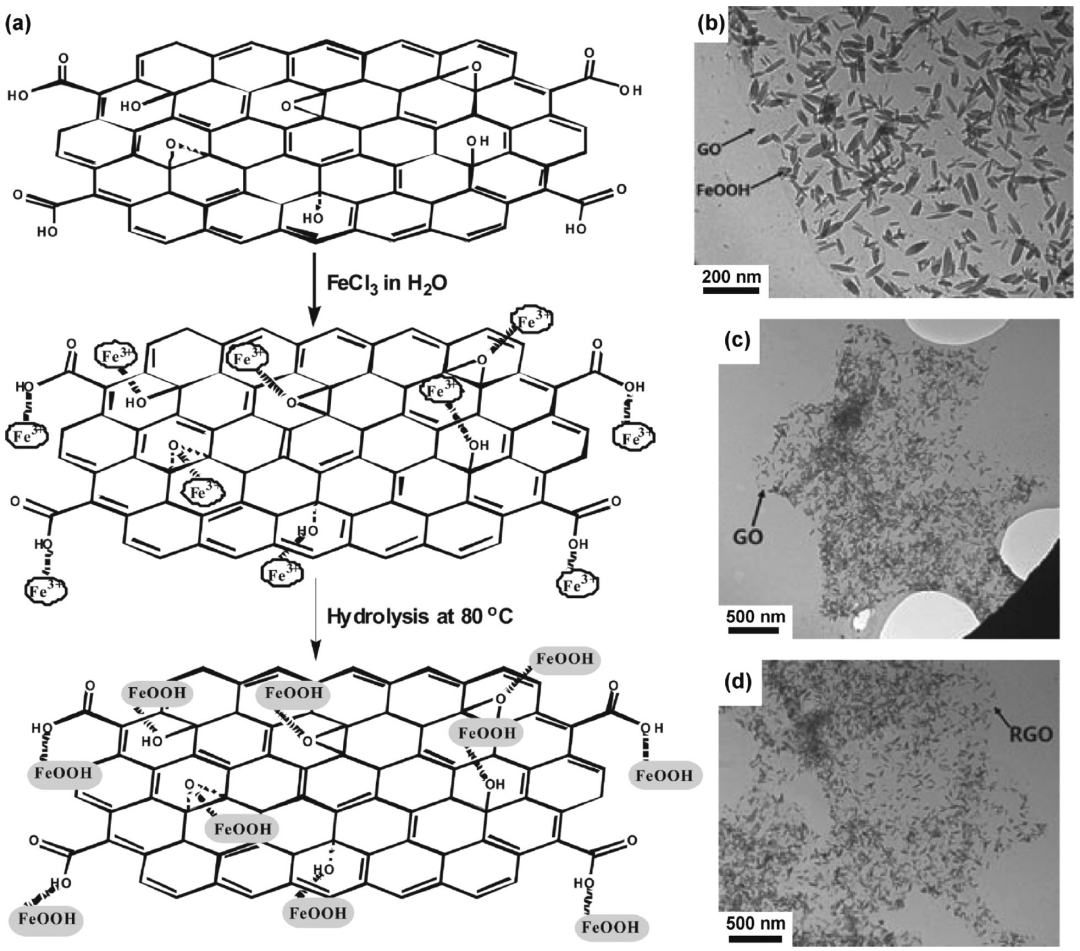


**Figure 21. (a) Scheme showing the reaction steps for preparation of a graphene/iron oxide hybrid with iron oxide nanoparticles directly grown on the surface of graphene. (b–d) TEM images monitoring individual reaction steps. Reprinted with permission from ref 233. Copyright 2011 Wiley-VCH.**

surfaces has been developed (see Figure 25);[246] the tight attachment of the iron oxide nanofilms was achieved by covalent chemical bonding *via* oxygen-containing defect sites on the graphene surface. Partially reduced thermally exfoliated graphene oxide and $Fe(NO_3)_3 \cdot 9H_2O$ were used as graphene matrix and precursor for iron oxide nanofilms, respectively. After the initial mixing of graphene nanosheets with $Fe(NO_3)_3 \cdot 9H_2O$ in ethanol solution, $Fe(NO_3)_3 \cdot 9H_2O$ was impregnated into the interspaces of the graphene nanosheets by ethanol evaporation. The resulting nanocomposite was then annealed at 200 °C in air to promote decomposition of $Fe(NO_3)_3 \cdot 9H_2O$ to iron oxide nanofilms. It is believed that the graphene substrate plays an important role in the process of accommodation of lithiation-induced strain of iron oxides as well as establishing electron conduction pathways for the iron oxide. In addition, the mesoporous structure of the iron oxide nanofilms provides a space to partly compensate lithiation-induced strain and enables electrolyte access and lithium-ion diffusion. The combination of these factors improves the cycling capability of the anode hybrid material.[246] As shown in Figure 25, the iron oxide nanofilms are still firmly bound to the graphene nanosheets after 60 cycles at 100 mA $g^{-1}$ and even 400 cycles at 1000 mA $g^{-1}$. Thus, the high performance of the graphene/iron oxide nanofilm composite as an anode material is understood in terms of its specific architecture.

Recently, an advanced architecture of hybrids comprising graphene sheets and core/double shell nanoparticles of $Fe/Fe_2O_3/Si-S-O$ nature has been proposed as an effective material for Cr(VI) removal (see Figure 26).[234] The reaction route toward such magnetic graphene nanocomposites involves two steps: (i) graphene sheets were dispersed in DMF using sodium dodecylbenzenesulfonate (SDBS) as a surfactant; to this dispersion was added $Fe(CO)_5$, and the mixture was heated to 153 °C, yielding formation of partially oxidized iron nanoparticles (*i.e.*, iron core and $Fe_2O_3$ shell) covered with SDBS; (ii) thermal annealing of the magnetically separated solid at 500 °C for 2 h under a $H_2$(5%)/Ar atmosphere promotes formation of $Fe/Fe_2O_3/Si-S-O$ nanoparticles on the graphene sheets. The resulting hybrid showed a high adsorption capacity for Cr(VI) which was attributed to single-layer

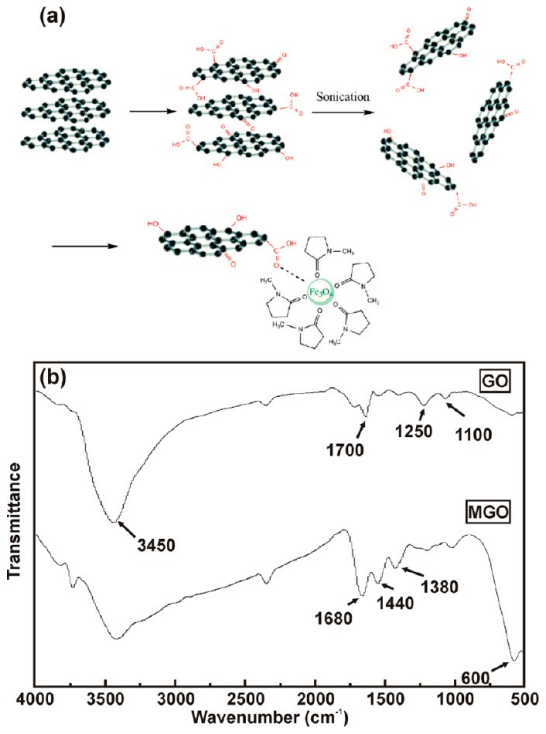


**Figure 22. (a) Scheme showing the reaction steps for preparation of a graphene/iron oxide hybrid where the two components are linked *via* metal−carboxyl bonds. (b) Fourier transform infrared spectra of the pristine graphene oxide (GO) and a graphene/iron oxide hybrid (MGO) (peaks at ∼1440 and ∼1380 cm$^{-1}$ were assigned to the formation of either a monodentate or bidentate complex between the carboxyl group and iron on the surface of iron oxide nanoparticles). Reprinted from ref 247. Copyright 2010 American Chemical Society.**

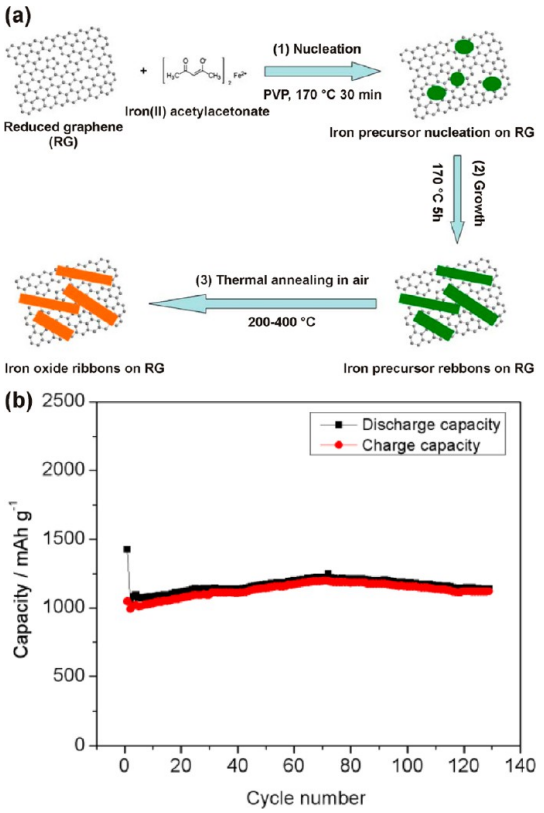


**Figure 23. (a) Scheme showing reaction steps for preparation of graphene/iron oxide ribbon hybrids for application in lithium batteries. (b) Cycle performance of graphene/iron oxide ribbon hybrids at a current density of 74 mA g$^{-1}$. Reprinted with permission from ref 248. Copyright 2012 Nature Publishing Group.**

adsorption on the graphene surface and surface complexation between sulfur of SDBS on the outer shell of the magnetic nanoparticles and Cr(VI) (see Figure 26). Moreover, this hybrid is magnetic (see Figure 26), and after use, it can easily be removed from the solution by applying an external magnetic field.

As can be expected, various authors have shown that, by altering the reaction conditions and reactants, it is possible to change the attached magnetic nanoparticles' distribution, size, and shape (Figure 27). These modifications of the attached nanoparticles can in turn help to tune the magnetic graphene nanocomposite properties, such as electrical conductivity, flexibility, giant magnetoresistance, negative permittivity, and paramagnetism.[27,203,207,249]

*Overview of Applications of Graphene/Iron Oxide Hybrids.* As already mentioned above, graphene/iron oxide nanocomposites offer a broad application portfolio. Magnetic graphene has predominantly been used in water purification applications, as was initially shown by Chandra *et al.*[240] In this study, it was demonstrated that a magnetite/graphene composite could be used to effectively remove 99.9% of As(III) and As(V) from contaminated water. One advantage of using this magnetic material is that the water-dispersible adsorbent can be easily removed from the solvent phase by application of an external magnetic field. Since this initial report by Chandra *et al.*,[240] this magnetite/graphene nanocomposite material has been used in the removal of various heavy metal ions (Cr(VI),[218] Pb(II),[250] U(VI),[251] Co(II)[252]) and organic materials (tetracycline,[253] 1-naphthol, 1-naphthylamine,[250] methylene blue,[243] polychlorinated biphenyls, polyaromatic hydrocarbons, phthalates,[254] Reactive Black 5,[255] ciprofloxacin, norfloxacin[256]).[257] The adsorption capacity of these magnetite/graphene materials is determined by the pH/ionic concentration/temperature of the polluted solution as well as the specific surface area of the individual components.[240,258]

If graphene oxide sheets are organized to form 3D macroscopic structures such as aerogels, sponges, and foams, the hybrid architecture then shows ultrahigh specific surface areas, enhanced mechanical strength, and fast mass and electron transport kinetics.[259−261] In the work of Lei *et al.*,[262] a nanocomposite made up of graphene oxide foam and $Fe_3O_4$ nanoparticles (∼7 nm in size) was tested for Cr(VI) removal. The hybrid exhibited a large surface area amounting to ∼574 m$^2$ g$^{-1}$ and excellent adsorption performance toward Cr(VI) removal with a maximum adsorption

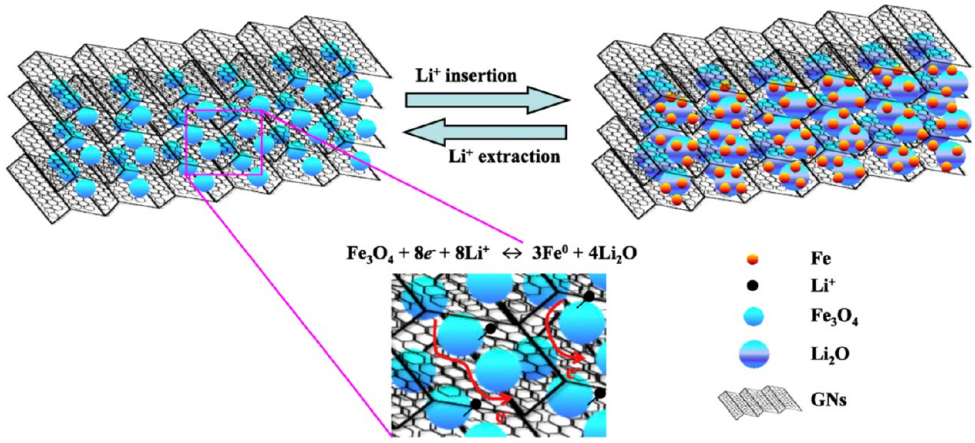


**Figure 24. Graphene/iron oxide hybrid as an anode material in lithium-ion batteries (GNs = graphene nanosheets). Reprinted with permission from ref 222. Copyright 2011 Elsevier Ltd.**

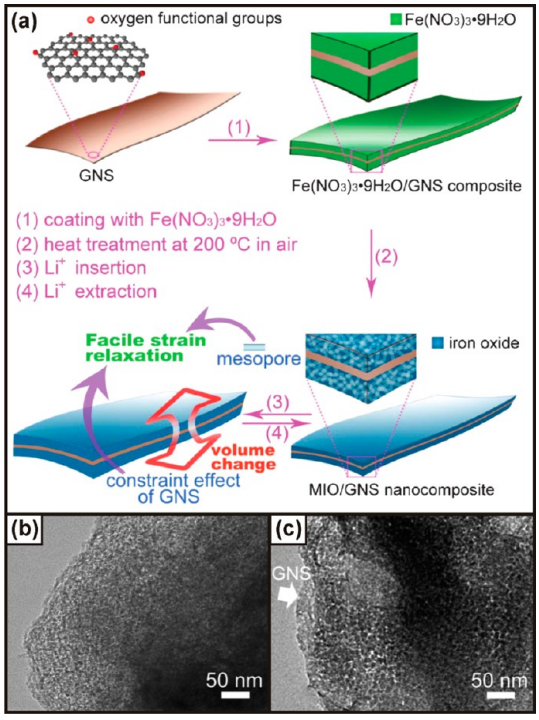


**Figure 25. (a) Preparation of a graphene/iron oxide nanofilm nanocomposite as an anode material in lithium-ion batteries (GNS = graphene nanosheets, MIO = magnetic iron oxide). TEM images of graphene nanofilm composites (b) after 60 discharge/charge cycles at 100 mA $g^{-1}$ and (c) after 400 discharge/charge cycles at 1000 mA $g^{-1}$. Reprinted with permission from ref 246. Copyright 2013 Royal Society of Chemistry.**

capacity of ~258 mg $g^{-1}$ and fast adsorption rate (100 mg $L^{-1}$, 20 min) at pH = 2, much higher than reported for current 2D graphene-based adsorbents and other traditional adsorbents. The adsorption capacity of such a magnetic 3D organized hybrid was explained in terms of synergetic effect involving reduction of Cr(VI) to Cr(III) and ion exchange between the hydroxyl groups and $Cr_2O_7^{2-}$/$HCrO^{4-}$.[262]

Other more advanced magnetic graphene water purification materials have been synthesized and applied. To promote the adsorption of As(V) ions, Luo *et al.*[263] showed that by including $MnO_2$ with the magnetite/graphene material, As(III) could be oxidized to As(V) without the need for additional external oxidizing agents. This report showed that the synthesized material could stably adsorb As(V) over a wide pH range (2−10), which is important as the magnetite/graphene material normally only affords stable adsorption at low pH values.[263]

In a similar manner, maghemite/graphene nanocomposites have been used in water purification as shown by Sinha and Jana.[239] In this study, the authors demonstrated that the endocrine disruptors—bisphenol A, atrazine, 1-naphthol, and dibutyl phthalate—could be efficiently (85−100%) removed from polluted water. By including ZnO in a maghemite/graphene nanocomposite material, Kumar and co-workers[264] showed that methylene blue could be effectively degraded and the water purification material efficiently separated using an external magnetic field. This material displayed a very high efficiency (95%) even after 5 cycles. These multiple reports demonstrate that even though these magnetic graphene materials do not show selective adsorption, they can still be applied in water purification as they are highly effective at adsorbing heavy metals and organic pollutants.

The affinity of these magnetic graphene materials for organic compounds and ions has been exploited in sensing and biosensing applications. Two studies have shown that magnetite/graphene nanocomposites offer a novel and stable environment for the immobilization of the biomolecules such as hemoglobin[265] and horseradish peroxidase.[266] These materials were then applied for mediator-free detection of hydrogen peroxide and displayed low detection limits of ~0.5 $\mu$M as well as large linear response ranges. The sensitivity toward hydrogen peroxide was attributed to fast electron transfer between the magnetite/graphene material and the immobilized enzyme. Jin *et al.*[267] showed that iron(II) phthalocyanine-decorated

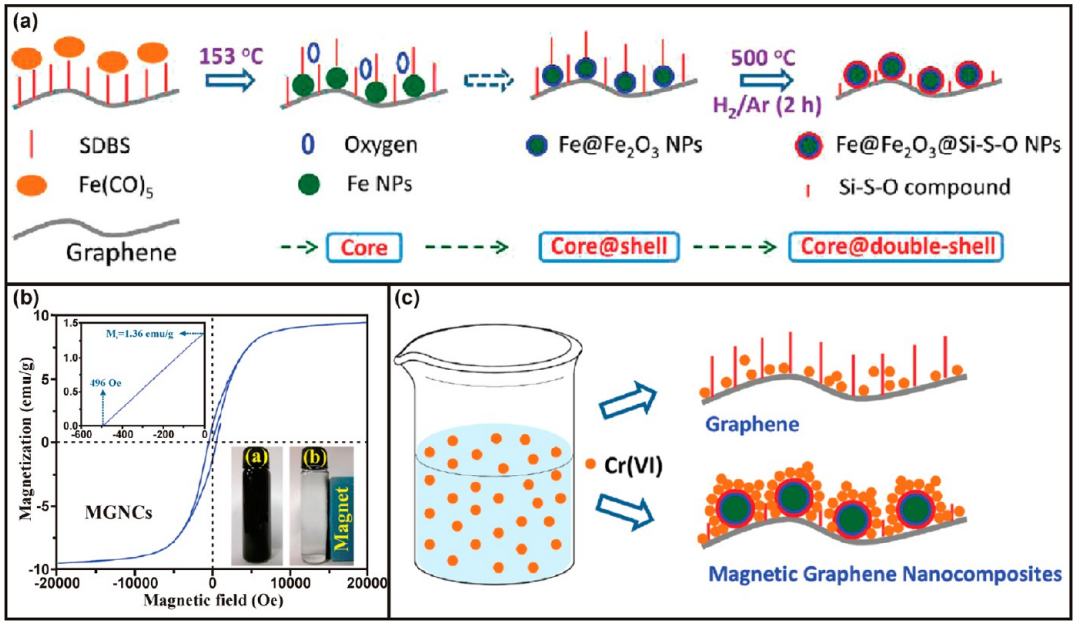


**Figure 26. (a) Preparation of the graphene/Fe/$Fe_2O_3$/Si−S−O hybrid (SDBS = sodium dodecylbenzenesulfonate, NPs = nanoparticles). (b) Room-temperature hysteresis loop of the graphene/Fe/$Fe_2O_3$/Si−S−O hybrid (the insets show behavior of the hybrid hysteresis loop around the origin and a response to a simple hand magnet; MGNCs = magnetic graphene nanocomposites). (c) Mechanism of adsorption of Cr(VI) by graphene and graphene/Fe/$Fe_2O_3$/Si−S−O hybrid. Reprinted from ref 234. Copyright 2012 American Chemical Society.**

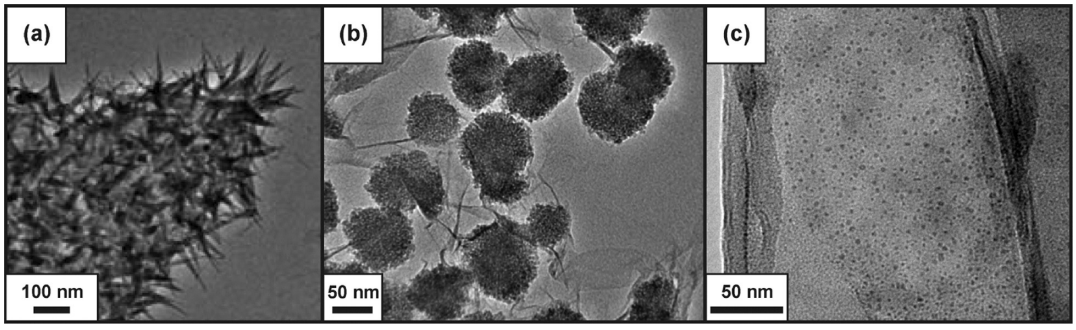


**Figure 27. (a) $Fe_3O_4$ nanoneedles grown on graphene sheets, (b) 60 nm $Fe_3O_4$ nanoparticles grown on graphene sheets, and (c) 3 nm $Fe_3O_4$ nanoparticles grown on graphene sheets. Panel (a) reprinted with permission from ref 203. Copyright 2011 Wiley-VCH Verlag GmbH&Co. KGaA, Weinheim. Panel (b) reprinted with permission from ref 208. Copyright 2010 Elsevier B. V. Panel (c) reprinted with permission from ref 242. Copyright 2011 Elsevier B. V.**

magnetite/graphene could be used in the electrochemical detection of *tert*-butyl hydroperoxide. This sensing ability was possibly due to the reduction of the organic peroxide by the iron-containing phthalocyanine. A study by Prakash and colleagues[268] demonstrated that a magnetite/graphene-modified electrode could be used to determine the concentration of Cr(III) in solution. By incorporating $Ru(bpy)_3^{2+}$ (bpy is 2,2′-bipyridine) into a porous magnetite/graphene material, Xu *et al.*[269] have showed that compounds containing tertiary amino groups and DNA could be detected using electrochemiluminescence. Application of an external magnetic field was found to stabilize the electrochemiluminescence of the material by stabilizing the electrostatic interactions between the $Ru(bpy)_3^{2+}$ and magnetite/graphene surface, thereby preventing leakage (see Figure 28).[269]

Recently, mesoporous $Fe_2O_3$ nanoparticles combined with graphene were proposed as a peroxidase mimetic potentially used as a reusable nanosensor for simple, rapid, and highly sensitive and selective optical detection of glucose.[270] The mechanism of glucose detection is schematically shown in Figure 29. In the presence of $Fe_2O_3$/graphene nanocomposites, $H_2O_2$ decomposes into a number of free radical species (*e.g.*, HO and $HO_2$) which oxidize 3,3,5,5-tetramethylbenzidine (TMB) owing to their strong oxidation capability, giving blue colored products. As $H_2O_2$ is the main oxidation product of glucose-oxidase-catalyzed reactions, glucose can be easily detected by colorimetric visualization. The improved catalytic activity of $Fe_2O_3$/graphene nanocomposites is governed by two factors: (i) mesoporous $Fe_2O_3$ nanoparticles with high surface area, providing a large number of catalytically active sites and

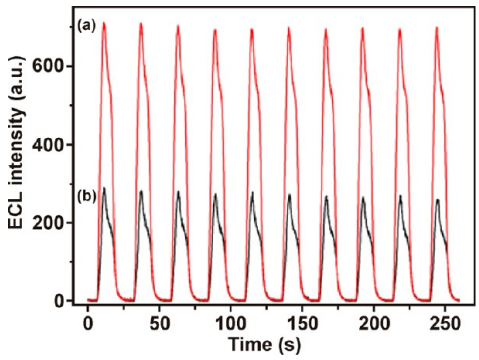


**Figure 28. Electrochemiluminescence (ECL) intensity *versus* time curve for 10 cyclic voltammetry cycles with (a) and without (b) the effect of an external magnetic field on paper-based chips in a solution of 100 mM phosphate buffered saline (PBS; pH = 7.4) at a scan rate of 100 mV $s^{-1}$. Reprinted with permission from ref 269. Copyright 2012 Springer-Verlag.**

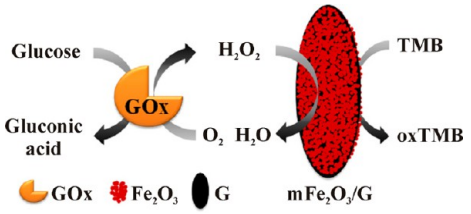


**Figure 29. Scheme describing optical detection of glucose employing graphene/iron oxide hybrid (GOx = glucose oxidase, TMB = 3,3,5,5-tetramethylbenzidine, oxTMB = oxidized 3,3,5,5-tetramethylbenzidine, G = graphene sheet, m$Fe_2O_3$/G = graphene/iron oxide hybrid). Reprinted with permission from ref 270. Copyright 2014 Elsevier B. V.**

encouraging the diffusion of TMB and $H_2O_2$ toward graphene surface, and (ii) graphene's $\pi$-rich two-dimensional structure promoting the adsorption and enrichment of TMB within the nanoparticle mesopores.[270]

Jiang *et al.*[271] have reported fabrication of paper-like $Fe_2O_3$/graphene nanosheets and tested the hybrid as $H_2S$ gas sensor. It was observed that the efficiency of the sensor strongly depends on the alignment of nanosheets decorated with iron oxide nanoparticles, imprinted during preparation by an external magnetic field. If $Fe_2O_3$/graphene nanosheets are aligned vertically, they are more sensitive to $H_2S$ than those showing horizontal arrangement.[271] This may be of crucial importance not only in sensing applications but also in lithium-ion batteries where higher storage capacities could be reached.

Magnetic graphene has been applied in biomedical applications other than biosensing, such as bioimaging,[272] magnetic resonance imaging (MRI),[241,273] and drug delivery.[272,274] A magnetite/graphene nanocomposite material has been employed to load anticancer drugs, such as 5-fluorouracil and doxorubicin hydrochloride, with a high loading capacity.[272,274] These studies showed that release of the drugs was determined by the cell pH of the targeted cells (see Figure 30).[272] Importantly, it was shown that the carrier material was nontoxic to Chang lung cancer cell lines.[274] The concept of using magnetic graphene as an MRI agent was proposed by Cong *et al.*,[241] who showed that $T_2$-weighted MRI could be conducted due to the excellent magnetic properties of the magnetite/graphene nanocomposite material. This initial work was expanded by Chen and co-workers[273] by showing that the magnetite/graphene nanocomposite material could be applied in cellular imaging. In this study, the magnetite/graphene nanocomposite was functionalized with aminodextran to induce larger $T_2$ shortening than observed for magnetite coated aminodextran nanoparticles. The magnetite/graphene nanocomposite material was confirmed to be nontoxic toward HeLa cell lines, which could be imaged at a limit of 1000 cells $mL^{-1}$. The nontoxicity and cell permeability of these magnetic graphene materials make them ideal candidates for future targeted bioimaging and drug delivery applications. However, no study, published so far, has addressed the issue of *in vivo* distribution of graphene/iron oxide nanocomposites inside the living organisms.

Recently, a new multifunctional theranostic agent exploiting iron-oxide-loaded poly(lactic acid) microcapsules coated with graphene oxide has been developed by Li *et al.*[275] This hybrid provides a trimodal imaging (ultrasound (US) imaging, photoacoustic (PA) tomography, and nuclear magnetic resonance imaging (MRI)) and, at the same time, enables performance of photothermal therapy of cancer by irradiating the graphene oxide with electromagnetic waves in the near-infrared region. Here, $Fe_3O_4$ nanoparticles loaded in the poly(lactic acid) microcapsules with ultrasound imaging capability serve as magnetic resonance imaging contrast agents and carriers driven to the cancer site in the living organism by the magnetic field gradient. On the other hand, graphene oxide, having a strong near-infrared light absorbance, acts as contrast enhanced photoacoustic imaging agent and tool for photothermal therapy. When irradiated with near-infrared light, graphene oxide strongly absorbs light that is converted to heat, destroying the tumor cells. It was found that as-designed iron oxide/poly(lactic acid)/graphene oxide nanocomposite effectively kills the cancer cells (HeLa cells) upon near-infrared laser irradiation under the guidance of the contrast enhanced US/PA/MRI imaging without damaging normal healthy cells. In addition, the efficiency of photothermal therapy can be increased by applying an alternating external magnetic field when iron oxide nanoparticles give extra heat due to hysteresis losses.[275]

The use of magnetite/graphene[201,276,277] and maghemite/graphene[237] nanocomposites in renewable energy applications has been demonstrated by employing these materials as anodes in lithium-ion batteries. Zhang and co-workers[276] showed that a magnetite/graphene nanocomposite could be synthesized using an efficient microwave method, which

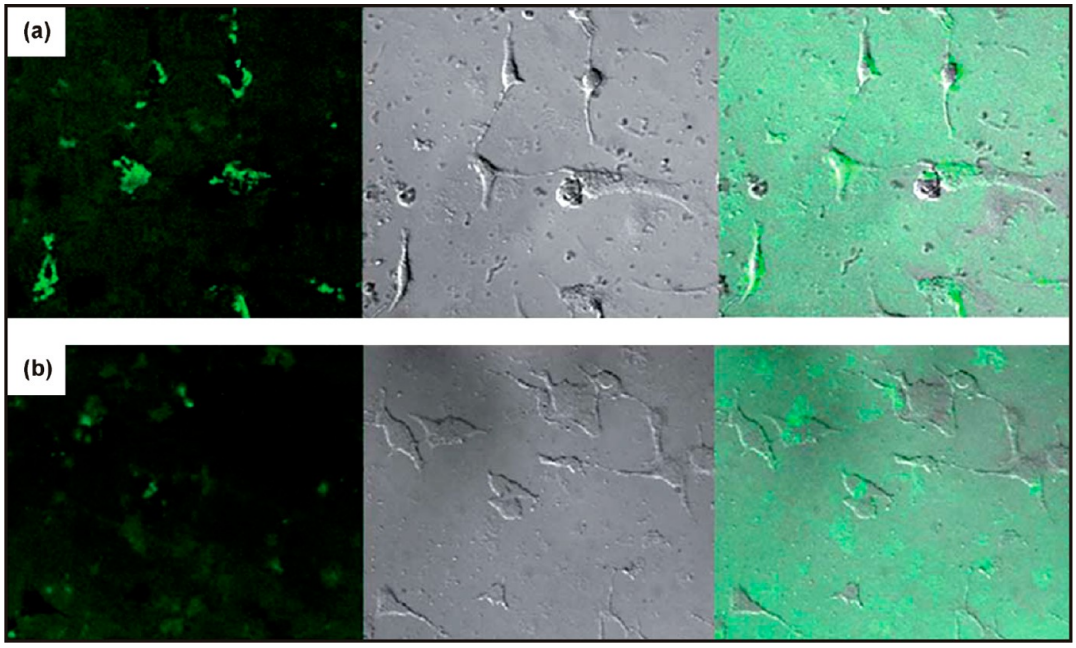


**Figure 30. Confocal fluorescence images of (a) magnetite/graphene–folic acid–fluorescein isothiocyanate (FTIC) and (b) magnetite/graphene-FITC after incubation with SK3 at 37 °C for 1 h. Reprinted with permission from ref 272. Copyright 2011 Royal Society of Chemistry.**

resulted in magnetite nanoparticles (20–70 nm) intercalated between graphene sheets. The material showed a stable capacity of 650 mA h $g^{-1}$ after 50 cycles. This stability was believed to be due to the interspaces and flexibility of the material, which is able to accommodate the volume changes upon lithium insertion and extraction. In a similar study, Zhou *et al.*[201] showed that the graphene substrate stabilizes the magnetite nanoparticles upon cycling with the average size of the nanoparticles staying almost constant (increases from 196 to 213 nm) compared to commercial magnetite nanoparticles (decreases from 735 to 428 nm). Behera[277] reported that magnetite/graphene nanocomposites with 10 nm sized magnetite nanoparticles showed a stable capacity of ~1100 mA h $g^{-1}$. This study demonstrated that the magnetite nanoparticle size, as well as graphene content and synthetic method, can affect the capacity of the material when used as an anode in lithium-ion batteries.

Similar to the magnetite/graphene material, Kim *et al.*[237] have shown that maghemite/graphene nanocomposite can be used as an anode in lithium-ion batteries. In this study, a stable capacity of 690 mA h $g^{-1}$ was obtained at a current density of 500 mA $g^{-1}$. This capacity is similar to that achieved in the other magnetite/graphene-focused studies, which again suggests that both forms of magnetic iron oxide may be formed during the synthetic procedures.[243]

Magnetite/graphene nanocomposite materials have also been applied as supercapacitors. Li *et al.*[278] obtained a specific capacitance of 85 F $g^{-1}$ by coating a gold electrode with a magnetite/graphene nanocomposite material. However, in another similar study, a specific capacitance of 358 F $g^{-1}$ was reported for the same magnetite/graphene nanocomposite.[279] The difference between these results is probably due to different component content in the magnetite/graphene nanocomposite materials, as reported previously by Cheng and co-workers,[280] who showed that the weight ratio of the components has a dramatic effect on the sample surface area as well as pore volume, which in turn affects the specific capacitance. This is an important observation as magnetite/graphene compounds with far larger surface areas have been reported.[281]

Recently, it has be shown if a nitrogen atom is introduced into the structure of graphene, it brings enhancement in the graphene electrical conductivity as extra lone pair electrons are induced.[282–284] Moreover, nitrogen-doped graphene provides more active and nucleation sites due to defects formed upon nitrogen substitution, thus preventing more effectively the aggregation of metal oxide nanoparticles and, at the same time, strengthening the binding energy both for combination of nitrogen-doped graphene and metal oxide nanoparticles and for the adsorption of electrolyte ions on the electrode surface. After 100 charge/discharge cycles, this hybrid maintained a reversible capacity of 1012 mA h $g^{-1}$ at a current density of 100 mA $g^{-1}$, much higher than that of $Fe_2O_3$ nanoparticles alone (~200 mA h $g^{-1}$, 100–500 nm in size) and graphene/$Fe_2O_3$ nanoparticles hybrid (~430 mA h $g^{-1}$, 100–500 in size).[283] Nitrogen-doped graphene/maghemite nanocomposite (with $Fe_2O_3$ nanoparticles having 20–100 nm in size) was also tested as a potential electrode material in supercapacitors.[285] The specific capacitance of nitrogendoped

graphene/maghemite electrode was found to ~260 F $g^{-1}$ and dropped to ~215 F $g^{-1}$ after 1000 cycles at a current density of 2 A $g^{-1}$. The enhanced capacitance of the nitrogen-doped graphene/maghemite electrode was explained in terms of increased binding energy promoting accommodation of higher number ions on the electrode surface and presence of pyrrolic nitrogen decreasing the electrode internal and charge transfer resistances.[285]

It is known that graphene nanoribbons—thin ribbons of graphene monolayers—combine properties of graphene (*e.g.*, high electrical conductivity) and long carbon nanotubes (*e.g.*, high aspect ratio). It has been thus suggested as a promising conductive platform for iron oxide nanoparticles providing mechanical flexibility to readily accommodate volume changes during charging and discharging cycles. Lin *et al.*[286] reported that if graphene nanoribbons are decorated with ~10 nm sized $\gamma$-$Fe_2O_3$ nanoparticles, the graphene nanoribbon/iron oxide nanocomposite anode shows a reversible capacity of ~1190 mA h $g^{-1}$, falling to ~910 mA h $g^{-1}$ after 134 charge/discharge cycles at a current density of 0.2 A $g^{-1}$. At a rate of 2 A $g^{-1}$, the electrode still maintains a high capacity performance amounting to ~540 mA h $g^{-1}$ due to the unique structure of $\gamma$-$Fe_2O_3$ nanoparticles conformally coated with conductive graphene nanoribbons. It is worth mentioning that the lithium storage performance is significantly affected by the temperature at which the electrode nanocomposite material is annealed. On an increase of the annealing temperature, $\gamma$-$Fe_2O_3$ transforms to $\alpha$-$Fe_2O_3$, raising the concentration of $\alpha$-$Fe_2O_3$ nanoparticles in the nanocomposite. It is known that contrary to $\gamma$-$Fe_2O_3$, $\alpha$-$Fe_2O_3$ shows a phase transition during lithium insertion, favoring irreversible lithium storage and thus drop in capacity after cycling. In addition, at higher annealed temperatures, graphene nanoribbons tend to oxidize easily, losing their electrical conductivity.[286]

Ni–Fe alkaline batteries are regarded as alternatives to lithium-ion batteries. However, their practical utilization is hindered by several drawbacks including high self-discharge,[287] relatively low energy efficiency,[288] and low power density[289] of the iron anode in aqueous media. Recently, Wang *et al.*[290] reported a 1000 times increase in the charging and discharging rates for strongly coupled $FeO_x$/graphene nanocomposite anode compared to those exhibited by traditional electrodes in Ni–Fe batteries. Similar approach was adopted by Jiang *et al.*,[291] who prepared graphene sheets on which $FeO_x$ nanoparticles were grown ($Fe_3O_4$ and FeO phases with the particle size of about 100 nm). The as-prepared nanocomposites were tested as an electrode in the Ni–Fe alkaline batteries, giving an initial discharge capacity of ~552 mA h $g^{-1}$ at a current density of 200 mA $g^{-1}$. The enhanced electrochemical performance of this electrode was attributed to a size of

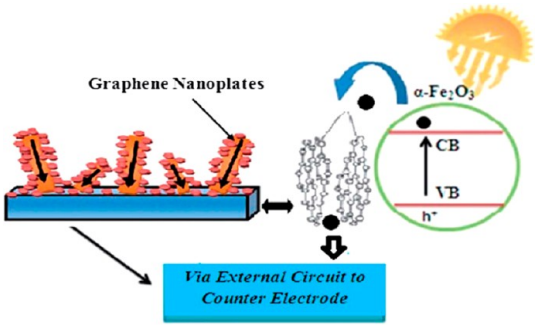


**Figure 31. Scheme describing electron transfer mechanism from $\alpha$-$Fe_2O_3$ to the transparent conducting oxide substrate mediated by the graphene sheets. Reprinted with permission from ref 293. Copyright 2014 Royal Society of Chemistry.**

$FeO_x$ nanoparticles decreasing significantly due to strong coupling during decomposition–crystallization progress providing larger available surface area and graphene layers promoting electron transfer through nanoparticles during charging and discharging.[291]

In the future, hydrogen is viewed as a promising candidate to store solar energy. Among all methods currently explored, direct splitting of water using solar energy in a photoelectrochemical (PEC) cell is viewed as one of the most attractive, economical, and environmentally friendly ways to produce hydrogen. The performance of the PEC cell is governed by the selection of a material for the photosensitive semiconductor electrode. Out of all potential materials for the electrode in the PEC cell, $\alpha$-$Fe_2O_3$ (hematite) has turned out to be promising as a photoelectrode owing to its suitable band gap (2.0–2.2 eV) absorbing almost 40% of incident sunlight, high abundance, and low cost. However, $\alpha$-$Fe_2O_3$ suffers from several drawbacks such as poor conductivity, high electron–hole pair recombination rate, and mismatch in the conduction band edge with respect to the redox level of the $H_2/H^+$ couple (~0.2 V *vs* normal hydrogen electrode).[292] In order to improve photoelectrochemical characteristics of $\alpha$-$Fe_2O_3$ (*i.e.*, electrode capacity and cycling stability) and enhance the efficiency of hydrogen production, $\alpha$-$Fe_2O_3$ has been recently combined with graphene sheets to overcome problems with poor charge transport property of $\alpha$-$Fe_2O_3$. In the $\alpha$-$Fe_2O_3$/graphene hybrid, graphene's role is to promote a quick pathway for electron transport from the semiconductor to the transparent conducting oxide substrate (*i.e.*, the charge collector) (see Figure 31). Such a hybrid in the form of a composite thin film has been, for example, developed by Rai *et al.*[293] and was tested as a photoanode in the PEC cell showing the highest photocurrent density of 2.5 mA $cm^{-2}$ (at 0.75 V/SCE under 150 mW $cm^{-2}$) and maximum solar-to-hydrogen conversion efficiency of 1.8% with 0.2 wt % of graphene sheets in the nanocomposite. The increased photocurrent was explained in terms of improved conductivity of $\alpha$-$Fe_2O_3$ with graphene sheets (restriction of

recombination of photoexcited electron−hole pairs at the surface or the interface), improved morphology, and decreased value of the net resistance.

$Fe_3O_4$/graphene nanocomposites have been suggested as effective electromagnetic absorbers in the microwave range. Both components play an active role in microwave absorption; however, due to very high carrier mobilities in graphene, nonmagnetic behavior, and unbalance of its dielectric permittivity and magnetic permeability, impedance mismatch is often observed degrading graphene's microwave absorption capability. Also, if $Fe_3O_4$ nanoparticles are left alone, they show bad thermal stability ($Fe^{2+}$ is easily oxidized to $Fe^{3+}$, and $Fe^{2+}$−$Fe^{3+}$ electron hopping mechanism is lost) and tend to agglomerate, negatively influencing microwave absorption properties. Once combined, problems with particle agglomeration and graphene impedance mismatch are significantly suppressed due to synergetic effects; $Fe_3O_4$/graphene nanocomposites then show improved absorption features (wider absorption bandwidth) as a result of combination of optimized dielectric and magnetic loss, geometrical effect (*i.e.*, thickness of the absorber), particle size, morphology, and chemical stoichiometry.[294−297] For example, in the work by Xue *et al.*,[297] ∼100 nm sized $Fe_3O_4$ nanoparticles decorating graphene sheets showed a multifrequency absorption covering C band and Ku band with a maximum reflection loss of −20 dB.

Large surface area magnetite/graphene nanocomposites have been reported by Zhou *et al.*,[281] who showed that a maximum BET specific surface area of 901 $m^2\ g^{-1}$ can be obtained by self-assembly of the components into a three-dimensional structure. Interestingly, this material exhibited a hydrogen storage capacity of 1.4 wt % at 77 K.

Hu and co-workers[298] have shown that a novel sulfonated graphene oxide/magnetite substrate can be used to support Pd nanoparticles. This material was applied as a catalyst in the Suzuki−Miyaura cross-coupling reaction. One benefit of using this material is that the catalyst can be easily removed from the reaction solution by application of an external magnetic field. The novel support also enabled even dispersion of the Pd catalyst over the surface, increasing the catalytic efficiency. In a related study, Li *et al.*[299] showed that Pt, Pd, and Pd/Pt nanoparticles can be uniformly deposited on a magnetite/graphene substrate. These catalysts were applied in the $NaBH_4$ reduction of 4-nitrophenol, where it was found that the Pd/Pt catalyst displayed the highest resistance to catalytic poisoning as well as a stable turnover frequency after 10 cycles. By reversing the synthetic method and first depositing Pd nanoparticles on graphene, Chandra *et al.*[300] succeeded in obtaining an even dispersion of magnetite nanoparticles. This catalytic material was used in the hydrogenation of vinyl acetate with a near 100% conversion efficiency after

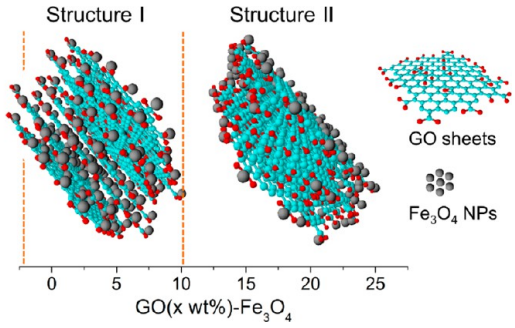


**Figure 32. Proposed two different structures of the graphene oxide/$Fe_3O_4$ hybrids at the transitional graphene oxide loading of 10 wt % (the cyan, red, and gray ball-and-stick model correspond to the structure of graphene oxide, oxygenated functional groups, and $Fe_3O_4$ nanoparticles, respectively). Reprinted with permission from ref 301. Copyright 2014 Nature Publishing Group.**

5 cycles. The stability of these catalysts was attributed to the stability introduced by electronic modulation between the graphene and the catalytic metal nanoparticles. In the work by Zubir *et al.*,[301] $Fe_3O_4$/graphene oxide nanocomposites were exploited in the degradation of Acid Orange 7 dye. It was found that the degradation occurs predominantly at the solid−liquid interfaces of the nanocomposites promoted by the formation of hydroxyl radicals ($HO^{\bullet}$) due to the catalyzed decomposition of hydrogen peroxide ($H_2O_2$) by the active sites ($Fe^{2+}$ and $Fe^{3+}$) of $Fe_3O_4$ nanoparticles. On the other hand, graphene oxide contains unpaired electrons originating from many semiconducting $\pi$-conjugated $sp^2$ domains on its basal plane, favoring electron transfer between graphene oxide and iron centers. This ensures regeneration of $Fe^{2+}$ ions to speed up the redox cycle between active sites, resulting in degradation and mineralization of Acid Orange 7 dye. Thus, several factors have been identified significantly participating in enhancement of the chemical reactivity: (i) high surface area of graphene oxide securing good dispersion of $Fe_3O_4$ nanoparticles over the graphene oxide sheets, supporting mass transfer of reactant to the active sites; (ii) large aromatic ring structure of graphene oxide promoting adsorption of Acid Orange 7; (iii) strong interaction between $Fe_3O_4$ nanoparticles and graphene oxide sheets *via* Fe−O−C bonds establishing electron transfer between the two hybrid components; (iv) partial reduction in graphene oxide speeding up the electron transfer and, hence, the redox cycle between the active sites accompanied by regeneration of ferrous ions.[301] In addition, it was observed that the efficiency of degradation strongly depends on the graphene oxide loading; above 10 wt % of graphene oxide loading (see Figure 32), the structure of graphene oxide changes due to dominant stacking of sheets and iron oxide nanoparticles mostly aggregated on the exterior surface of stacked sheets.[301]

Although there have been advances in the syntheses of graphene/iron oxide hybrids, some problems

and challenges remain that need to be addressed in order to produce high-quality nanocomposites with specific physicochemical properties for a given application. These include problems with the (i) solubility/dispersibility of the functionalized graphene nanosheets, (ii) prevention of stacking of graphene sheets before the introduction of the iron oxide precursors, (iii) control of the phase composition of the iron oxide nanoparticles (to avoid the presence of undesirable iron(III) oxide polymorphs as other nanoparticles or nanoparticle shells), (iv) control of the size and shape of the iron oxide nanoparticles, (v) control of the coverage of iron oxide nanoparticles on the graphene surface, and (vi) optimization of mutual interactions between both components involved in the hybrid (*via* suitable interaction pathways, *i.e.*, functional groups). In addition, most of the syntheses reported so far are relatively complex (involve several reaction steps) and hardly allow optimization. As such, they are time-consuming and relatively costly and often give low yields.

**Magnetic Fullerenes, Carbon Dots, Mesoporous Carbon, and Nanofoams in Theranostics, Dual Imaging, and Other Applications.** *Nanocomposites of Fullerenes and Iron Oxides: Syntheses and Applications.* Like carbon nanotubes and pure graphene, fullerene does not show long-range magnetic ordering. In general, the short-range magnetic properties of fullerene are driven by its structure, containing both pentagons and hexagons. The fullerene magnetic susceptibility involves two contributions, that is, a diamagnetic term originating from the hexagonal rings and a paramagnetic term stemming from the pentagonal rings.[302] Sometimes, the paramagnetic term is strengthened by the presence of oxygen.[303,304] Weak ferromagnetic behavior has been observed only in some fullerene derivatives, such as $C_{60}$ charge transfer complexes (*e.g.*, $C_{60}$-TDAE (tetrakisdimethylaminoethylene, $C_2N_4(CH_3)_8$), $C_{60}R_n$ compounds (where R = H, F, $CF_3$, and polymer fragments, and *n* is odd), and pressure-polymerized fullerenes (orthorhombic, tetragonal, and rhombohedral fullerene polymers).

To impart a strong magnetic response to fullerenes, they must be functionalized with magnetic species. Up to now, only a few studies have reported the preparation of fullerene/iron oxide hybrids where iron oxide nanoparticles are covalently bound to the fullerene surface *via* mediating functional groups (*e.g.*, −COOH groups).[305,306] However, no work has been published on the encapsulation of iron oxide nanoparticles inside the carbon cage (only metal atoms or simple molecules have been caged inside fullerenes so far—endohedral metallofullerenes[307−309]). Other types of linkages have also not been explored, most probably due to the weak forces that can develop between the two components.

Owing to very low biological toxicity of both fullerene and iron oxide nanoparticles, their hybrids are particularly promising for biomedical applications.

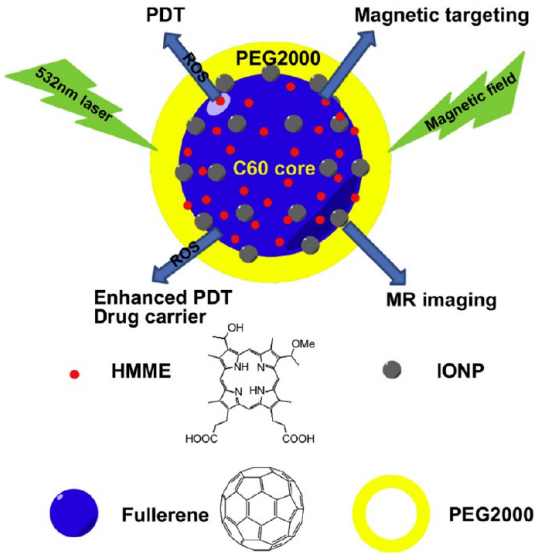


**Figure 33. Proposed architecture of the photodynamic agent based on fullerene/iron oxide nanoparticle hybrid. Reprinted with permission from ref 305. Copyright 2013 Elsevier Ltd.**

Recently, the potential of fullerene/iron oxide nanocomposites has been explored in photodynamic therapy, an alternative method developed to treat cancer and noncancer diseases.[305] Such therapy employs a photosensitizer, a compound selectively localized in the target tissue and activated by a specific wavelength of light, inducing photodamage and death of the target cells. However, this treatment strategy faces several challenges, including the low water solubility of many potential photosensitizers, tendency for the formation of aggregates under physiological conditions, accumulation rate at a target tissue, and limited target-selective recognition. It is known that nanoparticles can increase the solubility of hydrophobic drugs; if of magnetic nature, they can be driven to the target site by an external magnetic field where they accumulate. On the other hand, fullerenes which possess superior photo- and electrochemical features can effectively work as a photosensitizer owing to their capability to absorb visible light. Fullerene's light absorption is accompanied by the intersystem crossing to the long-lived triplet state, which equips fullerenes with the ability to generate oxygen-reactive species. Thus, if the fullerene surface is decorated with iron oxide nanoparticles, the hybrids can potentially act as photodynamic agents that can be delivered to the desired site in a controllable manner. Moreover, their presence at the site of action can easily be monitored by nuclear magnetic resonance imaging as magnetic nanoparticles behave as contrast agents. The proposed architecture of a new photodynamic anticancer drug composed of a fullerene/iron oxide hybrid further functionalized with hematoporphyrin monomethyl ether (HMME) is depicted in Figure 33, and the synthesis scheme is shown in Figure 34a.[305] The synthesis

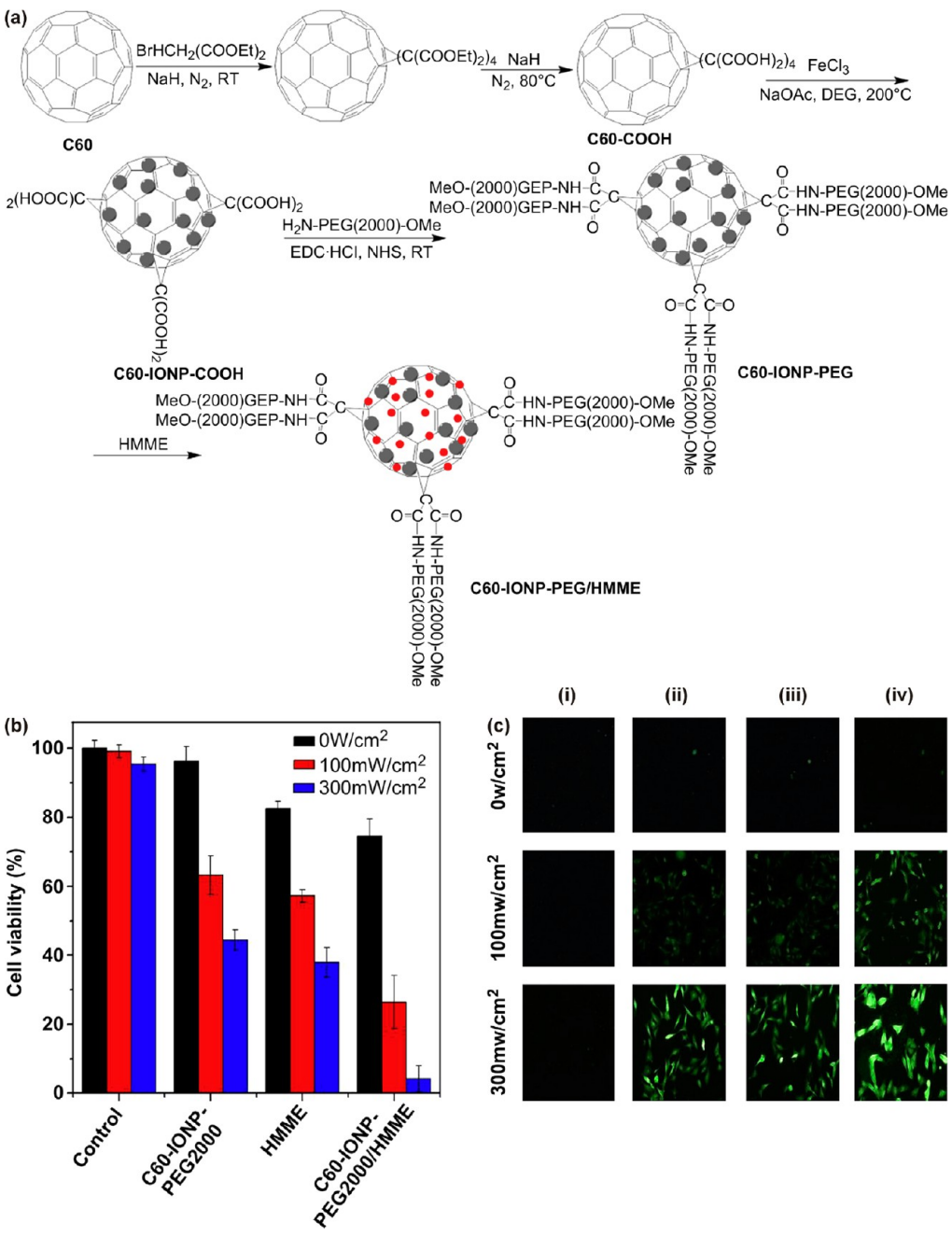


**Figure 34. (a) Scheme showing the reaction steps for preparing a fullerene/iron oxide photodynamic agent. (b) Relative viabilities of B16-F10 cells treated with $C_{60}$/iron oxide/PEG (C60-IONP-PEG2000), HMME, and $C_{60}$/iron oxide/PEG/HMME (C60-IONP-PEG2000/HMME) complex with or without laser irradiation (532 nm, 100 or 300 mW/cm$^2$, 5 min). (c) Detection of intracellular reactive oxygen production by DCFH-DA staining in B16-F10 cells incubated with C60-IONP-PEG/HMME complex: (i) control cells, (ii) C60-IONP-PEG, (iii) HMME, and (iv) C60-IONP-PEG/HMME. Reprinted with permission from ref 305. Copyright 2013 Elsevier Ltd.**

involves four steps: (i) functionalization of $C_{60}$ with −COOH groups by Bingle cycloaddition and ester hydrolysis reaction, (ii) a hydrothermal reaction promoting formation of iron oxide nanoparticles from an $FeCl_3 \cdot 6H_2O$ precursor on the surface of the fullerenes, (iii) PEGylation (PEG = polyethylene glycol) by condensation of carboxyl groups of the $C_{60}$/iron oxide and $NH_2$ groups of the MeO-PEG2000-$NH_2$ compound, and (iv) physical adsorption of the photodynamic HMME anticancer drug on the fullerene's surface. The functionalization with polyethylene glycol (PEG2000) provides the nanocomposite with the increased stability in physiological environment. As such, this $C_{60}$/iron oxide/PEG complex possesses a very low biological toxicity and may serve as a combined photodynamic therapy and contrast agent and magnetic-targeted drug delivery carrier, thus being regarded as a promising theranostic tool.[305] As demonstrated in Figure 34b, the $C_{60}$/iron oxide/PEG complex shows a relatively low cytotoxicity to B16-F10 cells

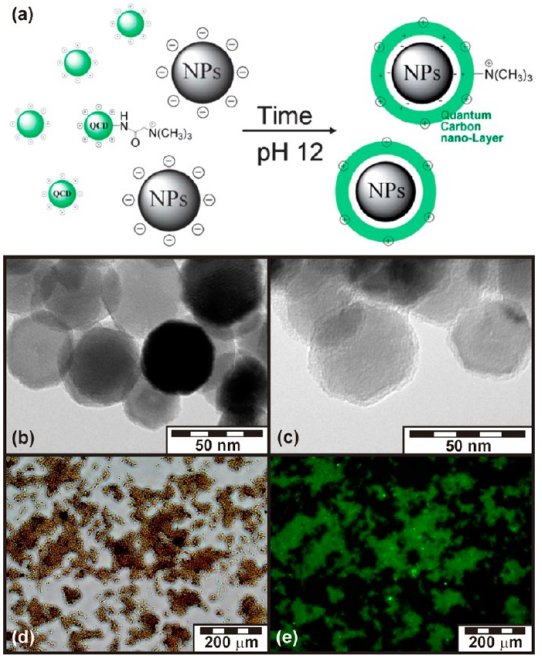


**Figure 35. (a) Preparation scheme of a nanocomposite composed of carbon quantum dots attached on the surface of iron oxide nanoparticles (QCD = carbon quantum dot, NPs = $Fe_3O_4$ nanoparticles). TEM images of (b) biogenic $Fe_3O_4$ nanoparticles and (c) carbon quantum dot/$Fe_3O_4$ hybrid (pH = 12, carbon quantum dot/$Fe_3O_4$ = 1/1). Carbon quantum dot/$Fe_3O_4$ hybrids imaged by a fluorescence microscope: (d) phase contrast and (e) phase contrast combined with a fluorescence mode. Reprinted with permission from ref 310. Copyright 2012 Royal Society of Chemistry.**

(mice melanoma cell line), whereas when irradiated with 532 nm laser, the cytotoxity of the hybrid greatly increases. Significant enhancement in killing of cancer cells was witnessed for $C_{60}$/iron oxide/PEG/HMME complex after exposure to laser; almost all cancer cells were killed with 300 mW/cm$^2$ laser power. In addition, a high level of generation of reactive oxygen species (ROS) was detected for $C_{60}$/iron oxide/PEG/HMME complex after laser exposure (greener fluorescence in Figure 34c), confirming its remarkable photodynamic therapy efficiency.[305]

*Nanocomposites of Carbon Quantum Dots and Iron Oxides: Syntheses and Applications.* If carbon quantum dots are combined with iron oxide nanoparticles, the resulting hybrid can be used as a dual fluorescent/magnetic imaging agent or as an efficient photocatalyst. Such a nanocomposite shows core/shell architecture, where the core is composed of an iron oxide phase to which quantum dots are attached either *via* covalent bond (*i.e.*, use of functional groups present on the surface of one of the hybrid components) or electrostatic interactions (*i.e.*, through electrostatically charged surfaces of the hybrid units). An example of a preparation route toward a carbon quantum dot/iron oxide hybrid for bioimaging purposes is shown schematically in Figure 35.[310] In this approach, carbon quantum dots are synthesized using

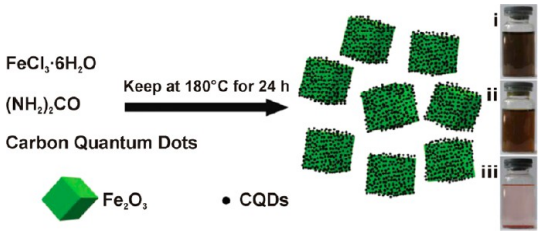


**Figure 36. Scheme describing the preparation of the carbon quantum dot/iron oxide nanocomposites acting as magnetically separable catalysts. The photographs show (i) carbon quantum dots dispersed in aqueous solution, (ii) reaction solution containing carbon quantum dots, $FeCl_3$, and $(NH_2)_2CO$, and (iii) product solution. Reprinted with permission from ref 311. Copyright 2011 Royal Society of Chemistry.**

tris(hydroxymethyl)aminomethane and betaine hydrochloride as a carbon source and surface modifier, respectively. The modifier provides the carbon quantum dot surface with $-N(CH_3)_3^+$ groups, which enables their immobilization on the negatively charged surface of the iron oxide nanoparticles (due to hydrolyzed hydroxyl group on the iron oxide nanoparticle surface) *via* electrostatic interactions, such as $Fe-O^- + {}^+N(CH_3)_3 \rightarrow Fe-O^{-+}N(CH_3)_3$.[310] The core/shell architecture is clearly seen in TEM images in Figure 35; different contrast reflects iron oxide nanoparticles as a core and carbon quantum dots as a shell. Thus, owing to the core/shell nature, hybrid nanoparticles combine fluorescence with magnetic response on a single platform (see Figure 35 where nanocomposite's fluorescence properties are highlighted).

Figure 36 shows a synthesis scheme for a carbon dot/iron oxide nanocomposite for photocatalytic applications.[311] It is believed that the presence of carbon quantum dots significantly enhances the photocatalytic activity of the iron oxide as they promote effective separation of photogenerated electrons and holes, preventing their rapid recombination. As all carbon nanostructures have a large electron storage capacity, the photon-excited electrons from $Fe_2O_3$ nanoparticles can be readily transported in the conducting network of carbon quantum dots. The electron–hole pairs can interact with adsorbed oxidants/reductants (*e.g.*, $O_2$ and $OH^-$), generating a large amount of active oxygen radicals (*i.e.*, $^\bullet O_2^-$ and $^\bullet OH$) with strong oxidation capability for degrading toxic gases (see Figure 37).[311] In addition, carbon quantum dots show upconversion photoluminescence by emitting light with a wavelength shorter than that of absorbed light, which excites $Fe_2O_3$ to produce electron–hole pairs. This hybrid has been proposed as a high-performance novel magnetically separable catalyst suitable for remediation applications. It has been successfully tested for degradation of gas-phase benzene and methanol.[317] As clearly seen from Figure 37, the degradation efficiency of benzene increased from 37% for $Fe_2O_3$ nanoparticles alone to nearly 80% in the case of carbon quantum dot/$Fe_2O_3$

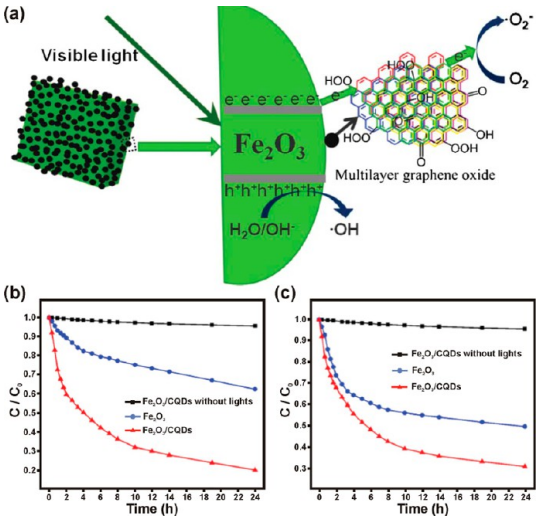


**Figure 37. (a) Proposed model of the mutual interactions between carbon quantum dots and iron oxide nanoparticles explaining the enhanced photocatalytic capability of the hybrid ($e^-$ = electron, $h^+$ = hole). Photocatalytic degradation of (b) gas-phase benzene and (c) gas-phase methanol over $Fe_2O_3$ nanoparticles and carbon quantum dot/$Fe_2O_3$ nanocomposite. Reprinted with permission from ref 311. Copyright 2011 Royal Society of Chemistry.**

nanocomposites. Similarly, carbon quantum dot/$Fe_2O_3$ hybrids show much higher activity for methanol degradation in comparison to that observed for $Fe_2O_3$ nanoparticles alone.

Recently, nanocomposites of graphene quantum dots and $Fe_3O_4$ nanoparticles have been proposed as a one of the promising peroxidase mimic systems and as a catalyst for removal of phenolic compounds from aqueous solutions.[312] As graphene quantum dots possess a defect-free 2D hexagonal lattice structure and enriched periphery carboxylic groups, they have been found to show much higher intrinsic peroxidase-like capability compared to that of micrometer-sized graphene oxide and improved performance and stability in $H_2O_2$ detection.[313,314] If combined with $Fe_3O_4$ nanoparticles through Fe−O chemical bonds (upon conversion of periphery carboxylic groups into carboxylate groups), electron transfer from electron-rich graphene quantum dots to $Fe_3O_4$ nanoparticles is significantly promoted, maintaining a higher number of $Fe^{2+}$ ions which play a dominant role in the catalytic peroxidase-like activity of $Fe_3O_4$. In addition, it was demonstrated that the magnetic graphene-quantum-dots-based hybrids show better or comparable catalytic efficiencies for some phenolic compounds as compared with those reported for horseradish peroxidase.[312]

*Nanocomposites of Mesoporous Carbon and Iron Oxides: Syntheses and Applications.* There have been several works reporting on embedding iron oxide nanoparticles in the mesoporous carbon matrix so far.[315−322] Mesoporous ordered carbon, frequently denoted as CMK-*n* (where *n* = 1−9), discovered in 1999,[323] has been explored as a suitable candidate, for example, in the field

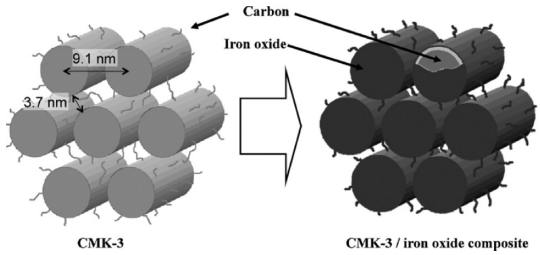


**Figure 38. Schematic picture of an electrode based on mesoporous carbon/iron oxide hybrid. Reprinted with permission from ref 322. Copyright 2011 Elsevier B. V.**

of energy storage and conversion or as an efficient adsorbent of various environment-polluting compounds.[324] Its application potential is encouraged by fascinating properties it shows such as high specific surface area, well-ordered pore structure, tunable mesopores, and pore size with high specific pore volume, hydrophobicity, intrinsic high electrical conductivity, good chemical and thermal stability, and biocompatibility.[324,325] Due to its porous structure, it can accommodate various nano-objects and is thus widely recognized as an important matrix component in the host/guest chemistry.[326] Commonly, mesoporous carbon is synthesized *via* an impregnation method employing well-ordered hexagonal and cubic mesoporous silica materials (*i.e.*, molecular sieves—MCM-48, SBA-1, SBA-15) as hard templates and sucrose as a carbon source.[327,328] To produce host/guest architectures, two strategies are often adopted, that is, either addition of metal ions during the synthesis of mesoporous carbon (one-step procedure) or postsynthetic incorporation of metals into the formed pore network (two- or more-step procedure). To do so, several techniques have been used including a cocasting method,[318] combined hydrolysis and pyrolysis method,[319] combined wet impregnation and calcination procedure,[317] method involving block copolymer self-assembly and carbonization processes,[316] and hydrothermal method.[320] Once assembled, the hybrids show improved properties as a result of synergetic and cooperative effects between the mesoporous carbon and well-dispersed active nanoparticles, extending thus significantly the application potential of the individual hybrid components. In case of nanocomposites based on iron oxides and mesoporous carbon, a number of applications have been envisaged such as electrodes in lithium-ion batteries (see Figure 38),[320,322] magnetically separable adsorbents of toxic elements (*e.g.*, arsenic, chromium),[316,319] and catalysts (*e.g.*, ammonia decomposition, selective oxidation of benzyl alcohol with molecular oxygen).[321,329]

A typical synthetic route toward mesoporous carbon/iron oxide hybrid is shown in Figure 39.[318] First, the mesoporous silica is filled with furfuryl alcohol and iron source; it is then polymerized, leaving small cavities into which $Fe^{3+}$ ions can be adsorbed.

Simultaneously with carbonization, $Fe^{3+}$-containing precursor decomposes into an iron oxide phase. The growth of iron oxide nano-objects is restricted by the channel size of the mesoporous silica and confinement during conversion of the of cross-linked polymer network into solid carbon. In the last step, the silica template is removed by applying NaOH aqueous solution. Depending on the content of $Fe^{3+}$-containing precursor introduced, iron oxide embedded inside the mesoporous carbon shows either nanoparticle (low content) or nanorod-like character as demonstrated by X-ray powder diffraction patterns (see Figure 39). On increasing the iron oxide loading, the iron oxide diffraction peaks get stronger and sharper, indicating growth of larger nanoparticles and nanorods.[318]

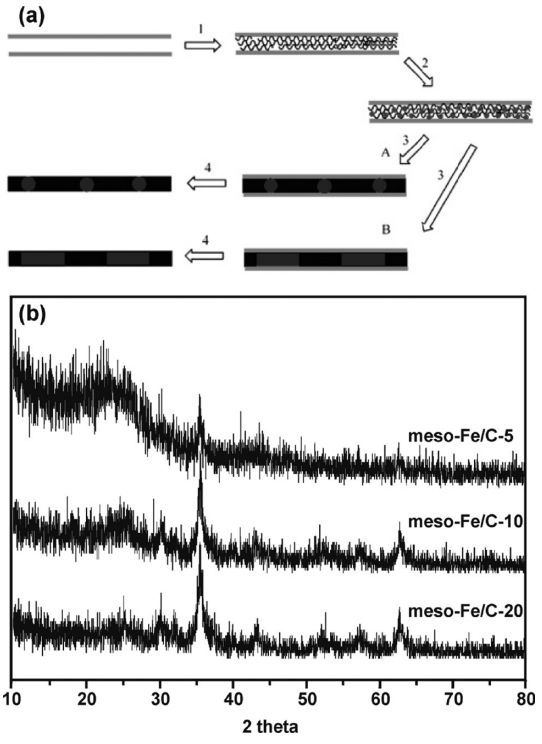


**Figure 39. (a) Scheme of synthetic steps toward mesoporous carbon/iron oxide architecture: (1) addition of furfuryl alcohol inside the pores of mesoporous silica and polymerization; (2) iron ion adsorption; (3) carbonization and formation of iron oxide (A) nanoparticles and/or (B) nanorods inside the pores of the mesoporous carbon; (4) removal of the silica template. (b) X-ray powder diffraction patterns of the mesoporous carbon/iron oxide hybrids with different levels of iron oxide loading (5, 10, and 20 wt %). Reprinted from ref 318. Copyright 2007 American Chemical Society.**

Alternative synthetic procedure of mesoporous carbon/iron oxide nanocomposite is depicted in Figure 40.[321] C-SBA-15 was used as a precursor for mesoporous carbon in order to secure a selective immobilization of iron oxide nanoparticles only in the pores within the tubes (not in the mesopores between the tubes). The preparation route requires three steps, that is, impregnation, drying, and calcination. The selection of the matrix and synthetic conditions provide a high iron oxide loading (up to 12 wt % in a single impregnation step). Moreover, upon leaching of the silica from the precursor, an additional pore system can be opened, enabling a controlled functionalization of the CMK-5 pores. The proposed nanocomposite has been tested as a promising catalyst for ammonia decomposition. The conversion rate, highest reported ever for any Fe-based catalyst employed in this reaction, was explained by high porosity of the CMK-5 support, being beneficial for the mass transfer, and the high dispersion of the iron oxide.[321]

To enhance the storage capacity and electrochemical performance of mesoporous carbon/iron oxide hybrids in lithium-ion batteries, Li *et al.*[320] proposed to use a mixture of $Fe_2O_3$ and $Fe_3O_4$ phases (*i.e.*, $FeO_x$) functionalizing the surface of the tubes from the mesoporous carbon. The synthetic procedure, shown in Figure 41, involves two steps, that is, covering the tube surfaces with a surfactant (CTAB) and hydrothermal process converting Fe-containing precursor into $FeO_x$ phase. As it is evident from Figure 41, the mesoporous carbon/iron oxide hybrid exhibits much better electrochemical performance than mesoporous carbon alone on increasing the current density. Even at the highest current density, the mesoporous carbon/iron oxide nanocomposite maintains a stable charge/discharge capacity of 320 mA h $g^{-1}$, about 5.4 times higher than pure mesoporous carbon. In addition, it is believed that employing the proposed mesoporous carbon/iron oxide architecture may shorten the path lengths for electron transfer and $Li^+$ transport, significantly improving the performance of the electrode.[320] Recently, Xu *et al.*[330] incorporated mesoporous $Fe_2O_3$ particles into mesoporous carbon matrix to improve cycling stability and capability rate. Similarly as $Fe_2O_3$ nanoparticles, mesoporous $Fe_2O_3$ particles show a long cycling life and high-rate performance; additionally, despite much smaller surface area

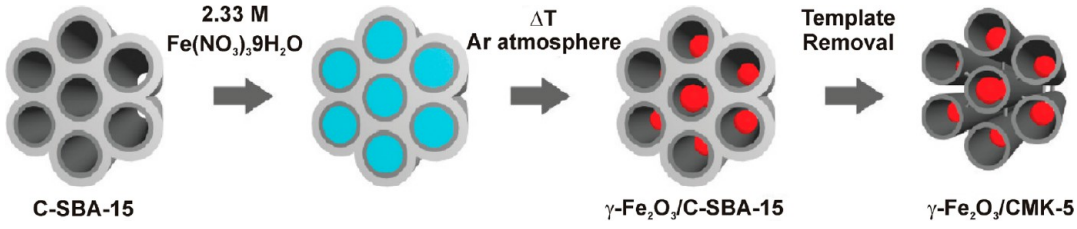


**Figure 40. Scheme of formation of $\gamma$-$Fe_2O_3$ nanoparticles confined inside the pores of CMK-5. Reprinted from ref 321. Copyright 2010 American Chemical Society.**

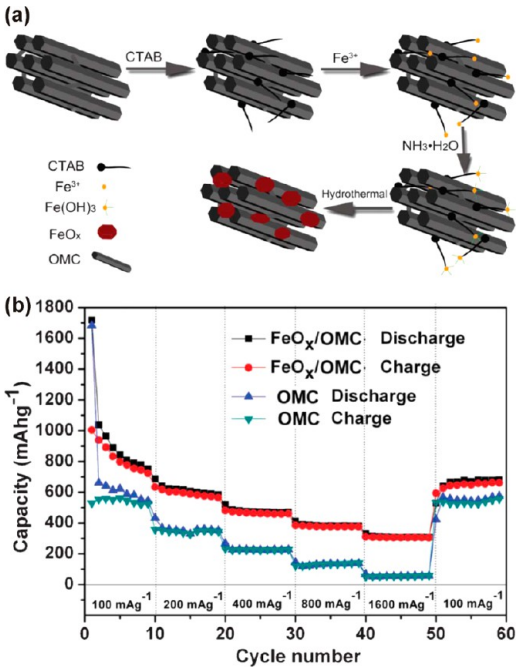


**Figure 41. (a) Schematic representation of preparation steps toward mesoporous carbon/$FeO_x$ hybrid. (b) Rate capacity of the ordered mesoporous carbon (OMC) and OMC/$FeO_x$ nanocomposite. Reprinted with permission from ref 320. Copyright 2013 Royal Society of Chemistry.**

than $Fe_2O_3$ nanoparticles, they have large tapping density and high Coulombic efficiency and provide extra voids for accommodating volume changes during lithium-ion insertion/extraction and relieving structural strain/stress during charge/discharge processes. The hybrid anode showed a high reversible capacity of ~800 mA h $g^{-1}$ maintained over 300 charge/discharge cycles at a current density of 100 mA $g^{-1}$, which is much better than those reported for solid $Fe_2O_3$ nanoparticles incorporated into the mesoporous carbon and/or between the graphene sheets. Thus, two factors have been identified to have a significant effect on the high-rate performance of mesoporous $Fe_2O_3$ nanoparticles, such as fast charge transfer reaction occurring at the large interface between electrode and liquid electrolyte and reduced Li-ion diffusion distances allowing fast kinetics.[330]

However, if iron oxide nanoparticles are incorporated into the pores of the mesoporous carbon or cover its surface, several problems must be faced and overcome in order to prepare hybrids with a desired combination of properties. Most importantly, iron oxide nanoparticles must be distributed homogeneously inside the pores and/or over the surface, must not be embedded into the mesopore walls, and must not aggregate. In addition, the surface of mesoporous carbon is suggested to be coated with a thin carbon layer to avoid the degradation of iron oxide nanoparticles in the environment (particularly in the case when iron oxide nanoparticles are attached to the surface of mesoporous carbon).

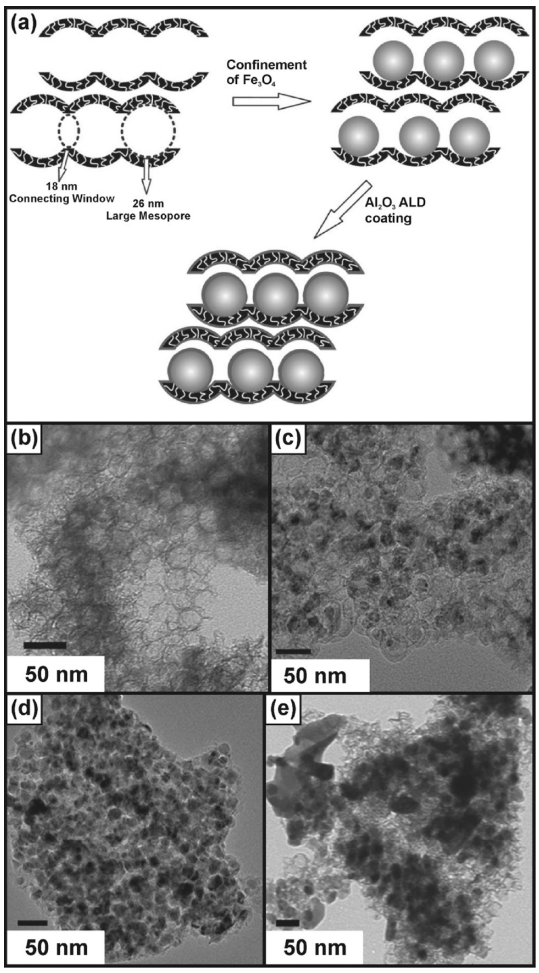


**Figure 42. (a) Scheme of preparation route toward carbon foam/iron oxide composite coated with $Al_2O_3$ thin layer for application as electrodes in lithium batteries (ALD = atomic layer deposition). (b–e) TEM images showing incorporation of $Fe_3O_4$ nanoparticles inside the pores of carbon foam (b, without loading; c–e, different loading level: 45, 61, and 71 wt %, respectively). Reprinted with permission from ref 333. Copyright 2011 Wiley VCH Verlag GmbH & Co. KGaA, Weinheim.**

*Nanocomposites of Carbon Foam and Iron Oxides: Syntheses and Applications.* Mesoporous carbon offers pores with ~3–4 nm, which limits the iron oxide loading capability and access of electrolyte to active nano-objects confined inside the pores. Thus, carbon foam has been suggested as an alternative for immobilization of iron oxide nanoparticles.[331,332] Carbon foam has a larger pore size (>20 nm) and large pore volume (>1.8 $cm^3$ $g^{-1}$). In addition, the pores of the carbon foam are opened in all directions owing to the inherently isotropic foam pore structure, making it more feasible, for example, for an electrolyte to reach iron oxide nanoparticles. An example of the preparation route toward a carbon foam/iron oxide hybrid, based on host/guest approach, is depicted in Figure 42.[333] The synthetic procedure involves three steps: (i) preparation of carbon foam with large interconnected pores from mesocellular silica as a hard

template; (ii) impregnation of pores by Fe-containing precursor (*e.g.*, $Fe(NO_3)_3 \cdot 9H_2O$); and (iii) heat treatment under Ar atmosphere inducing decomposition of Fe-containing precursor to $Fe_3O_4$. It turns out that the loading level may reach up to ~71 wt %. In order to enhance durability and rate capability of the carbon foam/iron oxide nanocomposite, an $Al_2O_3$ thin layer was used as a hybrid coating. A similar strategy to produce carbon foam/iron oxide nanocomposite is shown in Figure 43.[334] In this case, the iron oxide loading level was found to reach ~79 wt %. Several possible applications of carbon foam/iron oxide hybrids have been proposed, including anode materials in lithium-ion batteries[335,336] or magnetically recoverable Fenton catalyst for removal of phenol and arsenic (see Figure 44).[335]

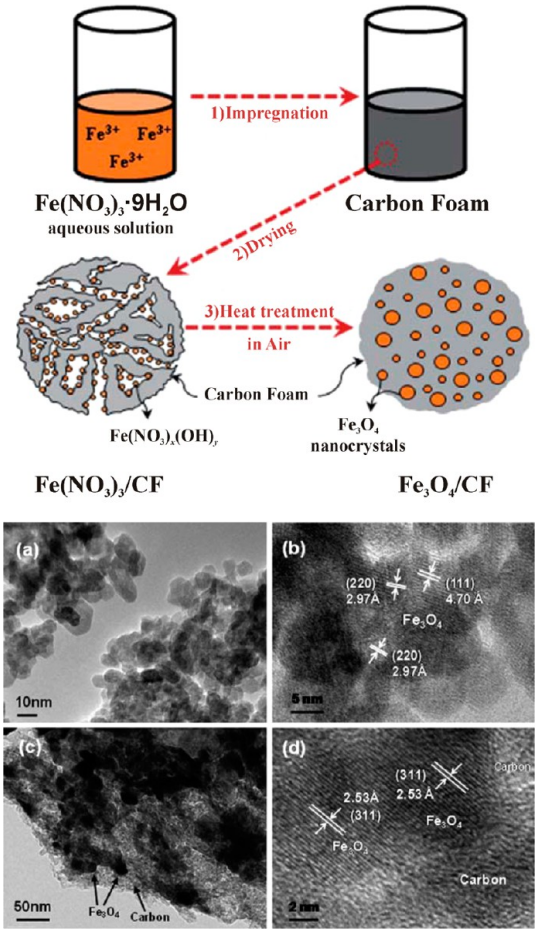


**Figure 43. (Top) Scheme of preparation route toward carbon foam (CF)/$Fe_3O_4$ hybrid. (Bottom) TEM images of $Fe_3O_4$ nanoparticles synthesized by the hydrothermal method (a,b), and the *in situ* formed $Fe_3O_4$ nanoparticles inside the pores of the carbon foam (c,d). Reprinted with permission from ref 334. Copyright 2011 Royal Society of Chemistry.**

*Iron Oxide/Carbon Core/Shell Nanoarchitectures: Syntheses and Applications.* Recently, a new architecture comprising an iron oxide core and a carbon shell has been developed.[336−338] These core/shell nanoparticles can be fabricated employing various techniques including chemical vapor deposition,[339] laser ablation,[340] arc-discharge,[341] sol−gel assembly process,[337] or salt template process.[338] They can be synthesized in one step (particularly in the cases when a single precursor is used as a source for metal oxide core and graphitic shell, such as a metal−oleate complex) or in two steps (independent synthesis of iron oxide nanoparticles followed by coating with carbon). The advantage of one-step procedures over the two-step routes mainly lies in a possibility to tune the average particle size and controllably alter the particle size distribution. This is achieved by the so-called "wrap-bake-peel" process,[342] which secures preservation of the size and shapes of the iron oxide nanocrystals during the heat treatment. The iron oxide/carbon core/shell nanoparticles have already been successfully tested as lithium-ion battery anodes,[338] showing a high performance comparable to that exhibited by graphene/iron oxide nanoarchitectures. In addition, $sp^2$ carbon coatings (*e.g.*, graphene sheets) can be covalently and noncovalently functionalized with diverse functional groups so that the iron oxide/carbon core/shell nanoparticles become dispersible in a physiological

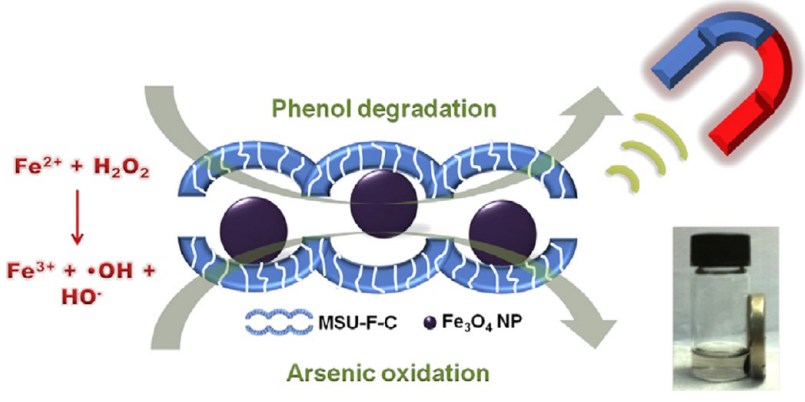


**Figure 44. Scheme showing mechanism of arsenic removal from aqueous solution employing carbon foam (MSU-F-C)/$Fe_3O_4$ hybrid. The inset shows removal of the (MSU-F-C)/$Fe_3O_4$ hybrid with adsorbed arsenic by a hand magnet. Reprinted with permission from ref 335. Copyright 2012 Elsevier Ltd.**

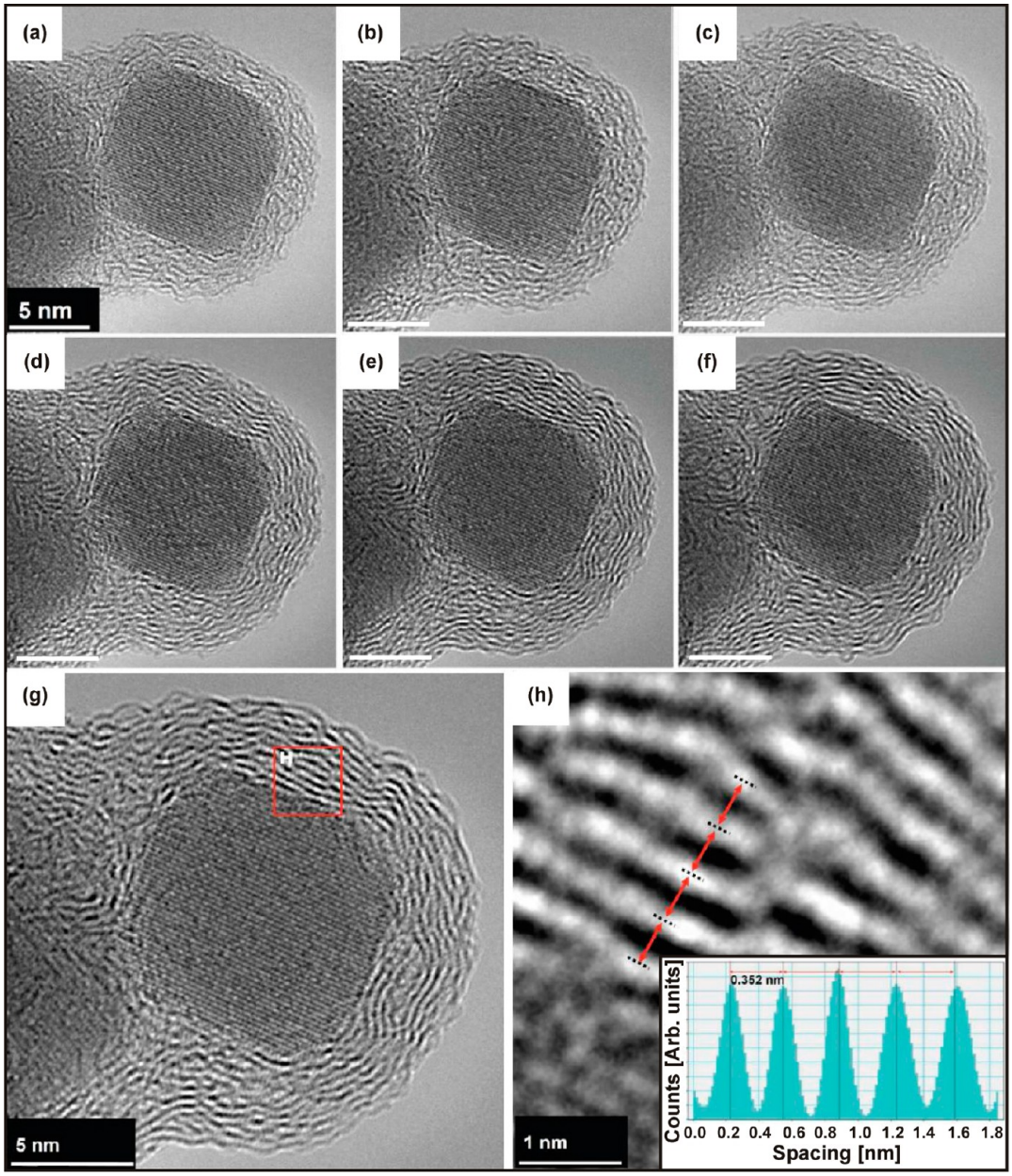


**Figure 45. (a−h) TEM images displaying evolution of graphene sheets on the surface of iron oxide nanoparticles from oleic acid coating upon thermal treatment under dynamic vacuum induced by electron irradiation. The inset in panel (h) shows the spacing between the individual graphene sheets on the surface of iron oxide nanoparticles. Reprinted from ref 336. Copyright 2012 American Chemical Society.**

environment and thus more biocompatible. This opens their possible exploitation in medical fields, especially in those focused on targeted delivery of biologically active molecules to desired sites in a living organism (*e.g.*, targeted delivery of anticancer drugs).

Figure 45 shows a formation of iron oxide/carbon core/shell nanoparticles by *in situ* graphitization of oleic acid on iron oxide nanoparticles.[336] Iron oxide nanoparticles were prepared *a priori* by a colloid chemistry approach using iron oleate complex (reaction product of iron(III) chloride and sodium oleate) as a precursor. The wet chemical synthesis yields nanoparticles with core/shell architecture when the core is made up of $\gamma$-$Fe_2O_3$ and the shell is of oleic acid nature. The shell is rich in carbon, and upon thermal treatment under dynamic vacuum, it is graphitized to form a few-layer graphene.

Alternatively, iron oxide/carbon core/shell hybrids can be prepared by adopting the combined sol−gel and pyrolysis procedure schematically described in Figure 46.[337] It involves three steps: (i) assembly of $Fe(CO)_5$/SBA-16 reaction system by a surfactant template route; (ii) thermally induced formation of iron oxide nanoparticles surrounded by a layer of carbon originating from carbonization of the F127 surfactant; and (iii) removal of silica by 5% HF. The resulting hybrid

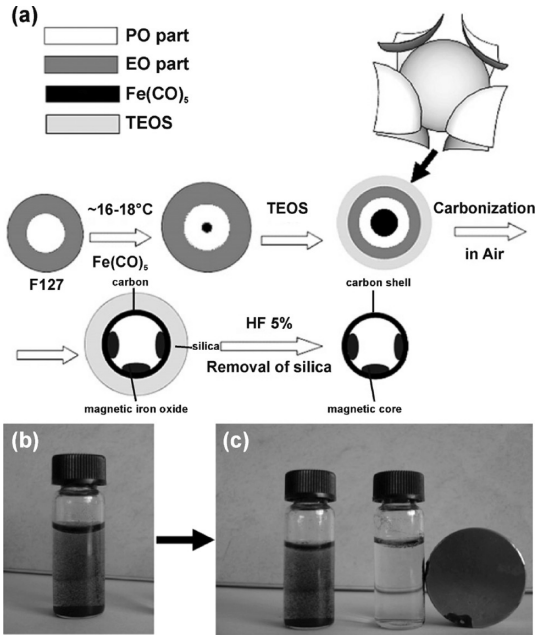


**Figure 46. (a) Scheme describing the synthetic steps toward iron oxide/carbon core/shell nanoparticles. Methylene blue aqueous solution (b) before and (c) after adsorption on the surface of iron oxide/carbon core/shell nanoparticles and their subsequent separation from solution by a magnet. Reprinted with permission from ref 337. Copyright 2009 Royal Society of Chemistry.**

shows a significant adsorption capability and can thus act as a recoverable adsorbent; it was successfully tested for removing methylene blue dye from an aqueous solution (see Figure 46).[337]

## SUMMARY AND FUTURE CHALLENGES

Herein we have shown the wide applicability and versatility of magnetic nanocarbon materials in fields such as water remediation, biosensing, bioimaging, drug delivery, theranostics, and Li-ion batteries. This versatility can be explained by the synergy between the suitable nanocarbon source and the magnetic material.

In the environmental applications, it turns out that iron oxides mostly play a passive role in the hybrid. They equip the nanocomposite with a property to be magnetically separable once pollutants of organic or inorganic nature are adsorbed on the surface provided by the carbon counterpart. This is highly desirable in the case when carbon nanotubes, due to their huge surface area and high reactivity, are used as adsorbents for the removal of toxic chemicals from water and gases. If not magnetically functionalized, it is difficult to separate them from aqueous solutions; most importantly, they show toxicity and may enter into cells, causing damage to plants, animals, and humans once released to the environment. Alternatively, mesoporous carbon or graphene may substitute the adsorption function of carbon nanotubes; however, higher efficiency and lower toxicity are redeemed by high cost, low yields, and purity.

On the other hand, iron oxides are active in carbon-based nanocomposites designed as promising materials in energy storage devices, sensing, and medical applications. In medical fields, both iron oxide and carbon components equally participate in the function of the hybrid; while carbon allotropes bring adsorption capability, fluorescent property, photocatalytic power or photo- and electrochemical features, iron oxides work as imaging and magnetically triggered therapeutic agents (*e.g.*, advanced architectures for combined targeted drug delivery and hyperthermia treatment). In lithium-ion batteries, iron oxides, possessing high theoretical specific capacities, serve as electrochemically active constituents providing intercalation and deintercalation of lithium ions during charging and discharging processes. However, if iron oxide nanoparticles are used alone as anode materials, three main problems are faced: (i) low electric conductivity; (ii) large stress and volume changes during charge/discharge processes disrupting the electric contact and causing structural collapse; and (iii) aggregation of iron/iron oxide nanoparticles during the cycle process (due to their large surface area and activity). Exploitation of carbon-based materials as a support for iron oxide nanoparticles improves electric conductivity, provides space to accommodate stress and volume changes, and prevents nanoparticle aggregation, preserving thus high reversible capacities (~1000 mA h $g^{-1}$) and cycling performance (>150 cycles). Contrary to other potentially exploitable electrochemically active compounds such as $Co_3O_4$, $SnO_2$, $Cu_2O$, and NiO, iron oxides offer eco-friendliness and are easily available and inexpensive, making them the most promising candidates for lithium storage.

It is believed that, in the future, the efficiency and applicability of many of these magnetic carbon-based nanocomposites can be enhanced by improving synergy between the hybrid components. This can be achieved by introduction of another component, functionalization of the carbon surface, control of magnetic particle loading and distribution (uniformly over the carbon allotrope surface or specifically around the edges), *etc*. In addition, the synergetic and cooperative effects are expected to be more promoted in the case of covalent and selective functionalization approaches when both counterparts actively affect each other, providing the possibility to tune their properties with respect to the intended practical exploitation of the nanocomposite. Through covalent linkage, magnetic nanoparticles may alter a magnetic state of various carbon allotropes (*e.g.*, similarly as doping of foreign atoms into the structure of carbon allotropes). Moreover, by covalent interactions, hybrid components are firmly bound to each other, avoiding their separation and release to the environment contrary to the nanocomposites in which the counterparts are held with each other by noncovalent interactions or simple physical adsorption.

Multiple research avenues remain unexplored in the field of magnetic carbon-based hybrids. Some of the areas include the introduction of magnetic iron oxide nanoparticles into fullerenes, magnetic functionalization of nanodiamonds toward theranostic applications, and enhancement and tuning of the intrinsic magnetic properties of carbon nanotubes. Thus, within these unchartered research areas, as well as the in-depth exploration of the versatility of carbon/iron oxide nanocomposites already synthesized, remarkable and cutting-edge research breakthroughs are expected to emerge.

*Conflict of Interest:* The authors declare no competing financial interest.

*Acknowledgment.* The authors acknowledge the support by the Operational Program Research and Development for Innovations—European Regional Development Fund (CZ.1.05/2.1.00/03.0058) and Operational Program Education for Competitiveness—European Social Fund (CZ.1.07/2.3.00/20.0017, CZ.1.07/2.3.00/20.0058, and CZ.1.07/2.3.00/20.0155) of the Ministry of Education, Youth and Sports of the Czech Republic, and the Korea National Research Foundation (National Honor Scientist Program: 2010-0020414).

## REFERENCES AND NOTES

1. Kroto, H. W.; Heath, J. R.; Obrien, S. C.; Curl, R. F.; Smalley, R. E. $C_{60}$ — Buckminsterfullerene. *Nature* **1985**, *318*, 162–163.
2. Danilenko, V. V. On the History of the Discovery of Nanodiamond Synthesis. *Phys. Solid State* **2004**, *46*, 595–599.
3. Xu, X. Y.; Ray, R.; Gu, Y. L.; Ploehn, H. J.; Gearheart, L.; Raker, K.; Scrivens, W. A. Electrophoretic Analysis and Purification of Fluorescent Single-Walled Carbon Nanotube Fragments. *J. Am. Chem. Soc.* **2004**, *126*, 12736–12737.
4. Sun, Y. P.; Zhou, B.; Lin, Y.; Wang, W.; Fernando, K. A. S.; Pathak, P.; Meziani, M. J.; Harruff, B. A.; Wang, X.; Wang, H. F.; *et al.* Quantum-Sized Carbon Dots for Bright and Colorful Photoluminescence. *J. Am. Chem. Soc.* **2006**, *128*, 7756–7757.
5. Iijima, S. Helical Microtubiles of Graphitic Carbon. *Nature* **1991**, *354*, 56–58.
6. Helveg, S.; Lopez-Cartes, C.; Sehested, J.; Hansen, P. L.; Clausen, B. S.; Rostrup-Nielsen, J. R.; Abild-Pedersen, F.; Norskov, J. K. Atomic-Scale Imaging of Carbon Nanofibre Growth. *Nature* **2004**, *427*, 426–429.
7. Nasibulin, A. G.; Pikhitsa, P. V.; Jiang, H.; Brown, D. P.; Krasheninnikov, A. V.; Anisimov, A. S.; Queipo, P.; Moisala, A.; Gonzalez, D.; Lientschnig, G.; *et al.* A Novel Hybrid Carbon Material. *Nat. Nanotechnol.* **2007**, *2*, 156–161.
8. Novoselov, K. S.; Geim, A. K.; Morozov, S. V.; Jiang, D.; Zhang, Y.; Dubonos, S. V.; Grigorieva, I. V.; Firsov, A. A. Electric Field Effect in Atomically Thin Carbon Films. *Science* **2004**, *306*, 666–669.
9. Kim, K. S.; Zhao, Y.; Jang, H.; Lee, S. Y.; Kim, J. M.; Kim, K. S.; Ahn, J. H.; Kim, P.; Choi, J. Y.; Hong, B. H. Large-Scale Pattern Growth of Graphene Films for Stretchable Transparent Electrodes. *Nature* **2009**, *457*, 706–710.
10. Li, X.; Cai, W.; An, J.; Kim, S.; Nah, J.; Yang, D.; Piner, R.; Velamakanni, A.; Jung, I.; Tutuc, E.; *et al.* Large-Area Synthesis of High-Quality and Uniform Graphene Films on Copper Foils. *Science* **2009**, *324*, 1312–1314.
11. Iijima, S.; Yudasaka, M.; Yamada, R.; Bandow, S.; Suenaga, K.; Kokai, F.; Takahashi, K. Nano-aggregates of Single-Walled Graphitic Carbon Nano-horns. *Chem. Phys. Lett.* **1999**, *309*, 165–170.
12. Son, Y.-W.; Cohen, M. M.; Louie, S. G. Half-Metallic Graphene Nanoribbons. *Nature* **2006**, *444*, 347–349.
13. Cai, J.; Ruffieux, P.; Jaafar, R.; Bieri, M.; Braun, T.; Blankenburg, S.; Muoth, M.; Seitsonen, A. P.; Saleh, M.; Feng, X.; *et al.* Atomically Precise Bottom-Up Fabrication of Graphene Nanoribbons. *Nature* **2010**, *466*, 470–473.
14. Chen, Y. C.; Oteyza, D. G. D.; Pedramrazi, Z.; Chen, C.; Fischer, F. R.; Crommie, M. F. Tuning the Band Gap of Graphene Nanoribbons Synthesized from Molecular Precursors. *ACS Nano* **2013**, *7*, 6123–6128.
15. Rode, A. V.; Gamaly, E. G.; Christy, A. G.; Gerald, J. G. F.; Hyde, S. T.; Elliman, R. G.; Luther-Davies, B.; Veinger, A. I.; Androulakis, J.; Giapintzakis, J. Unconventional Magnetism in All-Carbon Nanofoam. *Phys. Rev. B* **2004**, *70*, 054407.
16. Sun, L. T.; Gong, J. L.; Zhu, D. Z.; Zhu, Z. Y.; He, S. X. Diamond Nanorods from Carbon Nanotubes. *Adv. Mater.* **2004**, *16*, 1849–1853.
17. Barnard, A. S.; Snook, I. K. Phase Stability of Nanocarbon in One Dimension: Nanotubes *versus* Diamond Nanowires. *J. Chem. Phys.* **2004**, *120*, 3817–3821.
18. Zhou, X. F.; Qian, G. R.; Dong, X. A.; Zhang, L. X.; Tian, Y. J.; Wang, H. T. *Ab Initio* Study of the Formation of Transparent Carbon under Pressure. *Phys. Rev. B* **2010**, *82*, 134126.
19. Sheng, X. L.; Yan, Q. B.; Ye, F.; Zheng, Q. R.; Su, G. T-Carbon: A Novel Carbon Allotrope. *Phys. Rev. Lett.* **2011**, *106*, 155703.
20. Li, Q.; Ma, Y. M.; Oganov, A. R.; Wang, H. B.; Wang, H.; Xu, Y.; Cui, T.; Mao, H. K.; Zou, G. T. Superhard Monoclinic Polymorph of Carbon. *Phys. Rev. Lett.* **2009**, *102*, 175506.
21. Liu, M.; Artyukhov, V. I.; Lee, H.; Xu, F.; Yakobson, B. I. Carbyne from First Principles: Chain of C Atoms, a Nanorod or a Nanorope. *ACS Nano* **2013**, *7*, 10075–10082.
22. Openov, L. A.; Elesin, V. F. Prismane $C_8$: A New Form of Carbon? *JETP Lett.* **1998**, *68*, 726–731.
23. Tasis, D.; Tagmatarchis, N.; Bianco, A.; Prato, M. Chemistry of Carbon Nanotubes. *Chem. Rev.* **2006**, *106*, 1105–1136.
24. Diederich, F.; Thilgen, C. Covalent Fullerene Chemistry. *Science* **1996**, *271*, 317–323.
25. Nakamura, E.; Isobe, H. Functionalized Fullerenes in Water. The First 10 Years of Their Chemistry, Biology, and Nanoscience. *Acc. Chem. Res.* **2003**, *36*, 807–815.
26. Allen, M. J.; Tung, V. C.; Kaner, R. B. Honeycomb Carbon: A Review of Graphene. *Chem. Rev.* **2010**, *110*, 132–145.
27. Georgakilas, V.; Otyepka, M.; Bourlinos, A. B.; Chandra, V.; Kim, N.; Kemp, K. C.; Hobza, P.; Zboril, R.; Kim, K. S. Functionalization of Graphene: Covalent and Noncovalent Approaches, Derivatives and Applications. *Chem. Rev.* **2012**, *112*, 6156–6214.
28. Chen, D.; Feng, H. B.; Li, J. H. Graphene Oxide: Preparation, Functionalization, and Electrochemical Applications. *Chem. Rev.* **2012**, *112*, 6027–6053.
29. Yazyev, O. V. Emergence of Magnetism in Graphene Materials and Nanostructures. *Rep. Prog. Phys.* **2010**, *73*, 056501.
30. Kuzemsky, A. L. Unconventional and Exotic Magnetism in Carbon-Based Structures and Related Materials. *Int. J. Mod. Phys. B* **2013**, *27*, 1330007.
31. Lu, A. H.; Salabas, E. L.; Schuth, F. Magnetic Nanoparticles: Synthesis, Protection, Functionalization, and Application. *Angew. Chem., Int. Ed.* **2007**, *46*, 1222–1244.
32. Gupta, A. K.; Gupta, M. Synthesis and Surface Engineering of Iron Oxide Nanoparticles for Biomedical Applications. *Biomaterials* **2005**, *26*, 3995–4021.
33. Weissleder, R.; Stark, D. D.; Engelstad, B. L.; Bacon, B. R.; Compton, C. C.; White, D. L.; Jacobs, P.; Lewis, J. Superparamagnetic Iron Oxide: Pharmacokinetics and Toxicity. *Am. J. Roentgenol.* **1989**, *152*, 167–173.
34. Prato, M. [60]Fullerene Chemistry for Materials Science Applications. *J. Mater. Chem.* **1997**, *7*, 1097–1109.
35. Qiao, R.; Roberts, A. P.; Mount, A. S.; Klaine, S. J.; Ke, P. C. Translocation of $C_{60}$ and Its Derivatives Across a Lipid Bilayer. *Nano Lett.* **2007**, *7*, 614–619.
36. Eletskii, A. V.; Smirnov, B. M. Fullerenes. *Usp. Fiz. Nauk* **1993**, *163*, 33–60.

37. Diederich, F.; Rubin, Y. Synthetic Approaches toward Molecular and Polymeric Carbon Allotropes. *Angew. Chem., Int. Ed. Engl.* **1992**, *31*, 1101–1123.
38. Wang, Y.; Cheng, L. T. Nonlinear Optical Properties of Fullerenes and Charge-Transfer Complexes of Fullerenes. *J. Phys. Chem.* **1992**, *96*, 1530–1532.
39. Kawauchi, M.; Kawauchi, T.; Takeichi, T. Solubilization of [60]Fullerene Owing to Inclusion Complex Formation between Syndiotactic Poly(methyl methacrylate) and the Fullerenes in Polar Solvents. *Macromolecules* **2009**, *42*, 6136–6140.
40. Hebard, A. F.; Rosseinsky, M. J.; Haddon, R. C.; Murphy, D. W.; Glarum, S. H.; Palstra, T. T. M.; Ramirez, A. P.; Kortan, A. R. Superconductivity at 18 K in Potassium-Doped $C_{60}$. *Nature* **1991**, *350*, 600–601.
41. Stephens, P. W.; Cox, D.; Lauher, J. W.; Mihaly, L.; Wiley, J. B.; Allemand, P. M.; Hirsch, A.; Holczer, K.; Li, Q.; Thompson, J. D.; *et al.* Lattice Structure of the Fullerene Ferromagnet TDAE-$C_{60}$. *Nature* **1992**, *355*, 331–332.
42. Allemand, P. M.; Khemani, K. C.; Koch, A.; Wudl, F.; Holczer, K.; Donovan, S.; Gruner, G.; Thompson, J. D. Organic Molecular Soft Ferromagnetism in a Fullerene-$C_{60}$. *Science* **1991**, *253*, 301–303.
43. Bosi, S.; Da Ros, T.; Spalluto, G.; Prato, M. Fullerene Derivatives: An Attractive Tool for Biological Applications. *Eur. J. Med. Chem.* **2003**, *38*, 913–923.
44. Sijbesma, R.; Srdanov, G.; Wudl, F.; Castoro, J. A.; Wilkins, C.; Friedman, S. H.; Decamp, D. L.; Kenyon, G. L. Synthesis of a Fullerene Derivative for the Inhibition of HIV Enzymes. *J. Am. Chem. Soc.* **1993**, *115*, 6510–6512.
45. Lyon, D. Y.; Fortner, J. D.; Sayes, C. M.; Colvin, V. L.; Hughes, J. B. Bacterial Cell Association and Antimicrobial Activity of a $C_{60}$ Water Suspension. *Environ. Toxicol. Chem.* **2005**, *24*, 2757–2762.
46. He, Z. C.; Zhong, C. M.; Su, S. J.; Xu, M.; Wu, H. B.; Cao, Y. Enhanced Power-Conversion Efficiency in Polymer Solar Cells Using an Inverted Device Structure. *Nat. Photonics* **2012**, *6*, 591–595.
47. Peet, J.; Kim, J. Y.; Coates, N. E.; Ma, W. L.; Moses, D.; Heeger, A. J.; Bazan, G. C. Efficiency Enhancement in Low-Bandgap Polymer Solar Cells by Processing with Alkane Dithiols. *Nat. Mater.* **2007**, *6*, 497–500.
48. Brabec, C. J.; Gowrisanker, S.; Halls, J. J. M.; Laird, D.; Jia, S. J.; Williams, S. P. Polymer-Fullerene Bulk-Heterojunction Solar Cells. *Adv. Mater.* **2010**, *22*, 3839–3856.
49. Janssen, R. A. J.; Hummelen, J. C.; Saricifici, N. S. Polymer-Fullerene Bulk Heterojunction Solar Cells. *MRS Bull.* **2005**, *30*, 33–36.
50. Zhong, Y. W.; Matsuo, Y.; Nakamura, E. Lamellar Assembly of Conical Molecules Possessing a Fullerene Apex in Crystals and Liquid Crystals. *J. Am. Chem. Soc.* **2007**, *129*, 3052–3053.
51. Mihailetchi, V. D.; Koster, L. J. A.; Hummelen, J. C.; Blom, P. W. M. Photocurrent Generation in Polymer-Fullerene Bulk Heterojunctions. *Phys. Rev. Lett.* **2004**, *93*, 216601.
52. Sherigara, B. S.; Kutner, W.; D'Souza, F. Electrocatalytic Properties and Sensor Applications of Fullerenes and Carbon Nanotubes. *Electroanalysis* **2003**, *15*, 753–772.
53. Iijima, S.; Ichihashi, T. Single-Shell Carbon Nanotubes of 1-nm Diameter. *Nature* **1993**, *363*, 603–605.
54. Ajayan, P. M. Nanotubes from Carbon. *Chem. Rev.* **1999**, *99*, 1787–1799.
55. Hong, B. H.; Small, J. P.; Purewal, M. S.; Mullokandov, A.; Sfeir, M. Y.; Wang, F.; Lee, J. Y.; Heinz, T. F.; Brus, L. E.; Kim, P.; *et al.* Extracting Subnanometer Single Shells from Ultralong Multiwalled Carbon Nanotubes. *Proc. Natl. Acad. Sci. U.S.A.* **2005**, *102*, 14155–14158.
56. Hong, B. H.; Lee, J. Y.; Beetz, T.; Zhu, Y.; Kim, P.; Kim, K. S. Quasi-continuous Growth of Ultralong Carbon Nanotube Arrays. *J. Am. Chem. Soc.* **2005**, *127*, 15336–15337.
57. Dai, H. Carbon Nanotubes: Synthesis, Integration, and Properties. *Acc. Chem. Res.* **2002**, *35*, 1035–1044.
58. Thostenson, E. T.; Ren, Z.; Chou, T.-W. Advances in the Science and Technology of Carbon Nanotubes and Their Composites: A Review. *Compos. Sci. Technol.* **2001**, *61*, 1899–1912.
59. Charlier, J. C.; Blase, X.; Roche, S. Electronic and Transport Properties of Nanotubes. *Rev. Mod. Phys.* **2007**, *79*, 677–732.
60. Andrews, R.; Jacques, D.; Qian, D. L.; Rantell, T. Multiwall Carbon Nanotubes: Synthesis and Application. *Acc. Chem. Res.* **2002**, *35*, 1008–1017.
61. Wu, H. C.; Chang, X. L.; Liu, L.; Zhao, F.; Zhao, Y. L. Chemistry of Carbon Nanotubes in Biomedical Applications. *J. Mater. Chem.* **2010**, *20*, 1036–1052.
62. Bockrath, M.; Cobden, D. H.; McEuen, P. L.; Chopra, N. G.; Zettl, A.; Thess, A.; Smalley, R. E. Single-Electron Transport in Ropes of Carbon Nanotubes. *Science* **1997**, *275*, 1922–1925.
63. White, C. T.; Todorov, T. N. Carbon Nanotubes as Long Ballistic Conductors. *Nature* **1998**, *393*, 240–242.
64. Langer, L.; Bayot, V.; Grivei, E.; Issi, J. P.; Heremans, J. P.; Olk, C. H.; Stockman, L.; Van Haesendonck, C.; Bruynseraede, Y. Quantum Transport in a Multiwalled Carbon Nanotube. *Phys. Rev. Lett.* **1996**, *76*, 479–482.
65. Liu, K. H.; Hong, X. P.; Wu, M. H.; Xiao, F. J.; Wang, W. L.; Bai, X. D.; Ager, J. W.; Aloni, S.; Zettl, A.; Wang, E. G.; *et al.* Quantum-Coupled Radial-Breathing Oscillations in Double-Walled Carbon Nanotubes. *Nat. Commun.* **2013**, *4*, 1375.
66. Geim, A. K.; Novoselov, K. S. The Rise of Graphene. *Nat. Mater.* **2007**, *6*, 183–191.
67. Zhu, Y. W.; Murali, S.; Cai, W. W.; Li, X. S.; Suk, J. W.; Potts, J. R.; Ruoff, R. S. Graphene and Graphene Oxide: Synthesis, Properties, and Applications. *Adv. Mater.* **2010**, *22*, 3906–3924.
68. Rao, C. N. R.; Sood, A. K.; Subrahmanyam, K. S.; Govindaraj, A. Graphene: The New Two-Dimensional Nanomaterial. *Angew. Chem., Int. Ed.* **2009**, *48*, 7752–7777.
69. Castro Neto, A. H.; Guinea, F.; Peres, N. M. R.; Novoselov, K. S.; Geim, A. K. The Electronic Properties of Graphene. *Rev. Mod. Phys.* **2009**, *81*, 109–162.
70. Novoselov, K. S.; Geim, A. K.; Morozov, S. V.; Jiang, D.; Katsnelson, M. I.; Grigorieva, I. V.; Dubonos, S. V.; Firsov, A. A. Two-Dimensional Gas of Massless Dirac Fermions in Graphene. *Nature* **2005**, *438*, 197–200.
71. Myung, S.; Park, J.; Lee, H.; Kim, K. S.; Hong, S. Ambipolar Memory Devices Based on Reduced Graphene Oxide and Nanoparticles. *Adv. Mater.* **2010**, *22*, 2045–2049.
72. Zhang, Y. B.; Tan, Y. W.; Stormer, H. L.; Kim, P. Experimental Observation of the Quantum Hall Effect and Berry's Phase in Graphene. *Nature* **2005**, *438*, 201–204.
73. Schedin, F.; Geim, A. K.; Morozov, S. V.; Hill, E. W.; Blake, P.; Katsnelson, M. I.; Novoselov, K. S. Detection of Individual Gas Molecules Adsorbed on Graphene. *Nat. Mater.* **2007**, *6*, 652–655.
74. Kim, W. Y.; Kim, K. S. Prediction of Very Large Values of Magnetoresistance in a Graphene Nanoribbon Device. *Nat. Nanotechnol.* **2008**, *3*, 408–412.
75. Min, S. K.; Kim, W. Y.; Cho, Y.; Kim, K. S. Fast DNA Sequencing with a Graphene-Based Nanochannel Device. *Nat. Nanotechnol.* **2011**, *6*, 162–165.
76. Rajan, A. C.; Rezapour, M. R.; Yun, J.; Cho, Y.; Cho, W. J.; Min, S. K.; Lee, G.; Kim, K. S. Two Dimensional Molecular Electronics Spectroscopy for Molecular Fingerprinting, DNA Sequencing, and Cancerous DNA Recognition. *ACS Nano* **2014**, *8*, 1827–1833.
77. Loh, K. P.; Bao, Q. L.; Anga, P. K.; Yanga, J. X. The Chemistry of Graphene. *J. Mater. Chem.* **2010**, *20*, 2277–2289.
78. Karlický, F.; Datta, K. K. R.; Otyepka, M.; Zbořil, R. Halogenated Graphenes: Rapidly Growing Family of Graphene Derivatives. *ACS Nano* **2013**, *8*, 6434–6464.
79. Bae, S.; Kim, H.; Lee, Y.; Xu, X. F.; Park, J. S.; Zheng, Y.; Balakrishnan, J.; Lei, T.; Kim, H. R.; Song, Y. I.; *et al.* Roll-To-Roll Production of 30-Inch Graphene Films for Transparent Electrodes. *Nat. Nanotechnol.* **2010**, *5*, 574–578.
80. Li, X. L.; Wang, X. R.; Zhang, L.; Lee, S. W.; Dai, H. J. Chemically Derived, Ultrasmooth Graphene Nanoribbon Semiconductors. *Science* **2008**, *319*, 1229–1232.

81. Tapaszto, L.; Dobrik, G.; Lambin, P.; Biro, L. P. Tailoring the Atomic Structure of Graphene Nanoribbons by Scanning Tunnelling Microscope Lithography. *Nat. Nanotechnol.* **2008**, *3*, 397–401.
82. Lee, W. H.; Park, J.; Kim, Y.; Kim, K. S.; Hong, B. H.; Cho, K. Control of Graphene Field-Effect Transistors by Interfacial Hydrophobic Self-Assembled Monolayers. *Adv. Mater.* **2011**, *23*, 3460–3464.
83. Park, J.; Lee, W. H.; Huh, S.; Sim, S. H.; Kim, S. B.; Cho, K.; Hong, B. H.; Kim, K. S. Work-Function Engineering of Graphene Electrodes by Self-Assembled Monolayers for High-Performance Organic Field-Effect Transistors. *J. Phys. Chem. Lett.* **2011**, *2*, 841–845.
84. Ekiz, O. O.; Urel, M.; Guner, H.; Mizrak, A. K.; Dana, A. Reversible Electrical Reduction and Oxidation of Graphene Oxide. *ACS Nano* **2011**, *5*, 2475–2482.
85. Hecht, D. S.; Hu, L. B.; Irvin, G. Emerging Transparent Electrodes Based on Thin Films of Carbon Nanotubes, Graphene, and Metallic Nanostructures. *Adv. Mater.* **2011**, *23*, 1482–1513.
86. Liu, Z. F.; Liu, Q.; Huang, Y.; Ma, Y. F.; Yin, S. G.; Zhang, X. Y.; Sun, W.; Chen, Y. S. Organic Photovoltaic Devices Based on a Novel Acceptor Material: Graphene. *Adv. Mater.* **2008**, *20*, 3924–3930.
87. Wu, J. B.; Agrawal, M.; Becerril, H. A.; Bao, Z. N.; Liu, Z. F.; Chen, Y. S.; Peumans, P. Organic Light-Emitting Diodes on Solution-Processed Graphene Transparent Electrodes. *ACS Nano* **2010**, *4*, 43–48.
88. Liu, M.; Yin, X. B.; Ulin-Avila, E.; Geng, B. S.; Zentgraf, T.; Ju, L.; Wang, F.; Zhang, X. A Graphene-Based Broadband Optical Modulator. *Nature* **2011**, *474*, 64–67.
89. Stoller, M. D.; Park, S. J.; Zhu, Y. W.; An, J. H.; Ruoff, R. S. Graphene-Based Ultracapacitors. *Nano Lett.* **2008**, *8*, 3498–3502.
90. Liu, Z.; Robinson, J. T.; Sun, X. M.; Dai, H. J. PEGylated Nanographene Oxide for Delivery of Water-Insoluble Cancer Drugs. *J. Am. Chem. Soc.* **2008**, *130*, 10876–10877.
91. Zhang, L. M.; Xia, J. G.; Zhao, Q. H.; Liu, L. W.; Zhang, Z. J. Functional Graphene Oxide as a Nanocarrier for Controlled Loading and Targeted Delivery of Mixed Anticancer Drugs. *Small* **2010**, *6*, 537–544.
92. Lu, C. H.; Yang, H. H.; Zhu, C. L.; Chen, X.; Chen, G. N. A Graphene Platform for Sensing Biomolecules. *Angew. Chem., Int. Ed.* **2009**, *48*, 4785–4787.
93. Myung, S.; Kim, C.; Yin, P. T.; Park, J.; Solanki, A.; Reyes, P. I.; Lu, Y.; Kim, K. S.; Lee, K. B. Label-Free Polypeptide-Based Enzyme Detection Using a Graphene–Nanoparticle Hybrid Sensor. *Adv. Mater.* **2012**, *24*, 6081–6087.
94. Myung, S.; Solanki, A.; Kim, C.; Park, J.; Kim, K. S.; Lee, K. B. Graphene-Encapsulated Nanoparticle-Based Biosensor for the Selective Detection of Cancer Biomarkers. *Adv. Mater.* **2011**, *23*, 2221–2225.
95. Zhu, S. J.; Zhang, J. H.; Qiao, C. Y.; Tang, S. J.; Li, Y. F.; Yuan, W. J.; Li, B.; Tian, L.; Liu, F.; Hu, R.; *et al.* Strongly Green-Photoluminescent Graphene Quantum Dots for Bioimaging Applications. *Chem. Commun.* **2011**, *47*, 6858–6860.
96. Cao, L.; Meziani, M. J.; Sahu, S.; Sun, Y. P. Photoluminescence Properties of Graphene *versus* Other Carbon Nanomaterials. *Acc. Chem. Res.* **2013**, *46*, 171–180.
97. Li, H. T.; He, X. D.; Kang, Z. H.; Huang, H.; Liu, Y.; Liu, J. L.; Lian, S. Y.; Tsang, C. H. A.; Yang, X. B.; Lee, S. T. Water-Soluble Fluorescent Carbon Quantum Dots and Photocatalyst Design. *Angew. Chem., Int. Ed.* **2010**, *49*, 4430–4434.
98. Hola, K.; Bourlinos, A. B.; Kozak, O.; Berka, K.; Siskova, K. M.; Havrdova, M.; Tucek, J.; Safarova, K.; Otyepka, M.; Giannelis, E. P.; *et al.* Photoluminescence Effects of Graphitic Core Size and Surface Functional Groups in Carbon Dots: $COO^-$ Induced Red-Shift Emission. *Carbon* **2014**, *70*, 279–286.
99. Kozák, O.; Datta, K. K. R.; Greplová, M.; Ranc, V.; Kašlík, J.; Zbořil, R. Surfactant-Derived Amphiphilic Carbon Dots with Tunable Photoluminescence. *J. Phys. Chem. C* **2013**, *117*, 24991–24996.
100. Bourlinos, A. B.; Zboril, R.; Petr, J.; Bakandritsos, A.; Krysmann, M.; Giannelis, E. P. Luminescent Surface Quaternized Carbon Dots. *Chem. Mater.* **2012**, *24*, 6–8.
101. Bourlinos, A. B.; Stassinopoulos, A.; Anglos, D.; Zboril, R.; Georgakilas, V.; Giannelis, E. P. Photoluminescent Carbogenic Dots. *Chem. Mater.* **2008**, *20*, 4539–4541.
102. Bourlinos, A. B.; Stassinopoulos, A.; Anglos, D.; Zboril, R.; Karakassides, M.; Giannelis, E. P. Surface Functionalized Carbogenic Quantum Dots. *Small* **2008**, *4*, 455–458.
103. Bourlinos, A. B.; Karakassides, M. A.; Kouloumpis, A.; Gournis, D.; Bakandritsos, A.; Papagiannouli, I.; Aloukos, P.; Couris, S.; Hola, K.; Zboril, R.; *et al.* Synthesis, Characterization and Non-linear Optical Response of Organophilic Carbon Dots. *Carbon* **2013**, *61*, 640–643.
104. Li, H. T.; Liu, R. H.; Kong, W. Q.; Liu, J.; Liu, Y.; Zhou, L.; Zhang, X.; Lee, S. T.; Kang, Z. H. Carbon Quantum Dots with Photo-generated Proton Property as Efficient Visible Light Controlled Acid Catalyst. *Nanoscale* **2014**, *6*, 867–873.
105. Dong, Y. Q.; Chen, C. Q.; Lin, J. P.; Zhou, N. N.; Chi, Y. W.; Chen, G. N. Electrochemiluminescence Emission from Carbon Quantum Dot–Sulfite Coreactant System. *Carbon* **2013**, *56*, 12–17.
106. Cao, L.; Yang, S. T.; Wang, X.; Luo, P. J. G.; Liu, J. H.; Sahu, S.; Liu, Y. M.; Sun, Y. P. Competitive Performance of Carbon "Quantum" Dots in Optical Bioimaging. *Theranostics* **2012**, *2*, 295–301.
107. Bourlinos, A. B.; Bakandritsos, A.; Kouloumpis, A.; Gournis, D.; Krysmann, M.; Giannelis, E. P.; Polakova, K.; Safarova, K.; Hola, K.; Zboril, R. Gd(III)-Doped Carbon Dots as a Dual Fluorescent-MRI Probe. *J. Mater. Chem.* **2012**, *22*, 23327–23330.
108. Hirsch, A. Functionalization of Single-Walled Carbon Nanotubes. *Angew. Chem., Int. Ed.* **2002**, *41*, 1853–1859.
109. Sun, Y. P.; Fu, K. F.; Lin, Y.; Huang, W. J. Functionalized Carbon Nanotubes: Properties and Applications. *Acc. Chem. Res.* **2002**, *35*, 1096–1104.
110. Kim, O. K.; Je, J. T.; Baldwin, J. W.; Kooi, S.; Pehrsson, P. E.; Buckley, L. J. Solubilization of Single-Wall Carbon Nanotubes by Supramolecular Encapsulation of Helical Amylose. *J. Am. Chem. Soc.* **2003**, *125*, 4426–4427.
111. Wu, Y. H.; Qiao, P. W.; Qiu, J. J.; Chong, T. C.; Low, T. S. Magnetic Nanostructures Grown on Vertically Aligned Carbon Nanotube Templates. *Nano Lett.* **2002**, *2*, 161–164.
112. Watts, P. C. P.; Hsu, W. K.; Randall, D. P.; Kotzeva, V.; Chen, G. Z. Fe-Filled Carbon Nanotubes: Nano-electromagnetic Inductors. *Chem. Mater.* **2002**, *14*, 4505–4508.
113. Oymak, H.; Erkoc, S. Titanium Coverage on a Single-Wall Carbon Nanotube: Molecular Dynamics Simulations. *Chem. Phys.* **2004**, *300*, 277–283.
114. Chin, K. C.; Gohel, A.; Elim, H. I.; Ji, W.; Chong, G. L.; Lim, K. Y.; Sow, C. H.; Wee, A. T. S. Optical Limiting Properties of Amorphous $Si_xN_y$ and SiC Coated Carbon Nanotubes. *Chem. Phys. Lett.* **2004**, *383*, 72–75.
115. Wildgoose, G. G.; Banks, C. E.; Compton, R. G. Metal Nanopartictes and Related Materials Supported on Carbon Nanotubes: Methods and Applications. *Small* **2006**, *2*, 182–193.
116. Rao, C. N. R.; Satishkumar, B. C.; Govindaraj, A.; Nath, M. Nanotubes. *ChemPhysChem* **2001**, *2*, 78–105.
117. Pradhan, B. K.; Toba, T.; Kyotani, T.; Tomita, A. Inclusion of Crystalline Iron Oxide Nanoparticles in Uniform Carbon Nanotubes Prepared by a Template Carbonization Method. *Chem. Mater.* **1998**, *10*, 2510–2515.
118. Gao, Y.; Bando, Y. Carbon Nanothermometer Containing Gallium–Gallium's Macroscopic Properties Are Retained on a Miniature Scale in This Nanodevice. *Nature* **2002**, *415*, 599–609.
119. Menon, M.; Andriotis, A. N.; Froudakis, G. E. Curvature Dependence of the Metal Catalyst Atom Interaction with Carbon Nanotubes Walls. *Chem. Phys. Lett.* **2000**, *320*, 425–434.
120. Zhang, Y.; Zhang, H. B.; Lin, G. D.; Chen, P.; Yuan, Y. Z.; Tsai, K. R. Preparation, Characterization and Catalytic Hydroformylation Properties of Carbon Nanotubes-Supported

Rh-Phosphine Catalyst. *Appl. Catal., A* **1999**, *187*, 213–224.
121. Chen, W.; Fan, Z.; Pan, X.; Bao, X. Effect of Confinement in Carbon Nanotubes on the Activity of Fischer–Tropsch Iron Catalyst. *J. Am. Chem. Soc.* **2008**, *130*, 9414–9419.
122. Pan, X.; Bao, X. The Effects of Confinement inside Carbon Nanotubes on Catalysis. *Acc. Chem. Res.* **2011**, *44*, 553–562.
123. Ugarte, D.; Chatelain, A.; de Heer, W. A. Nanocapillarity and Chemistry in Carbon Nanotubes. *Science* **1996**, *274*, 1897–1899.
124. Shan, B.; Cho, K. First-Principles Study of Work Functions of Double-Wall Carbon Nanotubes. *Phys. Rev. B* **2006**, *73*, 081401.
125. Ajiki, H.; Ando, T. Magnetic Properties of Carbon Nanotubes. *J. Phys. Soc. Jpn.* **1993**, *62*, 2470–2480.
126. Leonhardt, A.; Ritschel, A.; Kozhuharova, R.; Graff, A.; Muhl, T.; Huhle, R.; Monch, I.; Elefant, D.; Schneider, C. M. Synthesis and Properties of Filled Carbon Nanotubes. *Diamond Relat. Mater.* **2003**, *12*, 790–793.
127. Murakami, H.; Hirakawa, M.; Tanaka, C.; Yamakawa, H. Field Emission from Well-Aligned, Patterned, Carbon Nanotube Emitters. *Appl. Phys. Lett.* **2000**, *76*, 1776–1778.
128. Sitharaman, B.; Kissell, K. R.; Hartman, K. B.; Tran, L. A.; Baikalov, A.; Rusakova, I.; Sun, Y.; Khant, H. A.; Ludtke, S. J.; Chiu, W.; *et al.* Superparamagnetic Gadonanotubes Are High-Performance MRI Contrast Agents. *Chem. Commun.* **2005**, *31*, 3915–3917.
129. Xie, J.; Lee, S.; Chen, X. Y. Nanoparticle-Based Theranostic Agents. *Adv. Drug Delivery Rev.* **2010**, *62*, 1064–1079.
130. Nasri, R.; Siblini, A.; Jorat, L.; Noyel, G. Magneto Dielectric Behavior of the Magnetic Fluid Manganese Ferrite in Carbon Tetrachloride. *J. Magn. Magn. Mater.* **1996**, *161*, 309–315.
131. Deng, L. J.; Han, M. G. Microwave Absorbing Performances of Multiwalled Carbon Nanotube Composites with Negative Permeability. *Appl. Phys. Lett.* **2007**, *91*, 023119.
132. Gao, X. P.; Zhang, Y.; Chen, X.; Pan, G. L.; Yan, J.; Wu, F. Carbon Nanotubes Filled with Metallic Nanowires. *Carbon* **2004**, *42*, 47–52.
133. Korneva, G.; Ye, H.; Gogotsi, Y.; Halverson, D.; Friedman, G.; Bradley, J. C.; Kornev, K. G. Carbon Nanotubes Loaded with Magnetic Particles. *Nano Lett.* **2005**, *5*, 879–884.
134. Adekunle, A. S.; Agboola, B. O.; Pillay, J.; Ozoemena, K. I. Electrocatalytic Detection of Dopamine at Single-Walled Carbon Nanotubes–Iron (III) Oxide Nanoparticles Platform. *Sens. Actuators, B* **2010**, *148*, 93–102.
135. Peng, X.; Li, Y.; Luan, Z.; Di, Z.; Wang, H.; Tian, B.; Jia, Z. Adsorption of 1,2-Dichlorobenzene from Water to Carbon Nanotubes. *Chem. Phys. Lett.* **2003**, *376*, 154–158.
136. Lu, C.; Chung, Y. L.; Chang, K. F. Adsorption of Trihalomethanes from Water with Carbon Nanotubes. *Water Res.* **2005**, *39*, 1183–1189.
137. Yan, H.; Gong, A.; He, H.; Zhou, J.; Wei, Y.; Lv, L. Adsorption of Microcystins by Carbon Nanotubes. *Chemosphere* **2006**, *62*, 142–148.
138. Li, Y. H.; Wang, S.; Cao, A.; Zhao, D.; Zhang, X.; Xu, C.; Luan, Z.; Ruan, D.; Liang, J.; Wu, D.; *et al.* Adsorption of Fluoride from Water by Amorphous Alumina Supported on Carbon Nanotubes. *Chem. Phys. Lett.* **2001**, *350*, 412–416.
139. Li, Y. H.; Wang, S.; Wei, J.; Zhang, X.; Xu, C.; Luan, Z.; Wu, D.; Wei, B. Lead Adsorption on Carbon Nanotubes. *Chem. Phys. Lett.* **2002**, *357*, 263–266.
140. Chen, C.; Wang, X. Adsorption of Ni(II) from Aqueous Solution Using Oxidized Multi-wall Carbon Nanotubes. *Ind. Eng. Chem. Res.* **2006**, *45*, 9144–9149.
141. Peng, X.; Luan, Z.; Ding, J.; Di, Z.; Li, Y.; Tian, B. Ceria Nanoparticles Supported on Carbon Nanotubes for the Removal of Arsenate from Water. *Mater. Lett.* **2005**, *59*, 399–403.
142. Chen, C. L.; Wang, X. K.; Nagatsu, M. Europium Adsorption on Multiwall Carbon Nanotube/Iron Oxide Magnetic Composite in the Presence of Polyacrylic Acid. *Environ. Sci. Technol.* **2009**, *43*, 2362–2367.
143. Gong, J. L.; Wang, B.; Zeng, G. M.; Yang, C. P.; Niu, C. G.; Niu, Q. Y.; Zhou, W. J.; Liang, Y. Removal of Cationic Dyes from Aqueous Solution Using Magnetic Multi-wall Carbon Nanotube Nanocomposite As Adsorbent. *J. Hazard. Mater.* **2009**, *164*, 1517–1522.
144. Gupta, V. K.; Agarwal, S.; Saleh, T. A. Chromium Removal by Combining the Magnetic Properties of Iron Oxide with Adsorption Properties of Carbon Nanotubes. *Water Res.* **2001**, *45*, 2207–2212.
145. Schnitzler, M. C.; Oliviera, M. M.; Ugarte, D.; Zabrin, A. J. G. One-Step Route to Iron Oxide-Filled Carbon Nanotubes and Bucky-Onions Based on the Pyrolysis of Organometallic Precursors. *Chem. Phys. Lett.* **2003**, *381*, 541–548.
146. Xu, L.; Zhang, W.; Ding, Y.; Peng, Y.; Zhang, S.; Yu, W.; Qian, Y. Formation, Characterization, and Magnetic Properties of $Fe_3O_4$ Nanowires Encapsulated in Carbon Microtubes. *J. Phys. Chem. B* **2004**, *108*, 10859–10862.
147. Xu, P.; Han, X. J.; Liu, X. R.; Zhang, B.; Wang, C.; Wang, X. H. A Study of the Magnetic and Electromagnetic Properties of Gamma-$Fe_2O_3$-Multiwalled Carbon Nanotubes (MWCNT) and Fe/$Fe_3C$-MWCNT Composites. *Mater. Chem. Phys.* **2009**, *114*, 556–560.
148. Huo, J. P.; Song, H. H.; Chen, X. H. Preparation of Carbon-Encapsulated Iron Nanoparticles by Co-carbonization of Aromatic Heavy Oil and Ferrocene. *Carbon* **2004**, *42*, 3177–3182.
149. Yu, F.; Wang, J. N.; Sheng, Z. N.; Su, L. F. Synthesis of Carbon-Encapsulated Magnetic Nanoparticles by Spray Pyrolysis of Iron Carbonyl and Ethanol. *Carbon* **2005**, *43*, 3018–3021.
150. Ajayan, P. M.; Iijima, S. Capillarity-Induced Filling of Carbon Nanotubes. *Nature* **1993**, *361*, 333–334.
151. Dujardin, E.; Ebbesen, T. W.; Hiura, H.; Tanigaki, K. Capillarity and Wetting of Carbon Nanotubes. *Science* **1994**, *265*, 1850–1852.
152. Ebbesen, T. W. Wetting, Filling and Decorating Carbon Nanotubes. *J. Phys. Chem. Solids* **1996**, *57*, 951–955.
153. Gao, C.; Li, W.; Morimoto, H.; Nagaoka, Y.; Maekawa, T. Magnetic Carbon Nanotubes: Synthesis by Electrostatic Self-Assembly Approach and Application in Biomanipulations. *J. Phys. Chem. B* **2006**, *110*, 7213–7220.
154. Zhenyu, S.; Zhimin, L.; Wang, Y.; Han, B.; Du, J.; Zhang, J. Fabrication and Characterization of Magnetic Carbon Nanotubes Composites. *J. Mater. Chem.* **2005**, *15*, 4497–4501.
155. Tsang, S. C.; Chen, Y. K.; Harris, P. J. F.; Green, M. L. H. A Simple Chemical Method of Opening and Filling Carbon Nanotubes. *Nature* **1994**, *372*, 159–162.
156. Pradhan, B. K.; Kyotani, T.; Tomita, A. Nickel Nanowires of 4 nm Diameter in the Cavity of Carbon Nanotubes. *Chem. Commun.* **1999**, *14*, 1317–1318.
157. Kamalakaran, R.; Lupo, F.; Grobert, N.; Lozano-Castello, D. D.; Jin-Phillipp, N. Y.; Ruhle, M. *In-Situ* Formation of Carbon Nanotubes in an Alumina–Nanotube Composite by Spray Pyrolysis. *Carbon* **2003**, *41*, 2737–2741.
158. Hang, B. T.; Hayashi, H.; Yoon, S. H.; Okada, S.; Yamaki, J. $Fe_2O_3$-Filled Carbon Nanotubes as a Negative Electrode for an Fe-Air Battery. *J. Power Sources* **2008**, *178*, 393–401.
159. Chen, W.; Pan, X.; Bao, X. Tuning of Redox Properties of Iron and Iron Oxides *via* Encapsulation within Carbon Nanotubes. *J. Am. Chem. Soc.* **2007**, *129*, 7421–7426.
160. Tan, F.; Fan, X.; Zhang, G.; Zhang, F. Coating and Filling of Carbon Nanotubes with Homogeneous Magnetic Nanoparticles. *Mater. Lett.* **2007**, *61*, 1805–1808.
161. Qiu, J.; Li, Q.; Wang, Z.; Sun, Y.; Zhang, H. CVD Synthesis of Coal-Gas-Derived Carbon Nanotubes and Nanocapsules Containing Magnetic Iron Carbide and Oxide. *Carbon* **2006**, *44*, 2565–2568.
162. Cava, C. E.; Possagno, R.; Schnitzler, M. C.; Roman, P. C.; Oliveira, M. M.; Lepiensky, C. M.; Zarbin, A. J. G.; Roman, L. S. Iron- and Iron Oxide-Filled Multi-walled Carbon Nanotubes: Electrical Properties and Memory Devices. *Chem. Phys. Lett.* **2007**, *444*, 304–308.
163. Xiong, Y.; Ye, J.; Gu, X.; Chen, Q. Synthesis and Magnetic Properties of Iron Oxide Nanoparticles/C and α-Fe/Iron Oxide Nanoparticles/C Composites. *J. Magn. Magn. Mater.* **2008**, *320*, 107–112.

164. Banerjee, S.; Wong, S. S. Functionalization of Carbon Nanotubes with a Metal Containing Molecular Complex. *Nano Lett.* **2002**, *2*, 49–53.
165. Richard, C.; Balavoine, F.; Schultz, P.; Ebbesen, T. W.; Mioskowski, C. Supramolecular Self-Assembly of Lipid Derivatives on Carbon Nanotubes. *Science* **2003**, *300*, 775–778.
166. Kong, H.; Cao, C.; Yan, D. Controlled Functionalization of Multiwalled Carbon Nanotubes by *In Situ* Atom Transfer Radical Polymerization. *J. Am. Chem. Soc.* **2004**, *126*, 412–413.
167. Baskaran, D.; Mays, J. W.; Bratcher, M. S. Polymer Grafted MWCNT through Surface Polymerization. *Angew. Chem., Int. Ed.* **2004**, *43*, 2138–2142.
168. Zhou, H.; Zhang, C.; Li, H.; Du, Z. Decoration of $Fe_3O_4$ Nanoparticles on the Surface of Poly(acrylic acid) Functionalized Multi-walled Carbon Nanotubes by Covalent Bonding. *J. Polym. Sci., Part A: Polym. Chem.* **2010**, *48*, 4697–4703.
169. Ko, S. W.; Yang, M. S.; Choi, H. J. Adsorption of Polymer Coated Magnetite Composite Particles onto Carbon Nanotubes and Their Magnetorheology. *Mater. Lett.* **2009**, *63*, 861–863.
170. Jia, B.; Gao, L.; Sun, J. Self-Assembly of Magnetite Beads along Multiwalled Carbon Nanotubes *via* a Simple Hydrothermal Process. *Carbon* **2007**, *45*, 1476–1481.
171. Lin, T. W.; Salzmann, C. G.; Shao, L. D.; Yu, C. H.; Green, M. L. H.; Tsang, S. C. Polyethylene Glycol Grafting and Attachment of Encapsulated Magnetic Iron Oxide Silica Nanoparticles onto Chlorosilanized Single-Wall Carbon Nanotubes. *Carbon* **2009**, *47*, 1415–1420.
172. Qin, C.; Shen, J.; Hu, Y.; Ye, M. Facile Attachment of Magnetic Nanoparticles to Carbon Nanotubes *via* Robust Linkages and Its Fabrication of Magnetic Nanocomposites. *Compos. Sci. Technol.* **2009**, *69*, 427–431.
173. Georgakilas, V.; Tzitzios, V.; Gournis, D.; Petridis, D. Attachment of Magnetic Nanoparticles on Carbon Nanotubes and Their Soluble Derivatives. *Chem. Mater.* **2005**, *17*, 1613–1617.
174. Choi, J. H.; Nguyen, F. T.; Barone, P. W.; Heller, D. A.; Moll, A. E.; Patel, D.; Boppart, S. A.; Strano, M. S. Multimodal Biomedical Imaging with Asymmetric Single-Walled Carbon Nanotube/Iron Oxide Nanoparticle Complexes. *Nano Lett.* **2007**, *7*, 861–867.
175. Kong, L.; Lu, X.; Zhang, W. Facile Synthesis of Multifunctional Multiwalled Carbon Nanotubes/$Fe_3O_4$ Nanoparticles/Polyaniline Composite Nanotubes. *J. Solid State Chem.* **2008**, *181*, 628–636.
176. Kornev, K. G.; Halverson, D.; Korneva, G.; Gogotsi, Y.; Friedman, G. Magnetostatic Interactions between Carbon Nanotubes Filled with Magnetic Nanoparticles. *Appl. Phys. Lett.* **2008**, *92*, 233117.
177. Kim, I. T.; Tannenbaum, A.; Tannenbaum, R. Anisotropic Conductivity of Magnetic Carbon Nanotubes Embedded in Epoxy Matrices. *Carbon* **2011**, *49*, 54–61.
178. Zhang, C.; Tjiu, W. W.; Liu, T.; Lui, W. Y.; Phang, I. Y.; Zhang, W.-D. Dramatically Enhanced Mechanical Performance of Nylon-6 Magnetic Composites with Nanostructured Hybrid One-Dimensional Carbon Nanotube-Two-Dimensional Clay Nanoplatelet Heterostructures. *J. Phys. Chem. B* **2011**, *115*, 3392–3399.
179. Cava, C. E.; Persson, C.; Zarbin, A. J. G.; Roman, L. S. Resistive Switching in Iron-Oxide-Filled Carbon Nanotubes. *Nanoscale* **2014**, *6*, 378–384.
180. Freedman, J. R.; Mattia, D.; Korneva, G.; Gogotsi, Y.; Friedman, G.; Fontecchio, A. K. Magnetically Assembled Carbon Nanotube Tipped Pipettes. *Appl. Phys. Lett.* **2007**, *90*, 103108.
181. Singhal, R.; Orynbayeva, Z.; Sundaram, R. V. K.; Niu, J. J.; Bhattacharyya, S.; Vitol, E. A.; Schrlau, M. G.; Papazoglou, E. S.; Friedman, G.; Gogotsi, Y. Multifunctional Carbon-Nanotube Cellular Endoscopes. *Nat. Nanotechnol.* **2011**, *6*, 57–64.
182. Syljukić, B.; Banks, C. E.; Compton, R. G. Iron Oxide Particles Are the Active Sites for Hydrogen Peroxide Sensing at Multiwalled Carbon Nanotube Modified Electrodes. *Nano Lett.* **2006**, *6*, 1556–1558.
183. Olivé-Monllau, R.; Muñoz-Pascual, F. X.; Baldrich, E. Characterization and Optimization of Carbon Nanotube Electrodes Produced by Magnetic Entrapment: Application to Paracetamol Detection. *Sens. Actuators, B* **2013**, *185*, 685–693.
184. Qu, S.; Wang, J.; Kong, J.; Yang, P.; Chen, G. Magnetic Loading of Carbon Nanotube/Nano-$Fe_3O_4$ Composite for Electrochemical Sensing. *Talanta* **2007**, *71*, 1096–1102.
185. Yin, M.; Wang, M.; Miao, F.; Ji, Y.; Tian, Z.; Shen, H.; Jia, N. Water-Dispersible Multiwalled Carbon Nanotube/Iron Oxide Hybrids as Contrast Agents for Cellular Magnetic Resonance Imaging. *Carbon* **2012**, *50*, 2162–2170.
186. Lamanna, G.; Garofalo, A.; Popa, G.; Wilhelm, C.; Begin-Colin, S.; Felder-Flesch, D.; Bianco, A.; Gazeau, F.; Menard-Moyon, C. Endowing Carbon Nanotubes with Superparamagnetic Properties: Applications for Cell Labeling, MRI Cell Tracking and Magnetic Manipulations. *Nanoscale* **2013**, *5*, 4412–4421.
187. Wang, H.; Wang, Z.; Ye, M.; Zong, S.; Li, M.; Chen, P.; Ma, X.; Cui, Y. Optically Encoded Nanoprobes Using Single Walled Carbon Nanotube as the Building Scaffold for Magnetic Field Guided Cell Imaging. *Talanta* **2014**, *119*, 144–150.
188. Shen, S.; Ren, J.; Zhu, X.; Pang, Z.; Lu, X.; Deng, C.; Zhang, R.; Jiang, X. Monodisperse Magnetites Anchored onto Carbon Nanotubes: A Platform for Cell Imaging, Magnetic Manipulation and Enhanced Photothermal Treatment of Tumors. *J. Mater. Chem. B* **2013**, *1*, 1939–1946.
189. Lu, Y.-J.; Wei, K.-C.; Ma, C.-C. M.; Yang, S.-Y.; Chen, J.-P. Dual Targeted Delivery of Doxorubicin to Cancer Cells Using Folate-Conjugated Magnetic Multi-walled Carbon Nanotubes. *Colloids Surf., B* **2012**, *89*, 1–9.
190. Chen, C.; Hu, J.; Shao, D.; Li, J.; Wang, X. Adsorption Behavior of Multiwall Carbon Nanotube/Iron Oxide Magnetic Composites for Ni(II) and Sr(II). *J. Hazard. Mater.* **2009**, *164*, 923–928.
191. Gupta, V. K.; Agarwal, S.; Saleh, T. A. Chromium Removal by Combining the Magnetic Properties of Iron Oxide with Adsorption Properties of Carbon Nanotubes. *Water Res.* **2011**, *45*, 2207–2212.
192. Ma, J.; Zhu, Z.; Chen, B.; Yang, M.; Zhou, H.; Li, C.; Yu, F.; Chen, J. One-Pot, Large-Scale Synthesis of Magnetic Activated Carbon Nanotubes and Their Applications for Arsenic Removal. *J. Mater. Chem. A* **2013**, *1*, 4662–4666.
193. Hu, J.; Shao, D.; Chen, C.; Sheng, G.; Li, J.; Wang, X.; Nagatsu, M. Plasma-Induced Grafting of Cyclodextrin onto Multiwall Carbon Nanotube/Iron Oxides for Adsorbent Application. *J. Phys. Chem. B* **2010**, *114*, 6779–6785.
194. Qu, S.; Huang, F.; Yu, S.; Chen, G.; Kong, J. Magnetic Removal of Dyes from Aqueous Solution Using Multi-walled Carbon Nanotubes Filled with $Fe_2O_3$ Particles. *J. Hazard. Mater.* **2008**, *160*, 643–647.
195. Goh, W. J.; Makam, V. S.; Hu, J.; Kang, L.; Zheng, M.; Yoong, S. L.; Udalagama, C. N. B.; Pastorin, G. Iron Oxide Filled Magnetic Carbon Nanotube–Enzyme Conjugates for Recycling of Amyloglucosidase: Toward Useful Applications in Biofuel Production Process. *Langmuir* **2012**, *28*, 16864–16873.
196. Zuo, X.; Peng, C.; Huang, Q.; Song, S.; Wang, L.; Li, D.; Fan, C. Design of a Carbon Nanotube/Magnetic Nanoparticle-Based Peroxidase-like Nanocomplex and Its Application for Highly Efficient Catalytic Oxidation of Phenols. *Nano Res.* **2009**, *2*, 617–623.
197. Samouhos, S.; McKinley, G. Carbon Nanotube–Magnetite Composites, with Applications To Developing Unique Magnetorheological Fluids. *J. Fluids Eng.* **2007**, *129*, 429–437.
198. Singhal, R.; Mochalin, V. N.; Lukatskaya, M. R.; Friedman, G.; Gogotsi, Y. Separation and Liquid Chromatography Using a Single Carbon Nanotube. *Sci. Rep.* **2012**, *2*, 510.
199. Hong, J.; Bekyarova, E.; de Heer, W. A.; Haddon, R. C.; Khizroev, S. Chemically Engineered Graphene-Based 2D Organic Molecular Magnet. *ACS Nano* **2013**, *7*, 10011–10022.

200. Kim, N.; Kim, K. S.; Jung, N.; Brus, L.; Kim, P. Synthesis and Electrical Characterization of Magnetic Bilayer Graphene Intercalate. *Nano Lett.* **2011**, *11*, 860–865.
201. Zhou, G. M.; Wang, D. W.; Li, F.; Zhang, L. L.; Li, N.; Wu, Z. S.; Wen, L.; Lu, G. Q.; Cheng, H.-M. Graphene-Wrapped $Fe_3O_4$ Anode Material with Improved Reversible Capacity and Cyclic Stability for Lithium Ion Batteries. *Chem. Mater.* **2010**, *22*, 5306–5313.
202. Guo, S. J.; Wen, D.; Zhai, Y. M.; Dong, S. J.; Wang, E. K. Platinum Nanoparticle Ensemble-on-Graphene Hybrid Nanosheet: One-Pot, Rapid Synthesis, and Used as New Electrode Material for Electrochemical Sensing. *ACS Nano* **2010**, *4*, 3959–3968.
203. Koo, H. Y.; Lee, H.-J.; Go, H.-A.; Lee, Y. B.; Bae, T. S.; Kim, J. K.; Choi, W. S. Graphene-Based Multifunctional Iron Oxide Nanosheets with Tunable Properties. *Chem.—Eur. J.* **2011**, *17*, 1214–1219.
204. Zhan, Y.; Meng, F.; Yang, X.; Liu, X. Magnetite−Graphene Nanosheets (GNs)/Poly(arylene ether nitrile) (PEN): Fabrication and Characterization of a Multifunctional Nanocomposite Film. *Colloids Surf., A* **2011**, *390*, 112–119.
205. Ban, C.; Wu, Z.; Gillaspie, D. T.; Chen, L.; Yan, Y.; Blackburn, J. L.; Dillon, A. C. Nanostructured $Fe_3O_4$/SWNT Electrode: Binder-Free and High-Rate Li-Ion Anode. *Adv. Mater.* **2010**, *22*, E145–E149.
206. Ren, L.; Huang, S.; Fan, W.; Liu, T. One-Step Preparation of Hierarchical Superparamagnetic Iron Oxide/Graphene Composites *via* Hydrothermal Method. *Appl. Surf. Sci.* **2011**, *258*, 1132–1138.
207. He, H.; Gao, C. Supraparamagnetic, Conductive, and Processable Multifunctional Graphene Nanosheets Coated with High-Density $Fe_3O_4$ Nanoparticles. *ACS Appl. Mater. Interfaces* **2010**, *2*, 3201–3210.
208. Shen, X.; Wu, J.; Bai, S.; Zhou, H. One-Pot Solvothermal Syntheses and Magnetic Properties of Graphene-Based Magnetic Nanocomposites. *J. Alloys Compd.* **2010**, *506*, 136–140.
209. Wang, C. Y.; Ravi, S.; Garapati, U. S.; Das, M.; Howell, M.; Mallela, J.; Alwarappan, S.; Mohapatra, S. S.; Mohapatra, S. Multifunctional Chitosan Magnetic−Graphene (CMG) Nanoparticles: A Theranostic Platform for Tumor-Targeted Co-delivery of Drugs, Genes and MRI Contrast Agents. *J. Mater. Chem. B* **2013**, *1*, 4396–4405.
210. Bai, L. Z.; Zhao, D. L.; Xu, Y.; Zhang, J. M.; Gao, Y. L.; Zhao, L. Y.; Tang, J. T. Inductive Heating Property of Graphene Oxide-$Fe_3O_4$ Nanoparticles Hybrid in an AC Magnetic Field for Localized Hyperthermia. *Mater. Lett.* **2012**, *68*, 399–401.
211. Wang, X.; Liu, D. P.; Song, S. Y.; Zhang, H. J. $CeO_2$-Based Pd(Pt) Nanoparticles Grafted onto $Fe_3O_4$/Graphene: A General Self-Assembly Approach To Fabricate Highly Efficient Catalysts with Magnetic Recyclable Capability. *Chem.—Eur. J.* **2013**, *19*, 5169–5173.
212. Verma, D.; Verma, S.; Sinha, A. K.; Jain, S. L. Iron Nanoparticles Supported on Graphene Oxide: A Robust, Magnetically Separable Heterogeneous Catalyst for the Oxidative Cyanation of Tertiary Amines. *ChemPlusChem* **2013**, *78*, 860–865.
213. Zhu, Y.; Murali, S.; Stoller, M. D.; Ganesh, K. J.; Cai, W.; Ferreira, P. J.; Pirkle, A.; Wallace, R. M.; Cychosz, K. A.; Thommes, M.; *et al.* Carbon-Based Supercapacitors Produced by Activation of Graphene. *Science* **2011**, *332*, 1537–1541.
214. Wang, Q. H.; Wang, D. W.; Li, Y. Q.; Wang, T. M. Superparamagnetic Magnetite Nanocrystals−Graphene Oxide Nanocomposites: Facile Synthesis and Their Enhanced Electric Double-Layer Capacitor Performance. *J. Nanosci. Nanotechnol.* **2012**, *12*, 4583–4590.
215. Kim, T. Y.; Jung, G.; Yoo, S.; Suh, K. S.; Ruoff, R. S. Activated Graphene-Based Carbons as Supercapacitor Electrodes with Macro- and Mesopores. *ACS Nano* **2013**, *7*, 6899–6905.
216. Zhou, L.; Deng, H. P.; Wan, J. L.; Zhang, R. J. Synthesis and Adsorption of Graphene-Based Iron Oxide Magnetic Nanocomposites. *Prog. Chem.* **2013**, *25*, 145–155.
217. Jabeen, H.; Chandra, V.; Jung, S.; Lee, J. W.; Kim, K. S.; Bin Kim, S. Enhanced Cr(VI) Removal Using Iron Nanoparticle Decorated Graphene. *Nanoscale* **2011**, *3*, 3583–3585.
218. Yang, K.; Feng, L. Z.; Shi, X. Z.; Liu, Z. Nano-graphene in Biomedicine: Theranostic Applications. *Chem. Soc. Rev.* **2013**, *42*, 530–547.
219. Bai, S.; Chen, S. Q.; Shen, X. P.; Zhu, G. X.; Wang, G. X. Nanocomposites of Hematite ($\alpha$-$Fe_2O_3$) Nanospindles with Crumpled Reduced Graphene Oxide Nanosheets as High-Performance Anode Material for Lithium-Ion Batteries. *RSC Adv.* **2012**, *2*, 10977–10984.
220. Wang, J.-Z.; Zhong, C.; Wexler, D.; Hayati Idris, N.; Wang, Z.-X.; Chen, L.-Q.; Liu, H.-K. Graphene-Encapsulated $Fe_3O_4$ Nanoparticles with 3D Laminated Structure as Superior Anode in Lithium Ion Batteries. *Chem.—Eur. J.* **2011**, *17*, 661–667.
221. Li, X.; Huang, X.; Liu, D.; Wang, X.; Song, S.; Zhou, L.; Zhang, H. Synthesis of 3D Hierarchical $Fe_3O_4$/Graphene Composites with High Lithium Storage Capacity and for Controlled Drug Delivery. *J. Phys. Chem. C* **2011**, *115*, 21567–21573.
222. Hsieh, C.-T.; Lin, J.-Y.; Mo, C.-Y. Improved Storage Capacity and Rate Capability of $Fe_3O_4$-Graphene Anodes for Lithium-Ion Batteries. *Electrochim. Acta* **2011**, *58*, 119–124.
223. Kuila, T.; Bose, S.; Mishra, A. K.; Khanra, P.; Kim, N. H.; Lee, J. H. Chemical Functionalization of Graphene and Its Applications. *Prog. Mater. Sci.* **2012**, *57*, 1061–1105.
224. Elias, D. C.; Nair, R. R.; Mohiuddin, T. M. G.; Morozov, S. V.; Blake, P. M.; Halsall, P.; Ferrari, A. C.; Boukhvalov, D. W.; Katsnelson, M. I.; Geim, A. K.; *et al.* Control of Graphene's Properties by Reversible Hydrogenation: Evidence for Graphane. *Science* **2009**, *323*, 610–613.
225. Kim, S.-W.; Seo, D.-H.; Gwon, H.; Kim, J.; Kang, K. Fabrication of $FeF_3$ Nanoflowers on CNT Branches and Their Application to High Power Lithium Rechargeable Batteries. *Adv. Mater.* **2010**, *22*, 5260–5264.
226. Rodriguez-Manzo, J. A.; Cretu, O.; Banhart, F. Trapping of Metal Atoms in Vacancies of Carbon Nanotubes and Graphene. *ACS Nano* **2010**, *4*, 3422–3428.
227. Lu, G.; Mao, S.; Park, S.; Ruoff, R. S.; Chen, J. Facile, Noncovalent Decoration of Graphene Oxide Sheets with Nanocrystals. *Nano Res.* **2009**, *2*, 192–200.
228. Combellas, C.; Delamar, M.; Kanoufi, F.; Pinson, J.; Podvorica, F. I. Spontaneous Grafting of Iron Surfaces by Reduction of Aryldiazonium Salts in Acidic or Neutral Aqueous Solution. Application to the Protection of Iron against Corrosion. *Chem. Mater.* **2005**, *17*, 3968–3975.
229. Kataby, G.; Cojocaru, M.; Prozorov, R.; Gedanken, A. Coating Carboxylic Acids on Amorphous Iron Nanoparticles. *Langmuir* **1999**, *15*, 1703–1708.
230. Li, H.; Xu, T.; Wang, C.; Chen, J.; Zhou, H.; Liu, H. Tribochemical Effects on the Friction and Wear Behaviors of Diamond-like Carbon Film Under High Relative Humidity Condition. *Tribol. Lett.* **2005**, *19*, 231–238.
231. Adenier, A.; Bernard, M.-C.; Chehimi, M. M.; Cabet-Deliry, E.; Desbat, B.; Fagebaume, O.; Pinson, J.; Podvorica, F. Covalent Modification of Iron Surfaces by Electrochemical Reduction of Aryldiazonium Salts. *J. Am. Chem. Soc.* **2001**, *123*, 4541–4549.
232. Zhou, J. S.; Song, H. H.; Ma, L. L.; Chen, X. H. Magnetite/Graphene Nanosheet Composites: Interfacial Interaction and Its Impact on the Durable High-Rate Performance in Lithium-Ion Batteries. *RSC Adv.* **2011**, *1*, 782–791.
233. Qu, Q.; Yang, S.; Feng, X. 2D Sandwich-like Sheets of Iron Oxide Grown on Graphene as High Energy Anode Material for Supercapacitors. *Adv. Mater.* **2011**, *23*, 5574–5580.
234. Zhu, J.; Wei, S.; Gu, H.; Rapole, S. B.; Wang, Q.; Luo, Z.; Haldolaarachchige, N.; Young, D. P.; Guo, Z. One-Pot Synthesis of Magnetic Graphene Nanocomposites Decorated with Core@Double-Shell Nanoparticles for Fast Chromium Removal. *Environ. Sci. Technol.* **2012**, *46*, 977–985.
235. Gao, Y. J.; Ma, D.; Hu, G.; Zhai, P.; Bao, X. H.; Zhu, B.; Zhang, B. S.; Su, D. S. Layered-Carbon-Stabilized Iron Oxide

Nanostructures as Oxidation Catalysts. *Angew. Chem., Int. Ed.* **2011**, *50*, 10236–10240.
236. Pilatos, G.; Vermisoglou, E. C.; Perdikaki, A.; Devlin, E.; Pappas, G. S.; Romanos, G. E.; Boukos, N.; Giannakopoulou, T.; Trapalis, C.; Kanellopoulos, N. K.; *et al.* One-Step, *In Situ* Growth of Unmodified Graphene–Magnetic Nanostructured Composites. *Carbon* **2014**, *66*, 467–475.
237. Kim, I. T.; Magasinski, A.; Jacob, K.; Yushin, G.; Tannenbaum, R. Synthesis and Electrochemical Performance of Reduced Graphene Oxide/Maghemite Composite Anode for Lithium Ion Batteries. *Carbon* **2013**, *52*, 56–64.
238. Szabo, T.; Bakandritsos, A.; Tzitzios, V.; Devlin, E.; Petridis, D.; Dekany, I. Magnetically Modified Single and Turbostratic Stacked Graphenes from Tris(2,2′-bipyridyl) Iron(II) Ion-Exchanged Graphite Oxide. *J. Phys. Chem. B* **2008**, *112*, 14461–14469.
239. Sinha, A.; Jana, N. R. Graphene-Based Composite with $\gamma$-$Fe_2O_3$ Nanoparticle for the High-Performance Removal of Endocrine-Disrupting Compounds from Water. *Chem.—Asian J.* **2013**, *8*, 786–791.
240. Chandra, V.; Park, J.; Chun, Y.; Lee, J. W.; Hwang, I. C.; Kim, K. S. Water-Dispersible Magnetite-Reduced Graphene Oxide Composites for Arsenic Removal. *ACS Nano* **2010**, *4*, 3979–3986.
241. Cong, H. P.; He, J. J.; Lu, Y.; Yu, S. H. Water-Soluble Magnetic-Functionalized Reduced Graphene Oxide Sheets: *In Situ* Synthesis and Magnetic Resonance Imaging Applications. *Small* **2010**, *6*, 169–173.
242. Li, Y.; Chu, J.; Qi, J. Y.; Li, X. An Easy and Novel Approach for the Decoration of Graphene Oxide by $Fe_3O_4$ Nanoparticles. *Appl. Surf. Sci.* **2011**, *257*, 6059–6062.
243. Guo, J.; Wang, R.; Tjiu, W. W.; Pan, J.; Liu, T. Synthesis of Fe Nanoparticles@Graphene Composites for Environmental Applications. *J. Hazard. Mater.* **2012**, *225–226*, 63–73.
244. Schwertmann, U.; Cornell, R. M. *Iron Oxides in the Laboratory: Preparation and Characterization*, 2nd ed.; Wiley-VCH: Weinheim, Germany, 2000.
245. Dreyer, D. R.; Park, S.; Bielawski, C. W.; Ruoff, R. S. The Chemistry of Graphene Oxide. *Chem. Soc. Rev.* **2010**, *39*, 228–240.
246. Zheng, M.; Qiu, D.; Zhao, B.; Ma, L.; Wang, X.; Lin, Z.; Pan, L.; Zheng, Y.; Shi, Y. Mesoporous Iron Oxide Directly Anchored on a Graphene Matrix for Lithium-Ion Battery Anodes with Enhanced Strain Accommodation. *RSC Adv.* **2013**, *3*, 699–703.
247. Shen, J.; Hu, Y.; Shi, M.; Li, N.; Ma, H.; Ye, M. One Step Synthesis of Graphene Oxide–Magnetic Nanoparticle Composite. *J. Phys. Chem. C* **2010**, *114*, 1498–1503.
248. Yang, S.; Sun, Y.; Chen, L.; Hernandez, Y.; Feng, X.; Mullen, K. Porous Iron Oxide Ribbons Grown on Graphene for High-Performance Lithium Storage. *Sci. Rep.* **2012**, *2*, 427.
249. Zhu, J.; Luo, Z.; Wu, S.; Haldolaarachchige, N.; Young, D. P.; Wei, S.; Guo, Z. Magnetic Graphene Nanocomposites: Electron Conduction, Giant Magnetoresistance and Tunable Negative Permittivity. *J. Mater. Chem.* **2012**, *22*, 835–844.
250. Jabeen, H.; Kemp, K. C.; Chandra, V. Synthesis of Nano Zerovalent Iron Nanoparticles—Graphene Composite for the Treatment of Lead Contaminated Water. *J. Environ. Manage.* **2013**, *130*, 429–435.
251. Zong, P. F.; Wang, S. F.; Zhao, Y. L.; Wang, H.; Pan, H.; He, C. H. Synthesis and Application of Magnetic Graphene/Iron Oxides Composite for the Removal of U(VI) from Aqueous Solutions. *Chem. Eng. J.* **2013**, *220*, 45–52.
252. Liu, M.; Chen, C.; Hu, J.; Wu, X.; Wang, X. Synthesis of Magnetite/Graphene Oxide Composite and Application for Cobalt(II) Removal. *J. Phys. Chem. C* **2011**, *115*, 25234–25240.
253. Zhang, Y.; Chen, B.; Zhang, L.; Huang, J.; Chen, F.; Yang, Z.; Yao, J.; Zhang, Z. Controlled Assembly of $Fe_3O_4$ Magnetic Nanoparticles on Graphene Oxide. *Nanoscale* **2011**, *3*, 1446–1450.
254. Karamani, A. A.; Douvalis, A. P.; Stalikas, C. D. Zero-Valent Iron/Iron Oxide-Oxyhydroxide/Graphene as a Magnetic Sorbent for the Enrichment of Polychlorinated Biphenyls, Polyaromatic Hydrocarbons and Phthalates Prior to Gas Chromatography-Mass Spectrometry. *J. Chromatogr. A* **2013**, *1271*, 1–9.
255. Travlou, N. A.; Kyzas, G. Z.; Lazaridis, N. K.; Deliyanni, E. A. Functionalization of Graphite Oxide with Magnetic Chitosan for the Preparation of a Nanocomposite Dye Adsorbent. *Langmuir* **2013**, *29*, 1657–1668.
256. Tang, Y.; Guo, H.; Xiao, L.; Yu, S.; Gao, N.; Wang, Y. Synthesis of Reduced Graphene Oxide/Magnetite Composites and Investigation of Their Adsorption Performance of Fluoroquinolone Antibiotics. *Colloids Surf., A* **2013**, *424*, 74–80.
257. Kemp, K. C.; Seema, H.; Saleh, M.; Le, N. H.; Mahesh, K.; Chandra, V.; Kim, K. S. Environmental Applications Using Graphene Composites: Water Remediation and Gas Adsorption. *Nanoscale* **2013**, *5*, 3149–3171.
258. Sheng, G.; Li, Y.; Yang, X.; Ren, X.; Yang, S.; Hu, J.; Wang, X. Efficient Removal of Arsenate by Versatile Magnetic Graphene Oxide Composites. *RSC Adv.* **2012**, *2*, 12400–12407.
259. Paul, R. K.; Ghazinejad, M.; Penchev, M.; Lin, J. A.; Ozkan, M.; Ozkan, C. S. Synthesis of a Pillared Graphene Nanostructure: A Counterpart of Three-Dimensional Carbon Architectures. *Small* **2010**, *6*, 2309–2313.
260. Xu, Y. X.; Wu, Q. O.; Sun, Y. Q.; Bai, H.; Shi, G. Q. Three-Dimensional Self-Assembly of Graphene Oxide and DNA into Multifunctional Hydrogels. *ACS Nano* **2010**, *4*, 7358–7362.
261. Li, C.; Shi, G. Q. Three-Dimensional Graphene Architectures. *Nanoscale* **2012**, *4*, 5549–5563.
262. Lei, Y. L.; Chen, F.; Luo, Y. J.; Zhang, L. Three-Dimensional Magnetic Graphene Oxide Foam/$Fe_3O_4$ Nanocomposite as an Efficient Absorbent for Cr(VI) Removal. *J. Mater. Sci.* **2014**, *49*, 4236–4245.
263. Luo, X. B.; Wang, C. C.; Luo, S. L.; Dong, R. Z.; Tu, X. M.; Zeng, G. S. Adsorption of As(III) and As(V) from Water Using Magnetite $Fe_3O_4$-Reduced Graphite Oxide-$MnO_2$ Nanocomposites. *Chem. Eng. J.* **2012**, *187*, 45–52.
264. Vijay Kumar, S.; Huang, N. M.; Yusoff, N.; Lim, H. N. High Performance Magnetically Separable Graphene/Zinc Oxide Nanocomposite. *Mater. Lett.* **2013**, *93*, 411–414.
265. He, Y. P.; Sheng, Q. L.; Zheng, J. B.; Wang, M. Z.; Liu, B. Magnetite–Graphene for the Direct Electrochemistry of Hemoglobin and Its Biosensing Application. *Electrochim. Acta* **2011**, *56*, 2471–2476.
266. Zhou, K.; Zhu, Y.; Yang, X.; Li, C. Preparation and Application of Mediator-Free $H_2O_2$ Biosensors of Graphene–$Fe_3O_4$ Composites. *Electroanalysis* **2011**, *23*, 862–869.
267. Jin, Y.; Qian, J.; Wang, K.; Yang, X.; Dong, X.; Qiu, B. Fabrication of Multifunctional Magnetic FePc@$Fe_3O_4$/Reduced Graphene Oxide Nanocomposites as Biomimetic Catalysts for Organic Peroxide Sensing. *J. Electroanal. Chem.* **2013**, *693*, 79–85.
268. Prakash, A.; Chandra, S.; Bahadur, D. Structural, Magnetic, and Textural Properties of Iron Oxide-Reduced Graphene Oxide Hybrids and Their Use for the Electrochemical Detection of Chromium. *Carbon* **2012**, *50*, 4209–4219.
269. Xu, Y.; Lv, Z.; Xia, Y.; Han, Y.; Lou, B.; Wang, E. Highly Porous Magnetite/Graphene Nanocomposites for a Solid-State Electrochemiluminescence Sensor on Paper-Based Chips. *Anal. Bioanal. Chem.* **2013**, *405*, 3549–3558.
270. Xing, Z. C.; Tian, J. Q.; Asiri, A. M.; Qusti, A. H.; Al-Youbi, A. O.; Sun, X. P. Two-Dimensional Hybrid Mesoporous $Fe_2O_3$-Graphene Nanostructures: A Highly Active and Reusable Peroxidase Mimetic toward Rapid, Highly Sensitive Optical Detection of Glucose. *Biosens. Bioelectron.* **2014**, *52*, 452–457.
271. Jiang, Z. X.; Li, J.; Aslan, H.; Li, Q.; Li, Y.; Chen, M. L.; Huang, Y. D.; Froning, J. P.; Otyepka, M.; Zboril, R.; *et al.* A High Efficiency $H_2S$ Gas Sensor Material: Paper Like $Fe_2O_3$/Graphene Nanosheets and Structural Alignment Dependency of Device Efficiency. *J. Mater. Chem. A* **2014**, *2*, 6714–6717.
272. Yang, X. Y.; Wang, Y. S.; Huang, X.; Ma, Y. F.; Huang, Y.; Yang, R. C.; Duan, H. Q.; Chen, Y. S. Multi-functionalized

Graphene Oxide Based Anticancer Drug-Carrier with Dual-Targeting Function and pH-Sensitivity. *J. Mater. Chem.* **2011**, *21*, 3448–3454.
273. Chen, W.; Yi, P.; Zhang, Y.; Zhang, L.; Deng, Z.; Zhang, Z. Composites of Aminodextran-Coated $Fe_3O_4$ Nanoparticles and Graphene Oxide for Cellular Magnetic Resonance Imaging. *ACS Appl. Mater. Interfaces* **2011**, *3*, 4085–4091.
274. Fan, X.; Jiao, G.; Zhao, W.; Jin, P.; Li, X. Magnetic $Fe_3O_4$-Graphene Composites as Targeted Drug Nanocarriers for pH-Activated Release. *Nanoscale* **2013**, *5*, 1143–1152.
275. Li, X. D.; Liang, X. L.; Yue, X. L.; Wang, J. R.; Li, C. H.; Deng, Z. J.; Jing, L. J.; Lin, L.; Qu, E. Z.; Wang, S. M.; *et al.* Imaging Guided Photothermal Therapy Using Iron Oxide Loaded Poly(lactic Acid) Microcapsules Coated with Graphene Oxide. *J. Mater. Chem. B* **2014**, *2*, 217–223.
276. Zhang, M.; Lei, D. N.; Yin, X. M.; Chen, L. B.; Li, Q. H.; Wang, Y. G.; Wang, T. H. Magnetite/Graphene Composites: Microwave Irradiation Synthesis and Enhanced Cycling and Rate Performances for Lithium Ion Batteries. *J. Mater. Chem.* **2010**, *20*, 5538–5543.
277. Behera, S. K. Enhanced Rate Performance and Cyclic Stability of $Fe_3O_4$—Graphene Nanocomposites for Li Ion Battery Anodes. *Chem. Commun.* **2011**, *47*, 10371–10373.
278. Li, B. J.; Cao, H. Q.; Shao, J.; Qu, M. Z.; Warner, J. H. Superparamagnetic $Fe_3O_4$ Nanocrystals@Graphene Composites for Energy Storage Devices. *J. Mater. Chem.* **2011**, *21*, 5069–5075.
279. Zhang, W.; Liu, F.; Li, Q.; Shou, Q.; Cheng, J.; Zhang, L.; Nelson, B. J.; Zhang, X. Transition Metal Oxide and Graphene Nanocomposites for High-Performance Electrochemical Capacitors. *Phys. Chem. Chem. Phys.* **2012**, *14*, 16331–16337.
280. Cheng, J. P.; Shou, Q. L.; Wu, J. S.; Liu, F.; Dravid, V. P.; Zhang, X. B. Influence of Component Content on the Capacitance of Magnetite/Reduced Graphene Oxide Composite. *J. Electroanal. Chem.* **2013**, *698*, 1–8.
281. Zhou, D.; Zhang, T.-L.; Han, B.-H. One-Step Solvothermal Synthesis of an Iron Oxide—Graphene Magnetic Hybrid Material with High Porosity. *Microporous Mesoporous Mater.* **2013**, *165*, 234–239.
282. Yang, S. H.; Song, X. F.; Zhang, P.; Gao, L. Facile Synthesis of Nitrogen-Doped Graphene Ultrathin $MnO_2$ Sheet Composites and Their Electrochemical Performances. *ACS Appl. Mater. Interfaces* **2013**, *5*, 3317–3322.
283. Du, M.; Xu, C. H.; Sun, J.; Gao, L. One Step Synthesis of $Fe_2O_3$/Nitrogen-Doped Graphene Composite as Anode Materials for Lithium Ion Batteries. *Electrochim. Acta* **2012**, *80*, 302–307.
284. Cai, D. D.; Li, D. D.; Wang, S. Q.; Zhu, X. F.; Yang, W. S.; Zhang, S. Q.; Wang, H. H. High Rate Capability of $TiO_2$/Nitrogen-Doped Graphene Nanocomposite as an Anode Material for Lithium-Ion Batteries. *J. Alloys Compd.* **2013**, *561*, 54–58.
285. Zhao, P. H.; Li, W. L.; Wang, G.; Yu, B. Z.; Li, X. J.; Bai, J. T.; Ren, Z. Y. Facile Hydrothermal Fabrication of Nitrogen-Doped Graphene/$Fe_2O_3$ Composites as High Performance Electrode Materials for Supercapacitor. *J. Alloys Compd.* **2014**, *604*, 87–93.
286. Lin, J.; Raji, A. R. O.; Nan, K. W.; Peng, Z. W.; Yan, Z.; Samuel, E. L. G.; Natelson, D.; Tour, J. M. Iron Oxide Nanoparticle and Graphene Nanoribbon Composite as an Anode Material for High- Performance Li-Ion Batteries. *Adv. Funct. Mater.* **2014**, *24*, 2044–2048.
287. Souza, C. A. C.; Carlos, I. A.; Lopes, M.; Finazzi, G. A.; de Almeida, M. R. H. Self-Discharge of Fe—Ni Alkaline Batteries. *J. Power Sources* **2004**, *132*, 288–290.
288. Malkhandi, S.; Yang, B.; Manohar, A. K.; Prakash, G. K. S.; Narayanan, S. R. Self-Assembled Monolayers of *n*-Alkanethiols Suppress Hydrogen Evolution and Increase the Efficiency of Rechargeable Iron Battery Electrodes. *J. Am. Chem. Soc.* **2013**, *135*, 347–353.
289. Periasamy, P.; Babu, B. R.; Iyer, S. V. Cyclic Voltammetric Studies of Porous Iron Electrodes in Alkaline Solutions Used for Alkaline Batteries. *J. Power Sources* **1996**, *58*, 35–40.
290. Wang, H. L.; Liang, Y. Y.; Gong, M.; Li, Y. G.; Chang, W.; Mefford, T.; Zhou, J. G.; Wang, J.; Regier, T.; Wei, F.; *et al.* An Ultrafast Nickel-Iron Battery from Strongly Coupled Inorganic Nanoparticle/Nanocarbon Hybrid Materials. *Nat. Commun.* **2012**, *3*, 917.
291. Jiang, W.; Liang, F.; Wang, J. W.; Su, L.; Wu, Y. M.; Wang, L. M. Enhanced Electrochemical Performances of $FeO_x$-Graphene Nanocomposites as Anode Materials for Alkaline Nickel—Iron Batteries. *RSC Adv.* **2014**, *4*, 15394–15399.
292. Deng, J. J.; Lv, X. X.; Gao, J.; Pu, A. W.; Li, M.; Sun, X. H.; Zhong, J. Facile Synthesis of Carbon-Coated Hematite Nanostructures for Solar Water Splitting. *Energy Environ. Sci.* **2013**, *6*, 1965–1970.
293. Rai, S.; Ikram, A.; Sahai, S.; Dass, S.; Shrivastav, R.; Satsangi, V. R. Morphological, Optical and Photoelectrochemical Properties of $Fe_2O_3$-GNP Composite Thin Films. *RSC Adv.* **2014**, *4*, 17671–17679.
294. Wang, T. S.; Liu, Z. H.; Lu, M. M.; Wen, B.; Ouyang, Q. Y.; Chen, Y. J.; Zhu, C. L.; Gao, P.; Li, C. Y.; Cao, M. S.; *et al.* Graphene-$Fe_3O_4$ Nanohybrids: Synthesis and Excellent Electromagnetic Absorption Properties. *J. Appl. Phys.* **2013**, *113*, 024314.
295. Sun, X.; He, J. P.; Li, G. X.; Tang, J.; Wang, T.; Guo, Y. X.; Xue, H. R. Laminated Magnetic Graphene with Enhanced Electromagnetic Wave Absorption Properties. *J. Mater. Chem. C* **2013**, *1*, 765–777.
296. Zheng, J.; Lv, H. L.; Lin, X. H.; Ji, G. B.; Li, X. G.; Du, Y. W. Enhanced Microwave Electromagnetic Properties of $Fe_3O_4$/Graphene Nanosheet Composites. *J. Alloys Compd.* **2014**, *589*, 174–181.
297. Xue, W. D.; Zhao, R.; Du, X.; Xu, F. W.; Xu, M.; Wei, K. X. Graphene-$Fe_3O_4$ Micro-Nano Scaled Hybrid Spheres: Synthesis and Synergistic Electromagnetic Effect. *Mater. Res. Bull.* **2014**, *50*, 285–291.
298. Hu, J. F.; Wang, Y. P.; Han, M.; Zhou, Y. M.; Jiang, X. Q.; Sun, P. P. A Facile Preparation of Palladium Nanoparticles Supported on Magnetite/s-Graphene and Their Catalytic Application in Suzuki—Miyaura Reaction. *Catal. Sci. Technol.* **2012**, *2*, 2332–2340.
299. Li, X.; Wang, X.; Song, S.; Liu, D.; Zhang, H. Selectively Deposited Noble Metal Nanoparticles on $Fe_3O_4$/Graphene Composites: Stable, Recyclable, and Magnetically Separable Catalysts. *Chem.—Eur. J.* **2012**, *18*, 7601–7607.
300. Chandra, S.; Bag, S.; Das, P.; Bhattacharya, D.; Pramanik, P. Fabrication of Magnetically Separable Palladium—Graphene Nanocomposite with Unique Catalytic Property of Hydrogenation. *Chem. Phys. Lett.* **2012**, *519—520*, 59–63.
301. Zubir, N. A.; Yacou, C.; Motuzas, J.; Zhang, X. W.; da Costa, J. C. D. Structural and Functional Investigation of Graphene Oxide—$Fe_3O_4$ Nanocomposites for the Heterogeneous Fenton-like Reaction. *Sci. Rep.* **2014**, *4*, 4594.
302. Luo, W. L.; Wang, H.; Ruoff, R. C.; Cioslowski, J.; Phelps, S. Susceptibility Discontinuity in Single-Crystal $C_{60}$. *Phys. Rev. Lett.* **1994**, *73*, 186–188.
303. Haddon, R. C.; Scheemeyer, L. F.; Waszczak, J. V.; Glarum, S. H.; Tycko, R.; Dabbah, G.; Kortan, A. R.; Muller, A. J.; Mujsce, A. M.; Rosseinsky, M. J.; *et al.* Experimental and Theoretical Determination of the Magnetic Susceptibility of $C_{60}$ and $C_{70}$. *Nature* **1991**, *350*, 46–47.
304. Ruoff, R. S.; Beach, D.; Cuomo, J.; McGuire, T.; Whetten, R. L.; Diederich, F. Confirmation of a Vanishingly Small Ring Current Magnetic Susceptibility of Icosahedral $C_{60}$. *J. Phys. Chem.* **1991**, *95*, 3457–3459.
305. Shi, J.; Yu, X.; Wang, L.; Liu, Y.; Gao, J.; Zhang, J.; Ma, R.; Liu, R.; Zhang, Z. PEGylated Fullerene/Iron Oxide Nanocomposites for Photodynamic Therapy, Targeted Drug Delivery and MR Imaging. *Biomaterials* **2013**, *34*, 9666–9677.
306. Snovski, R.; Grinblat, J.; Margel, S. Synthesis and Characterization of Magnetic Poly(divinyl benzene)/$Fe_3O_4$, C/$Fe_3O_4$/Fe, and C/Fe Onionlike Fullerene Micrometer-Sized Particles with a Narrow Size Distribution. *Langmuir* **2011**, *27*, 11071–11080.

307. Shinohara, H. Endohedral Metallofullerenes. *Rep. Prog. Phys.* **2000**, *63*, 843–892.
308. Chaur, M. N.; Melin, F.; Ortiz, A. L.; Echegoyen, L. *Angew. Chem., Int. Ed.* **2009**, *48*, 7514–7538.
309. Rodriguez-Fortea, A.; Balch, A. L.; Poblet, J. M. Endohedral Metallofullerenes: A Unique Host–Guest Association. *Chem. Soc. Rev.* **2011**, *40*, 3551–3563.
310. Markova, Z.; Bourlinos, A. B.; Safarova, K.; Polakova, K.; Tucek, J.; Medrik, I.; Siskova, K.; Petr, J.; Krysmann, M.; Giannelis, E. P.; *et al.* Synthesis and Properties of Core–Shell Fluorescent Hybrids with Distinct Morphologies Based on Carbon Dots. *J. Mater. Chem.* **2012**, *22*, 16219–16223.
311. Zhang, H.; Ming, H.; Lian, S.; Huang, H.; Li, H.; Zhang, L.; Liu, Y.; Kang, Z.; Leeb, S.-T. $Fe_2O_3$/Carbon Quantum Dots Complex Photocatalysts and Their Enhanced Photocatalytic Activity under Visible Light. *Dalton Trans.* **2011**, *40*, 10822–10825.
312. Wu, X. C.; Zhang, Y.; Han, T.; Wu, H. X.; Guo, S. W.; Zhang, J. Y. Composite of Graphene Quantum Dots and $Fe_3O_4$ Nanoparticles: Peroxidase Activity and Application in Phenolic Compound Removal. *RSC Adv.* **2014**, *4*, 3299–3305.
313. Zhou, X. J.; Zhang, Y.; Wang, C.; Wu, X. C.; Yang, Y. Q.; Zheng, B.; Wu, H. X.; Guo, S. W.; Zhang, J. Y. Photo-Fenton Reaction of Graphene Oxide: A New Strategy To Prepare Graphene Quantum Dots for DNA Cleavage. *ACS Nano* **2012**, *6*, 6592–6599.
314. Zhang, Y.; Wu, C. Y.; Zhou, X. J.; Wu, X. C.; Yang, Y. Q.; Wu, H. X.; Guo, S. W.; Zhang, J. Y. Graphene Quantum Dots/Gold Electrode and Its Application in Living Cell $H_2O_2$ Detection. *Nanoscale* **2013**, *5*, 1816–1819.
315. Baikousi, M.; Bourlinos, A. B.; Douvalis, A.; Bakas, T.; Anagnostopoulos, D. F.; Tucek, J.; Safarova, K.; Zboril, R.; Karakassides, M. A. Synthesis and Characterization of $\gamma$-$Fe_2O_3$/Carbon Hybrids and Their Application in Removal of Hexavalent Chromium Ions from Aqueous Solutions. *Langmuir* **2012**, *28*, 3918–3930.
316. Zhai, Y. P.; Dou, Y. Q.; Liu, X. X.; Tu, B.; Zhao, D. Y. One-Pot Synthesis of Magnetically Separable Ordered Mesoporous Carbon. *J. Mater. Chem.* **2009**, *19*, 3292–3300.
317. Huwe, H.; Froba, M. Synthesis and Characterization of Transition Metal and Metal Oxide Nanoparticles inside Mesoporous Carbon CMK-3. *Carbon* **2007**, *45*, 304–314.
318. Dong, X. P.; Chen, H. R.; Zhao, W. R.; Li, X.; Shi, J. L. Synthesis and Magnetic Properties of Mesostructured $\gamma$-$Fe_2O_3$/Carbon Composites by a Co-casting Method. *Chem. Mater.* **2007**, *19*, 3484–3490.
319. Wu, Z. X.; Li, W.; Webley, P. A.; Zhao, D. Y. General and Controllable Synthesis of Novel Mesoporous Magnetic Iron Oxide@Carbon Encapsulates for Efficient Arsenic Removal. *Adv. Mater.* **2012**, *24*, 485–491.
320. Li, Z. Q.; Wang, X. K.; Wang, C. B.; Yin, L. W. Hybrids of Iron Oxide/Ordered Mesoporous Carbon as Anode Materials for High-Capacity and High-Rate Capability Lithium-Ion Batteries. *RSC Adv.* **2013**, *3*, 17097–17104.
321. Lu, A. H.; Nitz, J. J.; Comotti, M.; Weidenthaler, C.; Schlichte, K.; Lehmann, C. W.; Terasaki, O.; Schuth, F. Spatially and Size Selective Synthesis of Fe-Based Nanoparticles on Ordered Mesoporous Supports as Highly Active and Stable Catalysts for Ammonia Decomposition. *J. Am. Chem. Soc.* **2010**, *132*, 14152–14162.
322. Nagao, M.; Otani, M.; Tomita, H.; Kanzaki, S.; Yamada, A.; Kanno, R. New Three-Dimensional Electrode Structure for the Lithium Battery: Nano-Sized $\gamma$-$Fe_2O_3$ in a Mesoporous Carbon Matrix. *J. Power Sources* **2011**, *196*, 4741–4746.
323. Ryoo, R.; Joo, S. H.; Jun, S. Synthesis of Highly Ordered Carbon Molecular Sieves *via* Template-Mediated Structural Transformation. *J. Phys. Chem. B* **1999**, *103*, 7743–7746.
324. Ryoo, R.; Joo, S. H.; Kruk, M.; Jaroniec, M. Ordered Mesoporous Carbons. *Adv. Mater.* **2001**, *13*, 677–681.
325. Vinu, A.; Mori, T.; Ariga, K. New Families of Mesoporous Materials. *Sci. Technol. Adv. Mater.* **2006**, *7*, 753–771.
326. Wan, Y.; Yang, H. F.; Zhao, D. Y. "Host–Guest" Chemistry in the Synthesis of Ordered Nonsiliceous Mesoporous Materials. *Acc. Chem. Res.* **2006**, *39*, 423–432.
327. Liang, C. D.; Li, Z. J.; Dai, S. Mesoporous Carbon Materials: Synthesis and Modification. *Angew. Chem., Int. Ed.* **2008**, *47*, 3696–3717.
328. Kruk, M.; Jaroniec, M.; Ryoo, R.; Joo, S. H. Characterization of Ordered Mesoporous Carbons Synthesized Using MCM-48 Silicas as Templates. *J. Phys. Chem. B* **2000**, *104*, 7960–7968.
329. Geng, L. L.; Zhang, X. Y.; Zhang, W. X.; Jia, M. J.; Liu, G. Highly Dispersed Iron Oxides on Mesoporous Carbon for Selective Oxidation of Benzyl Alcohol with Molecular Oxygen. *Chem. Commun.* **2014**, *50*, 2965–2967.
330. Xu, Y. H.; Jian, G. Q.; Liu, Y. H.; Zhu, Y. J.; Zachariah, M. R.; Wang, C. S. Superior Electrochemical Performance and Structure Evolution of Mesoporous $Fe_2O_3$ Anodes for Lithium-Ion Batteries. *Nano Energy* **2014**, *3*, 26–35.
331. Lee, J.; Sohn, K.; Hyeon, T. Fabrication of Novel Mesocellular Carbon Foams with Uniform Ultralarge Mesopores. *J. Am. Chem. Soc.* **2001**, *123*, 5146–5147.
332. Lee, J.; Sohn, K.; Hyeon, T. Low-Cost and Facile Synthesis of Mesocellular Carbon Foams. *Chem. Commun.* **2002**, 2674–2675.
333. Kang, E.; Jung, Y. S.; Cavanagh, A. S.; Kim, G. H.; George, S. M.; Dillon, A. C.; Kim, J. K.; Lee, J. $Fe_3O_4$ Nanoparticles Confined in Mesocellular Carbon Foam for High Performance Anode Materials for Lithium-Ion Batteries. *Adv. Funct. Mater.* **2011**, *21*, 2430–2438.
334. Yoon, T.; Chae, C.; Sun, Y. K.; Zhao, X.; Kung, H. H.; Lee, J. K. Bottom-Up *In Situ* Formation of $Fe_3O_4$ Nanocrystals in a Porous Carbon Foam for Lithium-Ion Battery Anodes. *J. Mater. Chem.* **2011**, *21*, 17325–17330.
335. Chun, J.; Lee, H.; Lee, S. H.; Hong, S. W.; Lee, J.; Lee, C.; Lee, J. Magnetite/Mesocellular Carbon Foam as a Magnetically Recoverable Fenton Catalyst for Removal of Phenol and Arsenic. *Chemosphere* **2012**, *89*, 1230–1237.
336. Mendes, R. G.; Bachmatiuk, A.; El-Gendy, A. A.; Melkhanova, S.; Klingeler, R.; Buchner, B.; Rummeli, M. H. A Facile Route To Coat Iron Oxide Nanoparticles with Few-Layer Graphene. *J. Phys. Chem. C* **2012**, *116*, 23749–23756.
337. Zhu, S. M.; Zhang, D.; Chen, Z. X.; Zhang, Y. M. Controlled Synthesis of Core/Shell Magnetic Iron Oxide/Carbon Systems *via* a Self-Template Method. *J. Mater. Chem.* **2009**, *19*, 7710–7715.
338. Jang, B.; Park, M.; Chae, O. B.; Park, S.; Kim, Y.; Oh, S. M.; Piao, Y.; Hyeon, T. Direct Synthesis of Self-Assembled Ferrite/Carbon Hybrid Nanosheets for High Performance Lithium-Ion Battery Anodes. *J. Am. Chem. Soc.* **2012**, *134*, 15010–15015.
339. Tristao, J. C.; Oliveira, A. A. S.; Ardisson, J. D.; Dias, A.; Lago, R. M. Facile Preparation of Carbon Coated Magnetic $Fe_3O_4$ Particles by a Combined Reduction/CVD Process. *Mater. Res. Bull.* **2011**, *46*, 748–754.
340. Moussa, S.; Atkinson, G.; El-Shall, M. S. Laser-Assisted Synthesis of Magnetic Fe/$Fe_2O_3$ Core: Carbon-Shell Nanoparticles in Organic Solvents. *J. Nanopart. Res.* **2013**, *15*, 1470.
341. Zhang, F.; Cui, L.; Lin, K.; Jin, F. M.; Wang, B.; Shi, S. X.; Yang, D. A.; Wang, H.; He, F.; Chen, X. P.; *et al.* Preparation of Carbon-Encapsulated Iron Nanoparticles in High Yield by DC Arc Discharge and Their Characterization. *J. Alloys Compd.* **2013**, *553*, 367–374.
342. Piao, Y.; Kim, J.; Bin Na, H.; Kim, D.; Baek, J. S.; Ko, M. K.; Lee, J. H.; Shokouhimehr, M.; Hyeon, T. Wrap-Bake-Peel Process for Nanostructural Transformation from $\beta$-FeOOH Nanorods to Biocompatible Iron Oxide Nanocapsules. *Nat. Mater.* **2008**, *7*, 242–247.